Geochimica et Cosmochimica Acta, Vol. 68, No. 24, pp. 5027–5057, 2004

0016-7037/04 $30.00 + .00

doi:10.1016/j.gca.2004.08.016

Dissolution mechanisms of water in depolymerized silicate melts: Constraints from ^{1}H and ^{29}Si NMR spectroscopy and ab initio calculations

XIANYU XUE* and MASAMI KANZAKI

Institute for Study of the Earth's Interior, Okayama University, Misasa, Tottori 682-0193, Japan

(*Received February* 23, 2004; *accepted in revised form August* 13, 2004)

Abstract—Dissolution of water in magmas significantly affects phase relations and physical properties. To shed new light on the this issue, we have applied ^{1}H and ^{29}Si nuclear magnetic resonance (NMR) spectroscopic techniques to hydrous silicate glasses (quenched melts) in the CaO-MgO-SiO_2 (CMS), Na_2O-SiO_2, Na_2O-CaO-SiO_2 and Li_2O-SiO_2 systems. We have also carried out ab initio molecular orbital calculations on representative clusters to gain insight into the experimental results.

The most prominent result is the identification of a major peak at ~1.1 to 1.7 ppm in the ^{1}H MAS NMR spectra for all the hydrous CMS glasses. On the basis of experimental NMR data for crystalline phases and ab initio calculation results, this peak can be unambiguously attributed to (Ca,Mg)OH groups. Such OH groups, like free oxygens, are only linked to metal cations, but not part of the silicate network, and are thus referred to as free hydroxyls in the paper. This represents the first direct evidence for a substantial proportion (~13~29%) of the dissolved water as free hydroxyl groups in quenched hydrous silicate melts. We have found that free hydroxyls are favored by (1) more depolymerized melts and (2) network-modifying cations of higher field strength (Z/R^2: Z: charge, R: cation-oxygen bond length) in the order Mg > Ca > Na. Their formation is expected to cause an increase in the melt polymerization, contrary to the effect of SiOH formation. The ^{29}Si MAS NMR results are consistent with such an interpretation. This water dissolution mechanism could be particularly important for ultramafic and mafic magmas.

The ^{1}H MAS NMR spectra for glasses of all the studied compositions contain peaks in the 4 to 17 ppm region, attributable to SiOH of a range of strength of hydrogen bonding and molecular H_2O. The relative population of SiOH with strong hydrogen bonding grows with decreasing field strength of the network-modifying cations. Ab initio calculations confirmed that this trend largely reflects hydrogen bonding with nonbridging oxygens. *Copyright © 2004 Elsevier Ltd*

1. INTRODUCTION

Water often constitutes the most abundant volatile component in natural magmas and can have a dramatic effect on their phase relations and physical properties. Dissolved water in silicate glasses is also a key factor affecting the properties of many technological materials. Knowledge of the dissolution mechanisms of water is thus necessary to gain a deep understanding of the properties and behavior of hydrous silicate melts and glasses. There have been extensive spectroscopic and diffraction studies using techniques such as infrared (IR), Raman, nuclear magnetic resonance spectroscopy (NMR) and neutron diffraction, aimed at elucidating the solubility and dissolution mechanisms of water in silicate melts and glasses (see reviews in McMillan, 1994; Kohn, 2000). Many of these studies have been carried out on glasses quenched from melts, and their structures (both the silicate network and water speciation) are usually regarded to approximate those of the melts at the glass transition temperature. It is now generally agreed from extensive studies, in particular, IR and wideline ^{1}H-NMR studies, that water is dissolved in silicate melts as both molecular H_2O and hydroxyls (OH), with the abundance of the former increasing with increasing total water content (e.g., Bartholomew and Schreurs, 1980; Stolper, 1982b; Acocella et al., 1984; Eckert et al., 1988; also see reviews in McMillan, 1994; Kohn, 2000). In the wideline ^{1}H-NMR spectra of silicate glasses measured at low temperature, molecular H_2O typically exhibit a broad doublet shape ("Pake doublet"), arising from strong intramolecular H-H dipolar interaction, whereas hydroxyls show a narrower peak (e.g., Bartholomew and Schreurs, 1980; Eckert et al., 1988; Riemer et al., 2000). The nature of the dissolved hydroxyls is, however, not thoroughly understood. Particularly for aluminosilicate compositions for which there have been extensive studies, controversy remains as to the form of dissolved hydroxyls (McMillan and Holloway, 1987; Kohn et al., 1989b, 1992; Kubicki and Sykes, 1993; Sykes et al., 1997; Schmidt et al., 2000, 2001). This is partly because the interpretations of NMR and Raman spectra are complicated by the presence of aluminum (see reviews in McMillan, 1994; Kohn, 2000). Spectral interpretations are expected to be more straightforward for aluminum-free silicate compositions, which are thus ideal starting point for identifying and quantifying the variety of water species. Despite this advantage, there have been only limited spectroscopic studies, in particular NMR studies, on aluminum-free silicate compositions, and most of the NMR studies have been concentrated on silica and sodium silicate compositions (Farnan et al., 1987; Koller et al., 1990, 1995; Kümmerlen et al., 1992; Schaller and Sebald, 1995; Zotov and Keppler, 1998; Robert et al., 2001).

The structure of glasses and melts in the metal oxide-silica systems at relatively low pressure can be described as a network of interconnected SiO_4 tetrahedra, partially interrupted by the presence of metal oxides (network-modifiers). The connec-

* Author to whom correspondence should be addressed (xianyu@misasa.okayama-u.ac.jp).

tivity of such network structure may be expressed by the distribution of Si Q^n species, i.e., SiO_4 tetrahedra linked with n other SiO_4 tetrahedra (where $n = 0 \sim 4$). ^{29}Si-NMR is useful in distinguishing and quantifying the Q^n speciation. From the perspective of oxygen environments, three types of sites can be distinguished: (1) bridging oxygen (BO), oxygen that bridges two neighboring SiO_4 tetrahedra within the network structure; (2) nonbridging oxygen (NBO), oxygen that is coordinated to only one Si and to one or more metal cations (M), and thus terminates the network structure, and (3) free oxygen, oxygen that is only coordinated to M cations and is thus not part of the network structure. For relatively polymerized systems, the abundance of free oxygens is generally assumed to be negligible, and the parameter NBO/T (NBO per tetrahedrally coordinated cation) is often conveniently used as a measure of the average degree of polymerization of silicate melts.

In principle, the dissolved hydroxyl groups in hydrous glasses and melts in a metal oxide-silica system can be linked either to Si forming silanol (SiOH) groups, or to the metal cations forming MOH groups. Because the latter groups, like free oxygens, are only coordinated to metal cations, but not directly linked to the silicate network, we will denote them as free hydroxyls. This should not be confused with non-hydrogen-bonded SiOH groups that are also sometimes referred to as "free hydroxyls" in the glass literature (e.g., Scholze, 1959a,b; Wu, 1980). ^{29}Si magic angle spinning (MAS) and ^{1}H-^{29}Si cross-polarization (CP) MAS NMR results on silica and sodium silicate glasses and melts (Farnan et al., 1987; Koller et al., 1990, 1995; Kümmerlen et al., 1992; Schaller and Sebald, 1995; Zotov and Keppler, 1998; Robert et al., 2001) have revealed that the glass and melt structures become more depolymerized with water dissolution, suggesting that the formation of SiOH through the rupture of Si-O-Si linkages is a major water dissolution mechanism. The reported ^{1}H MAS NMR spectra for hydrous silica, and sodium-, barium-, and strontium-silicate glasses show peaks in the range between 2.7 and 17 ppm that have been attributed to molecular H_2O and SiOH groups (Kohn et al., 1989a; Kümmerlen et al., 1992; Schaller and Sebald, 1995; Robert et al., 2001).

Whereas SiOH groups are often regarded as the principle hydroxyl species in aluminum-free silicate melts and glasses, the dissolution of water as free hydroxyls was also long suggested, mainly on the basis of conflicting water solubility results (e.g., Kurkjian and Russell, 1957; Uys and King, 1963). Until recently, there had been few direct spectroscopic evidences for the presence of free hydroxyls in silicate melts and glasses, largely because of the scarcity of such studies. Mysen and coauthors indirectly inferred the presence of NaOH and CaOH groups in hydrous sodium and calcium silicate glasses from mass balance considerations using silicate speciation information derived from deconvolution of Raman spectra in the 900 to 1200 cm^{-1} region (Mysen et al., 1980b; Mysen and Virgo, 1986). However, the Raman spectral interpretation is controversial (e.g., McMillan, 1994; Zotov and Keppler, 1998), and the inferred increase in the degree of polymerization with water dissolution for sodium silicate glasses is contradictory to conclusions from subsequent ^{29}Si-NMR results (Kümmerlen et al., 1992; Zotov and Keppler, 1998). ^{29}Si and ^{1}H-^{29}Si CP MAS NMR studies on lithium silicate gels (Dupree et al., 1990; Wies et al., 1990) have revealed that the gels are more polymerized than anhydrous glasses of similar Li_2O/SiO_2 ratio, again indirectly suggesting the presence of LiOH groups in the gel structure from mass balance requirement. However, it is unclear to what extent the structure of these gels may reflect those of the melts or quenched glasses. Our recent preliminary ^{1}H and ^{29}Si-NMR study on hydrous silicate glasses near the diopside ($CaMgSi_2O_6$) composition containing 2 and 3.8 wt% H_2O revealed a major ^{1}H-NMR peak near 1.3 ppm, which had not been observed in hydrous silica or aluminum-free silicate glasses studied previously, and is most likely attributable to the free hydroxyl group, (Ca,Mg)OH, from comparison with experimental data for similar groups in crystalline phases and ab initio calculation results (Xue et al., 2001; Kanzaki and Xue, 2002). This was a significant result that warrants further investigation into a wider range of compositions, because it provided the first direct evidence for the presence of a significant amount of free hydroxyl groups in quenched silicate melts. The identification of different types of OH groups is important, because they may have contrasting effects on the liquidus phase relations, and the network structure and physical properties of silicate melts (cf. Kurkjian and Russell, 1957; Uys and King, 1963; Mysen et al., 1980b; Mysen and Virgo, 1986). More recently, Mysen and Cody (2003) also extended ^{29}Si and ^{1}H MAS NMR and Raman spectroscopic studies to sodium silicate glasses of a broader range of compositions and interpreted their results in terms of the formation of molecular H_2O, SiOH and NaOH groups.

One of the objectives of this study is to systematically investigate the effect of compositions on the water dissolution mechanisms, especially on the formation of free hydroxyls, using ^{1}H and ^{29}Si MAS NMR spectroscopy. The two important compositional parameters are the degree of polymerization and the type of metal cations. We will use the bulk NBO/T values calculated from the anhydrous compositions to approximate the average degree of polymerization. The type of cations is known to have a large influence on the mixing properties (e.g., Q^n speciation distribution) of anhydrous silicate glasses and melts (cf. Hess, 1995; Navrotsky, 1995). The properties of metal cations have been expressed in the literature in terms of several different parameters, such as the electronegativity of various scales, the field potential (Z/r, Z: charge, r: ionic radii), or field strength (Z/R^2, R: M-O bond length), with more or less the same order: Mg > Ca > Li > Na > K. We will use cation field strength as a simple parameter to sort out variations in different structural and NMR parameters with cation type. The samples we investigated in this study include glasses in the CaO-MgO-SiO_2 (CMS) system with a range of Mg/Ca ratio (0 to 1), NBO/T (1.42 to 2.26) and H_2O content (1 to 2 wt%), and $Na_2Si_4O_9$, $Na_2Si_2O_5$, $Na_2CaSi_4O_{10}$ and $Li_2Si_2O_5$ glasses containing 0.5 to 3.8 wt% H_2O. The relatively low water contents are advantageous in that they allow better quantification of the different types of OH species from ^{1}H MAS NMR spectra. The CMS system represents an ideal system for systematically examining changes in the abundance of free hydroxyls with both cation type (Ca vs. Mg) and NBO/T. This system is also relevant geologically, because Mg and Ca are among the most abundant network-modifying cations in natural magmas. The compositions we chose are more depolymerized than most previously studied systems. Melting experiments on mantle materials have suggested that melts become progressively more

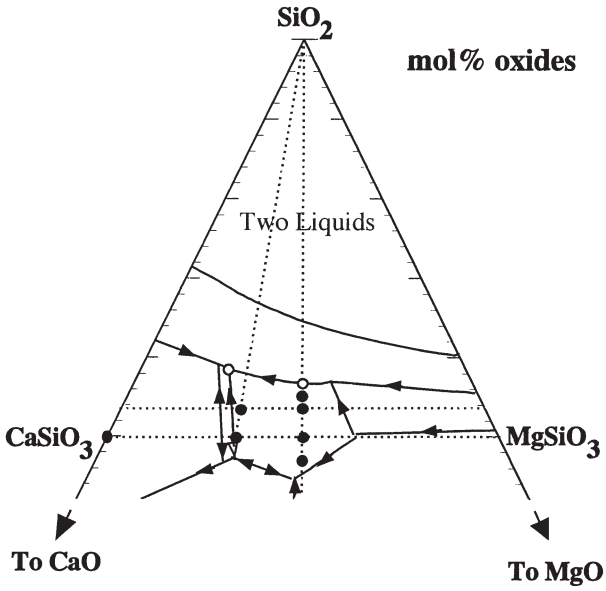

Fig. 1. A portion of the CaO-MgO-SiO_2 triangle diagram showing the compositions of hydrous glasses investigated in this study. Solid circles stand for homogeneous glasses, and open circles for phase-separated, milky white glasses. Also shown for reference are the phase boundaries for the anhydrous system at ambient pressure (Levin et al., 1964). We observed phase separation well beyond the two-liquid region of the latter. Dotted lines are guides to the eyes.

depolymerized with increasing depth of generation, from andesitic (NBO/T <0.5) at 1 GPa (e.g., Kushiro, 1972), to komatiitic or kimberlitic (NBO/T >2) above 5 GPa (e.g., Kawamoto and Holloway, 1997). Thus, these compositions are in particular relevant to mantle-derived magmas from depths. The additional more polymerized alkali silicate compositions provide complementary information concerning the compositional effects. This wide range of compositions is also useful in unraveling the compositional dependence of hydrogen bonding strength for water species, suggested previously from IR and ^{1}H-NMR studies (e.g., Scholze, 1959a,b; Kohn et al., 1989a). A second objective of this study is to provide a theoretical basis for the interpretations of experimental results. We have carried out ab initio molecular orbital (MO) calculations on clusters simulating possible SiOH and free hydroxyl groups in hydrous silicate glasses and melts. We have paid particular attention to the hydrogen bond forming tendencies and ^{1}H-NMR characteristics of these hydroxyl groups.

2. EXPERIMENTAL PROCEDURES AND CALCULATION METHODS

2.1. Sample Syntheses

We have synthesized hydrous glasses of a range of compositions (Mg/Ca = 0 to 1, NBO/T = 1.42 to 2.26) in the CMS system (all except one within the $CaSiO_3$ (Wo)-$CaMgSi_2O_6$(Di)-SiO_2 (Qz) subsystem) (Fig. 1 and Table 1). We will refer to the anhydrous compositions, except for end-member compositions, as CxMySz, where x, y and z stand for mol% of oxide components (C = CaO, M = MgO and S = SiO_2). We have produced these hydrous glasses in sealed platinum capsules at 2 kbar and 1425 to 1500°C using an internally heated gas pressure vessel (IHPV) apparatus. After a desired heating duration, we quenched the melts into glasses by breaking the hanging Mo wire with a current to allow the sample capsules to drop to the cold bottom of the pressure vessel ($\leq$ 300°C) under pressure. Three types of starting materials were used: One is anhydrous glass of the desired silicate composition plus deionized H_2O. The anhydrous glasses were, in turn, synthesized from mixtures of MgO, $CaCO_3$ and SiO_2 by decarbonization and subsequent melting at ambient pressure and 1450 to 1600°C. For some compositions, we have synthesized both glasses without any paramagnetic impurities and those with 0.2 wt% Gd_2O_3; the latter was added to improve the efficiency of ^{29}Si-NMR experiments. The second type of starting materials is a synthetic crystalline sample ($CaMgSi_2O_6$ diopside or $CaSiO_3$ wollastonite) plus deionized H_2O without doping with any paramagnetic impurities. The third is a mixture of MgO, SiO_2, $CaSiO_3$ (wollastonite) and $Mg(OH)_2$ (brucite) of appropriate proportions, again without any paramagnetic impurities. The NMR spectra for the resultant glasses employing different types of starting materials are similar for a given bulk composition (including paramagnetic impurity) and P-T condition. We have checked for the presence of quench crystals in the glass starting materials and in samples recovered from high-pressure experiments by optical microscopy and ^{1}H and ^{29}Si MAS NMR. It turned out to be rather tricky to produce quench crystal-free hydrous glasses for such depolymerized melts. At least three factors affect the glass-forming ability of the quenched melts. Firstly, the addition of only 0.2 wt% Gd_2O_3 enhances quench crystal formation, so that it was difficult to produce quench crystal-free glasses for certain compositions (e.g., Di) when 0.2 wt% Gd_2O_3 was doped (Table 1). Secondly, the water content also affects the glass-forming ability: all the synthesized hydrous CMS glasses contain $\sim$1 to 2 wt% H_2O, and quench crystals were formed in some experiments with more than 2 wt% H_2O. Thirdly, the size of the samples affects the quench rate, and thus we have chosen to use relatively small 3 mm-outer diameter capsules (60 to 70 mg samples) for most of the CMS glass syntheses (Table 1).

It is known that two-liquid phase separation occurs near the silica-rich region of the anhydrous CMS system at ambient pressure (Levin et al., 1964). We also observed phase separation for silica-rich compositions: milky white glasses with 2 wt% H_2O that are homogeneous under optical microscope were formed near the compositions for the Wo-Di-Qz eutectic (C30.3M11.2S58.5) and Di-Qz eutectic (C21.7M21.7S56.6) in the phase diagram for anhydrous CMS system at ambient pressure (see Fig. 1). These compositions are however, well outside the reported two-liquid region of the latter (Levin et al., 1964). The enlarged region of phase separation for hydrous glasses produced at 2 kbar could be due to different phase relations and/or lower glass transition temperature.

We have checked the compositions for all the starting glasses (dio, dis, disgd, diss, diwogd, diwos, and digd), and some of the hydrous glasses that were synthesized from oxide mixtures (diwo2w, diwoseu2w, and diseu2w) in the CMS system (see Table 1 for sample notation), using a JEOL JXA-8800 electron microprobe analyzer (EPMA). We have performed measurements on more than ten spots for each sample at an accelerating voltage of 15 kV, a beam current of 1.0 nA, and a beam diameter of 20 μm. The deviations between the analyzed compositions, taken as the average of all the measurements (not shown), and the respective nominal compositions are $\pm$ 0.0$\sim$0.8 wt% (oxide components), within uncertainties of the EPMA measurements (standard deviation of 0.2$\sim$0.9 wt%). We detected no spatial compositional variations for all the analyzed samples, including the two phase-separated samples (diwoseu2w and diseu2w) with beam diameters of 1 to 20 μm, consistent with microscopic observations.

We have also prepared several hydrous alkali silicate glass samples, including $Na_2Si_4O_9$ glasses containing 1.0 and 3.7 wt% H_2O, $Na_2Si_2O_5$ glasses containing 1.9 and 3.8 wt% H_2O, a $Na_2CaSi_4O_{10}$ glass containing 2.0 wt% H_2O and a $Li_2Si_2O_5$ glass containing 0.5 wt% H_2O, all doped with 0.2 wt% Gd_2O_3. We synthesized these samples from $\sim$200 mg of starting materials of anhydrous glasses (doped with 0.2 wt% Gd_2O_3) plus deionized water at 2 kbar and 1100 to 1300°C in sealed 4 mm-diameter Pt capsules using the IHPV apparatus. They were all clear and free from quench crystals, as confirmed by optical examinations and ^{1}H and ^{29}Si-NMR measurements. The anhydrous compositions of these glasses are all more polymerized (NBO/T = 0.5 to 1) than those in the CMS system described above. An attempt to synthesize less polymerized hydrous glasses along the Na_2SiO_3-$CaSiO_3$ join (with or without Gd_2O_3) resulted in quench crystals.

The quoted water contents (Table 1) for the hydrous glasses are those

Table 1. Synthesis conditions for samples measured with NMR.

Sample	Composition[a]	NBO/T[a]	H_2O content wt% (mol%)[a]	Paramagnetic impurites added	Starting materials[b]	Capsule size (mm)	Synthesis conditions	Sample description
				CaO-MgO-SiO_2 system				
dio1w	C26.5M26.5S47	2.26	1.0 (2.9)	None	G(dio) + W	3	2 kbar, 1500°C, 2 h	Clear glass
di1w	$CaMgSi_2O_6$	2.0	1.1 (3.2)	None	Di + W	3	2 kbar, 1450°C, 4.5 h	Clear glass
di1.5w	$CaMgSi_2O_6$	2.0	1.5 (4.4)	None	Di + W	3	2 kbar, 1450°C, 4 h	Clear glass
di2w	$CaMgSi_2O_6$	2.0	2.0 (5.8)	None	MIX	3	2 kbar, 1450°C, 4 h	Glass + quench crystal (minor)
di2wgd	$CaMgSi_2O_6$	2.0	1.9 (5.5)	0.2 wt% Gd_2O_3	G(digd) + W	4	2 kbar, 1425°C, 2 h	Quench crystal + Glass (minor)
dis1w	C23.3M23.3S53.3	1.75	0.9 (2.7)	None	G(dis) + W	3	2 kbar, 1500°C, 2 h	Clear glass
dis2w	C23.3M23.3S53.3	1.75	1.9 (5.5)	None	MIX	3	2 kbar, 1450°C, 4 h	Clear glass
dis2wgd[c]	C23.3M23.3S53.3	1.75	1.8 (5.2)	0.2 wt% Gd_2O_3	G(disgd) + W	3	2 kbar, 1450°C, 4 h	Clear glass
diss1w	C22.5M22.5S55	1.64	0.8 (2.4)	None	G(diss) + W	3	2 kbar, 1500°C, 2 h	Clear glass
diwo2w	C33.6M16.5S49.9	2.0	2.0 (5.9)	None	MIX	3	2 kbar, 1450°C, 4 h	Clear glass
diwo2wgd[c]	C33.6M16.5S49.9	2.0	1.8 (5.3)	0.2 wt% Gd_2O_3	G(diwogd) + W	3	2 kbar, 1450°C, 4 h	Clear glass
diwos2w	C31.3M15.4S53.3	1.75	1.8 (5.3)	None	G(diwos) + W	3	2 kbar, 1500°C, 2 h	Clear glass
wo1w	$CaSiO_3$	2.0	1.0 (3.1)	None	Wo + W	3	2 kbar, 1500°C, 4 h	Clear glass
wo2w	$CaSiO_3$	2.0	2.0 (6.2)	None	Wo + W	3	2 kbar, 1500°C, 4 h	Clear glass
diwoseu2w	C30.3M11.2S58.5	1.42	2.0 (6.0)	None	MIX	3	2 kbar, 1425°C, 2 h	Milky white Glass
diseu2w	C21.7M21.7S56.6	1.53	2.0 (5.9)	None	MIX	3	2 kbar, 1425°C, 2 h	Milky white Glass
				Other compositions				
lds0.5wgd	$Li_2Si_2O_5$	1.0	0.5 (1.4)	0.2 wt% Gd_2O_3	G(ldsgd) + W	4	2 kbar, 1250°C, 2 h	Clear glass
nds1wgd	$Na_2Si_2O_5$	1.0	1.9 (6.2)	0.2 wt% Gd_2O_3	G(ndsgd) + W	4	2 kbar, 1300°C, 3 h	Clear glass
nds3.8wgd	$Na_2Si_2O_5$	1.0	3.8 (12)	0.2 wt% Gd_2O_3	G(ndsgd) + W	4	2 kbar, 1300°C, 3 h	Clear glass
nts1wgd	$Na_2Si_4O_9$	0.5	1.0 (3.3)	0.2 wt% Gd_2O_3	G(ntsgd) + W	4	2 kbar, 1100°C, 20 h	Clear glass
nts3.7wgd	$Na_2Si_4O_9$	0.5	3.7 (11)	0.2 wt% Gd_2O_3	G(ntsgd) + W	4	2 kbar, 1100°C, 20 h	Clear glass
n2cs42wgd	$Na_2CaSi_4O_{10}$	1.0	2.0 (6.3)	0.2 wt% Gd_2O_3	G(n2cs4gd) + W	4	2 kbar, 1250°C, 2 h	Clear glass

[a] Nominal compositions; C = CaO; M = MgO; S = SiO_2, NBO/T calculated from anhydrous compositions ignoring free oxygens; H_2O mol% denotes mol% among oxide components.

[b] Wo and Di: crystalline $CaSiO_3$ wollastonite and $CaMgSi_2O_6$ diopside, respectively; G: anhydrous glass with sample label in bracket; W: deionized water; MIX: mixture of MgO, $Mg(OH)_2$ (brucite), $CaSiO_3$ (wollastonite) and SiO_2.

[c] Two (diwo2wgd) or three (dis2wgd) samples combined for NMR measurements.

added to the sample capsules. We have carefully monitored the weights of the sample capsules before and after the high-pressure experiments. In addition, we have checked for the presence of free liquid phase by monitoring the sample weights before and after the recovered capsules were pierced and heated in an oven at 110°C overnight. In general, samples that were glassy under optical microscope did not show weight loss with this procedure, whereas those contained quench crystals showed some weight loss. This is expected because all the water contents are well below the solubility limits at the P-T conditions of the present experiments (Rosenhauer and Eggler, 1975; Eggler and Rosenhauer, 1978). The intensities of ^{1}H MAS NMR spectra for glass samples that do not contain paramagnetic impurities also confirmed that the added water was quantitatively retained in the structure. Complications arise for samples doped with 0.2 wt% Gd_2O_3, as will be described in the next section.

2.2. NMR Spectroscopy

We have obtained ^{29}Si and ^{1}H MAS NMR spectra at a resonance frequency of 79.5 and 400.4 MHz, respectively, using a Varian Unity-Inova 400 MHz spectrometer and a Jakobsen-type 5 mm CP-MAS probe. We used tetramethylsilane (TMS) as an external reference standard of chemical shifts for both nuclei. To avoid complications due to contamination, we have handled all the samples with clean gloves and tweezers during both sample preparations and NMR measurements, and have carefully cleaned the Si_3N_4 sample rotors and Kel-F and Torlon rotor caps with ethyl alcohol.

We have acquired the ^{1}H MAS NMR spectra with either a single-pulse sequence, or the DEPTH sequence that consists of three back-to-back pulses ($\pi/2$-π-π) with a phase cycle of 16 (Cory and Ritchey, 1988). The probe contributes a broad ^{1}H background signal that has a much longer $\pi/2$ pulse time (about five times) and smaller ^{1}H spin-lattice relaxation time (T_1) than the samples. This probe background is largely suppressed with the DEPTH sequence. All the reported spectra are those after subtraction of the background signal; the latter was carefully measured on the same rotor/cap under identical conditions immediately before each measurement with the sample in. The ^{1}H MAS NMR spectra after background subtraction are similar with either the single-pulse sequence or the DEPTH sequence, although the latter gives better baseline because only minor intensity from the background signal needs to be subtracted. For the single-pulse experiments, we used a 4-μs ($\pi/2$) or 1-μs pulse, a 1 MHz spectral width with a 5-MHz analog-to-digital converter (ADC) or a 500 kHz spectral width with a 500-kHz ADC. For the DEPTH experiments, we adopted a spectral width of 1 MHz. The dead time was ~3 μs for the 5-MHz ADC and 6 μs for the 500-kHz ADC; signals in the free induction decay (FID) during this period were reconstructed using the linear prediction algorithm in the Varian VNMR software. We have acquired spectra using a range of recycle delay times between 5 s and greater than $5T_1$ for most samples to check for differential relaxations of different peaks, and have also varied the sample spinning speeds between 10 and 13 kHz. All the reported ^{1}H MAS NMR spectra have been acquired with a sample spinning speed of 10 kHz and a recycle delay greater than $5T_1$, unless otherwise explicitly stated.

We have also obtained rotor-synchronized ^{1}H Hahn-echo MAS NMR spectra using the Hahn-echo ($\pi/2$-τ-π-τ-acquisation) pulse sequence for all the glass samples. This pulse sequence is known to refocus dephased signals due to external magnetic field inhomogeneity and heteronuclear dipolar interactions, and is also effective in suppressing probe background from outside the sample coil (e.g., Zeng et al., 1999a). We have also found that background signal from the probe is insignificant with this pulse sequence. The Hahn-echo pulse sequence

Table 2. ^{1}H NMR results for samples in the CaO-MgO-SiO_2 system described in Table 1.

Sample	Composition[a]	H_2O content (wt%)	δ_i^H (ppm)[b]	FWHM (ppm)[c]	Abundance (%)[c]	^{1}H T_1 (s)	Comment
dio1w	C26.5M26.5S47	1.0	4.6				Glass
			1.3 (1.34)	2.0	29.2	37 ± 2	Glass
di1w	$CaMgSi_2O_6$	1.1	4.9			63 ± 3	Glass
			1.2 (1.28)	1.8	25.4	66 ± 2	Glass
di1.5w	$CaMgSi_2O_6$	1.5	4.9			29 ± 0.5	Glass
			1.3 (1.25)	1.9	24.9	29 ± 0.4	Glass
di2w	$CaMgSi_2O_6$	2.0	4.8			13 ± 0.5	Glass
			1.3			15 ± 0.3	Glass
			4.8	0.35	Minor	Shorter than above	Fluid inclusion
di2wgd	$CaMgSi_2O_6$ (Gd)	1.9	4.8	0.35		0.13 ± 0.004	Fluid inclusion
dis1w	C23.3M23.3S53.3	0.9	4.7			21 ± 1	Glass
			1.3 (1.21)	1.8	21.1	24 ± 1	Glass
dis2w	C23.3M23.3S53.3	1.9	4.7			15 ± 0.5	Glass
			1.2 (1.19)	1.8	20.4	15 ± 0.4	Glass
dis2wgd	C23.3M23.3S53.3(Gd)	1.8	4.8			2.8 ± 0.1	Glass
			1.3			2.8 ± 0.1	Glass
diss1w	C22.5M22.5S55	0.8	4.6			30 ± 2	Glass
			1.3 (1.20)	1.7	20.2	35 ± 1	Glass
diwo2w	C33.6M16.5S49.9	2.0	5.2			14 ± 0.2	Glass
			1.3 (1.25)	1.9	20.2	14 ± 0.2	Glass
diwo2wgd	C33.6M16.5S49.9(Gd)	1.8	5.2			3.7 ± 0.06	Glass
			1.4			3.7 ± 0.05	Glass
diwos2w	C31.3M15.4S53.3	1.8	4.9			8.8 ± 0.1	Glass
			1.3 (1.22)	1.8	17.1	9.2 ± 0.1	Glass
wo1w	$CaSiO_3$	1.0	5.7			57 ± 2	Glass
			1.7 (1.47)	2.0	14.1	60 ± 1	Glass
wo2w	$CaSiO_3$	2.0	5.6			18 ± 0.3	Glass
			1.5 (1.44)	1.9	13.2	18 ± 0.2	Glass
diwoseu2w	C30.3M11.2S58.5	2.0	4.5			14 ± 0.3	Main phase
			1.3 (1.20)	1.7	13.0	14 ± 0.2	Main phase
			(3.0)	1.5		Longer than above	Silicalike phase
diseu2w	C21.7M21.7S56.6	2.0	4.5			16 ± 0.3	Main phase
			1.1 (1.13)	1.7	20.2	15 ± 0.3	Main phase
			(3.0)	1.5		Longer than above	Silicalike phase

[a] Same notation as for Table 1; Gd in brackets stands for sample doped with 0.2 wt% Gd_2O_3;
[b] Numbers without brackets are positions of peak maxima; those in brackets are chemical shifts from deconvolution.
[c] Estimation from deconvolution of the central band of the ^{1}H MAS NMR spectra. The abundances for the phase-separated glasses are for the main, silica-poor phase (excluding the peak near 3.0 ppm).

has previously been applied in ^{1}H dipolar dephasing experiments to distinguish protons with contrasting strength of dipolar interactions in silica gels and hydrous silicate glasses (e.g., Bronnimann et al., 1988; Zeng et al., 1999a; Robert et al., 2001). This is based on the fact that incompletely averaged homogeneous H-H dipolar interaction, due to finite sample spinning speed compared to the strength of the latter interaction, results in incomplete refocusing of the signal during a Hahn-echo experiment, so that protons with stronger homonuclear dipolar interaction are preferentially suppressed. We have acquired most of the rotor-synchronized ^{1}H Hahn-echo MAS NMR spectra with a sample spinning speed of 10 kHz, a recycle delay time of greater than $3T_1$, and evolution time period, τ, values of 0.1 to 80 ms. We have used Kel-F caps for all the Hahn-echo experiments because they produce negligible ^{1}H background signal.

We have measured the ^{1}H spin-lattice relaxation time, T_1 for most of the hydrous glass samples with either the saturation-recovery or inversion-recovery method. The hydrous silicate glasses doped with 0.2 wt% Gd_2O_3 yield ^{1}H T_1 values of ~3 to 8 s, and those not doped with any paramagnetic impurities are longer (9 to 66 s). There is a general trend of decreasing ^{1}H T_1 with increasing H_2O contents within each group of glasses with and without Gd_2O_3 (Table 2).

We have performed ^{29}Si MAS NMR measurements on all the glass samples doped with 0.2 wt% Gd_2O_3 and on some of the samples not doped with paramagnetic impurities. The ^{29}Si T_1 of the anhydrous and hydrous glasses doped with 0.2 wt% Gd_2O_3 glasses are ~24 to 60 s; those of glasses without paramagnetic impurities are much longer. We have acquired the ^{29}Si MAS NMR spectra with either the single pulse sequence or the DEPTH pulse sequence. For the single-pulse MAS NMR experiments, a small, broad signal centered near −110 ppm from the probe background was detected, and was subtracted from the reported sample spectra. This probe background is suppressed to a negligible level with the DEPTH pulse sequence. The ^{29}Si MAS NMR spectra with either pulse sequences are identical in peak shape after probe background subtraction. We have acquired single-pulse MAS NMR spectra only for samples doped with 0.2 wt% Gd_2O_3, using a pulse of 2.2 μs (π/4), a recycle delay of 20 s, and sample spinning speeds of 6 to 8 kHz. Longer recycle delays (up to 1000 s) were also tested and were found to yield identical peak shapes. We have acquired the ^{29}Si MAS NMR spectra with the DEPTH pulse sequence at a sample spinning speed of 8 kHz, and recycle delays of ~40 to 60 s for samples doped with 0.2 wt% Gd_2O_3, and 1000 to 1600 s for those without paramagnetic impurities.

We have also collected ^{1}H-^{29}Si CP-MAS NMR spectra for samples doped with 0.2 wt% Gd_2O_3. This technique is often invoked to obtain information about the spatial relations between Si and H and to enhance the signal/noise ratio of samples containing protons (e.g., Kümmerlen et al., 1992; Uchino et al., 1992a; Phillips et al., 1997; Oglesby and Stebbins, 2000). The experiment detects the magnetization generated by polarization transfer from ^{1}H to ^{29}Si during a period of 'contact time' when the radiofrequency fields for both ^{1}H and ^{29}Si with amplitudes satisfying the Hartmann-Hahn matching condition are applied. The observed signal intensity with contact time (t) can by described by two exponential functions representing the cross-polarization between the ^{1}H and ^{29}Si spin systems (with a time constant T_{SiH}) and the

relaxation of the ^{1}H magnetization in the rotating frame of the applied radiofrequency field (with a time constant $T_{1\rho}(H)$):

$$I = I_0[\exp(-t/T_{1\rho}(H)) - \exp(-t/T_{SiH})]/[1 - T_{SiH}/T_{1\rho}(H)]$$

It has been suggested that the T_{SiH} values for minerals correlate with the Si-H distances (e.g., Phillips et al., 1997; Oglesby and Stebbins, 2000), and the $T_{1\rho}(H)$ values are related to the H-H distances (e.g., Oglesby and Stebbins, 2000). We have collected the ^{1}H-^{29}Si CP-MAS NMR spectra with a recycle delay of 5 s, a sample spinning speed of 4 kHz and contact times of 0.05 to 16 ms. The Hartmann-Hahn matching condition was adjusted using a natural pyrophyllite sample. The T_{SiH} and $T_{1\rho}(H)$ values were obtained from analyses of the intensities using the Varian VNMR software.

The effect of 0.2 wt% Gd_2O_3, added to some of the samples, on the ^{1}H and ^{29}Si-NMR spectra warrants commenting. It is a general practice to add a small amount (0.1 to 0.2 wt%) of paramagnetic impurities, such as Gd_2O_3, Fe_2O_3 or Mn_2O_3, to silicate glasses to reduce the otherwise extremely long ^{29}Si T_1 values (e.g., 7000 to 11,000 s for SiO_2 glasses not doped with any paramagnetic impurities: Gladden et al. (1986)). Gd_2O_3 is particularly useful for samples synthesized using Pt capsules at high pressure, because of its lower tendency of being reduced and absorbed by the metal capsules, compared with other oxides such as Fe_2O_3. The effect of such a small amount of paramagnetic impurities on the ^{29}Si-NMR spectra is generally considered to be negligible. However, we found that the addition of 0.2 wt% Gd_2O_3 causes a significant broadening and some loss of intensity for the ^{1}H MAS NMR spectra, although the overall features are retained (see section 3.1.2). Thus, for glasses doped with 0.2 wt% Gd_2O_3, the ^{29}Si-NMR spectra are most likely quantitatively reliable, but the ^{1}H MAS NMR spectra should be treated only in a qualitative manner.

2.3. Ab Initio Molecular Orbital Calculations

We have performed all the ab initio MO calculations on small clusters containing the OH groups of interest using the Gaussian 98 program (Frisch et al., 1998). The MacMolPlot graphic software (Bode and Gordon, 1998) was utilized to prepare the drawing for the clusters. Because a major purpose of these calculations is to evaluate the hydrogen bond forming tendency of OH groups in silicates, it is important that the calculations yield reliable geometry parameters, in particular, reliable hydrogen bonding distances. The results reported here are all for clusters with geometries optimized at B3LYP/6-31+G(d,p), where B3LYP stands for the Becke's three parameter hybrid functional using the correlation functional of Lee, Yang and Parr (Frisch et al., 1998), a typical density-functional theory (DFT) method. We have also performed some additional calculations on clusters optimized with a larger basis set (B3LYP/6-311+G(2df,p)), as for our previous paper (Xue and Kanzaki, 2001), and found only small differences in the geometries and calculated ^{1}H chemical shifts (not shown). Optimizations at B3LYP/6-31+G(d,p) or B3LYP/6-311+G(2df,p) both yield reliable O-H and O-H . . . O distances, superior to the Hartree-Fork (HF) method. For example, the O-H and O-H . . . O distances in H_2O and H_2O-H_2O dimer are reproduced within 0.008 Å and 0.06 Å of the respective experimental value at B3LYP/6-31+G(d,p) (also see Xue and Kanzaki, 2001).

The ^{1}H isotropic chemical shift (δ_i^H) (in ppm) was calculated as the difference in isotropic magnetic shielding (σ_i^H) (in ppm) between the reference TMS cluster ($Si(CH_3)_4$ with T_d symmetry) and the cluster of interest. We have used the gauge-independent atomic orbital (GIAO) method (Cheeseman et al., 1996) at HF/6-311+G(2df,p) for the calculation of NMR shielding tensors. As will be described in section 3.3, the calculated ^{1}H chemical shifts agree well with experimental data.

3. RESULTS

3.1. ^{1}H MAS NMR Results

3.1.1. ^{1}H-NMR results for the CMS system

In Figure 2 to 4 are shown the ^{1}H MAS NMR spectra for the clear, quench crystal-free hydrous CMS glasses containing ~1 to 2 wt% H_2O, and with Ca/(Ca + Mg) ratios of 0.5 to 1 and

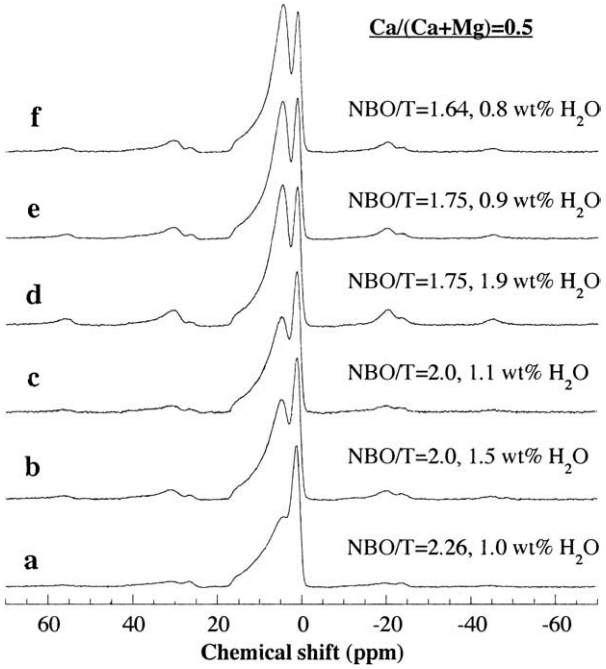

Fig. 2. ^{1}H MAS NMR spectra of hydrous silicate glasses along the $CaMgSiO_4$-SiO_2 join, all not doped with any paramagnetic impurities. (a) C26.5M26.5S47 glass containing 1.0 wt% H_2O (dio1w), (b) $CaMgSi_2O_6$ glass containing 1.5 wt% H_2O (di1.5w), (c) $CaMgSi_2O_6$ glass containing 1.1 wt% H_2O (di1w), (d) C23.3M23.3S53.3 glass containing 1.9 wt% H_2O (dis2w), (e) C23.3M23.3S53.3 glass containing 0.9 wt% H_2O (dis1w), and (f) C22.5M22.5S55 glass containing 0.8 wt% H_2O (diss1w). All the spectra were acquired using the DEPTH pulse sequence, with a spectral width of 1 MHz, a spinning rate of 10 kHz and recycle delay times of 100 to 400 s (all $>5T_1$).

NBO/T values of 1.64 to 2.26. Only the results for samples not doped with any paramagnetic impurities will be described in this section. All these ^{1}H MAS NMR spectra contain two

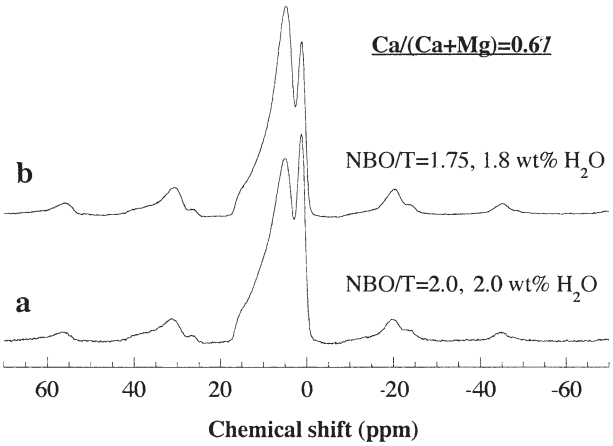

Fig. 3. ^{1}H MAS NMR spectra of hydrous silicate glasses along the C33.6M16.5S49.9-SiO_2 join, both not doped with any paramagnetic impurities. (a) C33.6M16.5S49.9 glass containing 2 wt% H_2O (diwo2w); (b) C31.3M15.4S53.3 glass containing 1.8 wt% H_2O (diwos2w). Both spectra were acquired using the DEPTH pulse sequence, with a spectral width of 1 MHz, a spinning rate of 10 kHz and recycle delay times of 80 to 100 s ($>5T_1$).

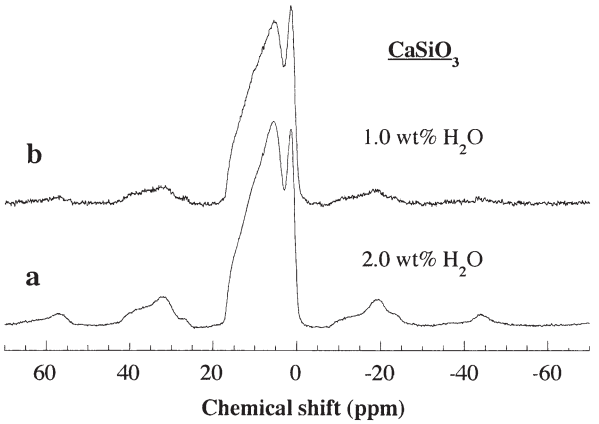

Fig. 4. ^{1}H MAS NMR spectra of hydrous $CaSiO_3$ glasses containing 1 and 2 wt% H_2O and not doped with any paramagnetic impurities. (a) 2.0 wt% H_2O (wo2w); (b) 1.0 wt% H_2O (wo1w). These spectra were acquired using the DEPTH pulse sequence, with a spectral width of 1 MHz, a spinning rate of 10 kHz and recycle delay times of 120 to 360 s (>5T_1).

partially resolved peaks: an asymmetric peak with a maximum near 4.6 to 5.7 ppm, and a second narrower and nearly symmetric peak centered at ~1.2 to 1.7 ppm. Peaks near 1.2 to 1.7 ppm have not been observed for hydrous silica and aluminum-free silicate glasses of other compositions, including $Na_2Si_4O_9$, $Na_2Si_2O_5$, $BaSi_2O_5$ and $SrSi_2O_5$ glasses (Kohn et al., 1989a; Kümmerlen et al., 1992; Schaller and Sebald, 1995; Robert et al., 2001), although some of the latter spectra are of unsatisfactory quality due to overlapping spinning sidebands and probe background signals. As mentioned in the Introduction, from comparison with experimental data for crystalline phases and ab initio calculation results, the most likely assignment for this peak is the (Ca,Mg)OH, free hydroxyl groups. Because the assignment of this peak is of utter importance for unraveling this hitherto unconfirmed water species, we will leave full discussions of its assignment to section 4.1, after the ab initio calculation results are presented. The lack of extensive spinning sidebands for this peak suggests that these OH species are relatively isolated from one another and from other water species.

The higher-frequency peak with maxima near 4 to 6 ppm in these ^{1}H MAS NMR spectra all show a similar range of frequencies, with a well-defined shoulder extending to ~17 ppm. Peaks in this region have also been observed for hydrous silica and silicate glasses of other compositions (see next section). The relative intensities of the region near 4 to 6 ppm show a small increase with increasing water content; this increase is more pronounced in the spinning sidebands than in the central band. As a matter of fact, this region gives more pronounced spinning sidebands, which also extend to a further frequency range, than the lower- or higher-frequency regions. These features are consistent with partial contribution of molecular H_2O to the 4 to 6 ppm region, because molecular H_2O is known to give more intense spinning sidebands than OH groups due to the strong intramolecular H-H dipolar interaction, and its relative abundance is expected to increase with total water content. Not all of the intensities in the 4 to 6 ppm region, however, could be attributed to molecular H_2O, because changes in the relative intensities with water content are much smaller in the central band than in the spinning sidebands, indicating contributions from additional component(s) with smaller strength of H-H dipolar interaction, most likely SiOH groups. The intensities in the remaining parts of the high-frequency peak are also most likely from SiOH groups with weak homonuclear H-H dipolar interaction. The shape of the high-frequency peak show systematic changes with composition: at a given NBO/T, the main change with increasing Ca/(Ca + Mg) ratio is enhancement of the higher-frequency shoulder (between 8 to 17 ppm); and at a given Ca/(Ca + Mg) ratio, the main change with increasing silica content is the growth of a relatively symmetric component near 4 to 6 ppm (Figs. 2 to 4). As suggested for silicate glasses of other compositions (Kohn et al., 1989a; Kümmerlen et al., 1992; Schaller and Sebald, 1995; Robert et al., 2001) and further discussed in section 3.3., the shape of the high-frequency peak reflects the distribution of hydrogen bonding strength. Our results are consistent with increasing relative population of strongly hydrogen-bonded SiOH groups (large chemical shifts between 8 to17 ppm) with increasing Ca/(Ca + Mg) ratio, and increasing relative population of relatively weakly hydrogen-bonded SiOH (and perhaps also molecular H_2O) (near 4 to 6 ppm) with increasing silica content.

To estimate the abundance of free hydroxyl groups (1.2 to 1.7 ppm peak), we have performed deconvolution for the ^{1}H MAS NMR spectra shown in Figure 2 to 4. Because the peak near 1.2 to 1.7 ppm is reasonably well resolved from the broader, higher-frequency peak, unconstrained deconvolution with a single Gaussian peak for the 1.2 to 1.7 ppm peak, and four to five Gaussians for the higher-frequency peak gives consistent results for the relative area of the former (within ~2%) for most samples. Considering the systematic changes in the shape of the higher-frequency peak with composition, we have used for the final reported results one Gaussian for the 1.2 to 1.7 ppm peak with unconstrained chemical shift and width, and five Gaussians for the higher-frequency peak: two Gaussians with fixed chemical shifts (15.5 and 13.6 ppm) and widths that reproduce well the highest-frequency shoulder of all spectra, two Gaussians with chemical shifts near 4 to 6 ppm and unconstrained widths to account for the intensity change in this region with silica content, and a fifth Gaussian with a chemical shift near 8 to 10 ppm and an unconstrained width to account for the intensity change in this region with Ca/(Ca + Mg) ratio (see Fig. 5 for an example). Deconvolution with this procedure yielded relatively constant chemical shifts of the lowest-frequency peak for all the calcium-magnesium silicate glasses (1.2 to 1.3 ppm), and slightly larger values (1.4 to 1.5 ppm) for the calcium silicate glasses (Table 2). The resultant full-widths-at-half-maximum-height (FWHM) of this peak are ~1.7 to 2.0 ppm, with a slight increase with increasing NBO/T (Table 2). The reported abundances for the peak near 1.2 to 1.5 ppm (Table 2) are those from deconvolution of the central band. When the spinning side bands are also considered, the relative abundances are lowered by ~1 to 2%, depending on the water content. Because molecular H_2O are in general under-represented in the central band, due to more extensive spread of intensities in the spinning sidebands, and because their abundances are expected to be low at total water contents of 1 to 2 wt%, the deconvolution results for the central band may be

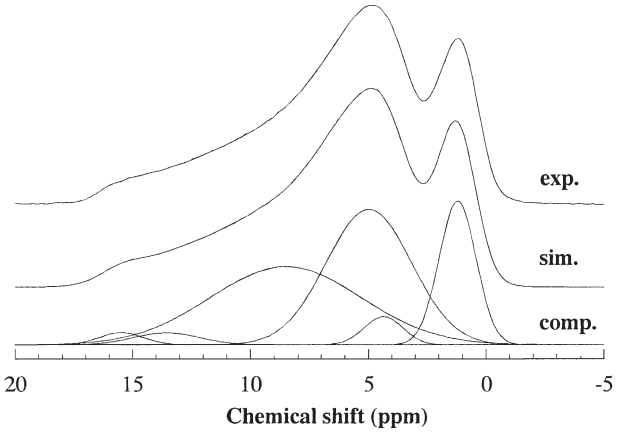

Fig. 5. An example of deconvolution for the ^{1}H MAS NMR spectra of the C31.3M15.4S53.3 glass containing 1.8 wt% H_2O and not doped with any paramagnetic impurities (diwos2w) shown in Figure 3b.

considered to approximate (the lower limit of) the proportion of free OH groups among total OH groups. In Figure 6, the estimated abundances of free OH groups are plotted as a function of NBO/T and Ca/(Ca + Mg) ratio. There is a general trend of increasing abundance with increasing NBO/T and decreasing Ca/(Ca + Mg) ratio, as is also clear from visual inspection of the spectra shown in Figure 2 to 4. Changes in the abundances of Gaussian peaks within the higher-frequency region are also in accordance with those expected from visual inspection. These results will not be presented because the choice of components is not unique, and the peak shape may reflect a continuous distribution of hydrogen bonding distances.

We have also acquired rotor-synchronized ^{1}H MAS Hahn-echo spectra for all these glasses with a spinning speed of 10 kHz and τ values between 0.1 to 80 ms. Changes in the spectra with increasing τ values are similar for all these compositions. An example is shown in Figure 7a for the C31.3M15.4S53.3 glass containing 1.8 wt% H_2O (diwos2w). The overall intensity decreases with increasing τ, but changes in the peak shape are relatively small. There is a small decrease in the relative intensity in the 4 to 6 ppm region; the decrease is more pronounced in the spinning sidebands than in the central band. Changes in relative intensities are somewhat less prominent for glasses with lower water contents. These observations are in agreement with partial contribution of molecular H_2O to the 4 to 6 ppm region, because peaks due to molecular H_2O tend to be preferentially attenuated than those due to relatively isolated OH groups during the evolution time period of Hahn-echo experiments, as a result of the stronger intramolecular H-H dipolar coupling (Bronnimann et al., 1988; Zeng et al., 1999a; Robert et al., 2001).

It is important to ascertain that the peaks described above are not due to quench crystals. We have purposely acquired ^{1}H MAS NMR spectra for some samples that contain quench crystals to exemplify the ^{1}H MAS NMR features associated with quench crystal formation. Examples are given in Figure 8a and c for two samples of a $CaMgSi_2O_6$ composition with ~2 wt% added H_2O: one doped with 0.2 wt% Gd_2O_3 (di2wgd), and the other not doped with any paramagnetic impurities (di2w). The former sample contains mostly quench crystals of diopside, as confirmed by ^{29}Si MAS NMR, and only a small amount of clear glass. It also exhibited weight loss after the capsule was pierced and heated at 110°C overnight, suggesting

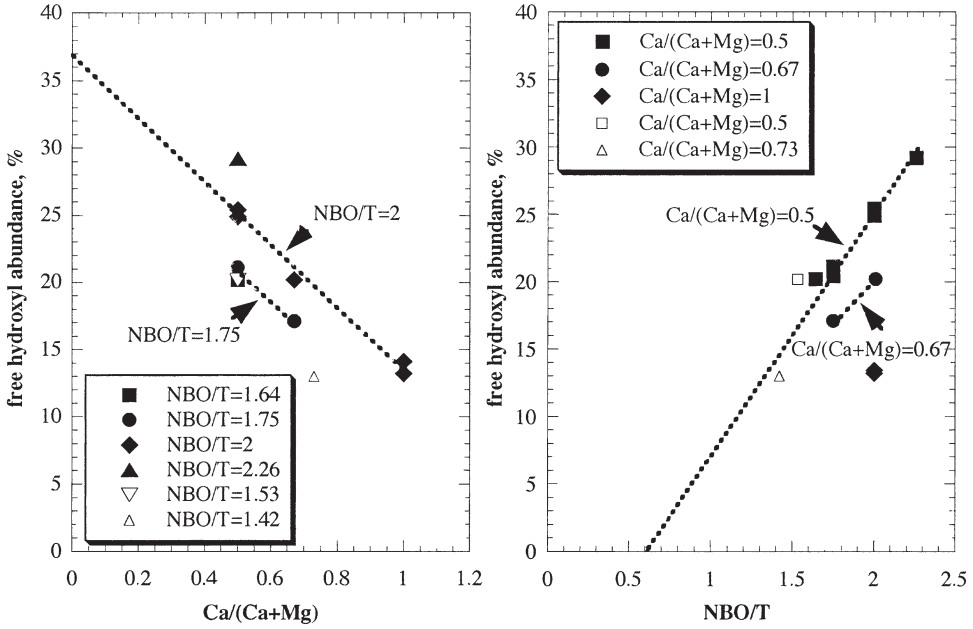

Fig. 6. Free hydroxyl abundance, estimated as the relative area of the peak near 1.2 to 1.5 ppm in the central band of the ^{1}H MAS NMR spectra, as a function of Ca/(Ca + Mg) ratio and bulk NBO/T for the hydrous CMS glasses not doped with any paramagnetic impurities. Solid symbols denote clear, homogeneous glasses, and open symbols denote phase-separated, milky white glasses. For the latter, the estimated abundance in the main phase (excluding the 3.0 ppm peak), and the bulk NBO/T and Ca/(Ca + Mg) ratios are used (Table 2). Dotted lines are guides to the eyes. There is a general trend of increasing abundance of free hydroxyls with decreasing Ca/(Ca + Mg) ratio and increasing NBO/T.

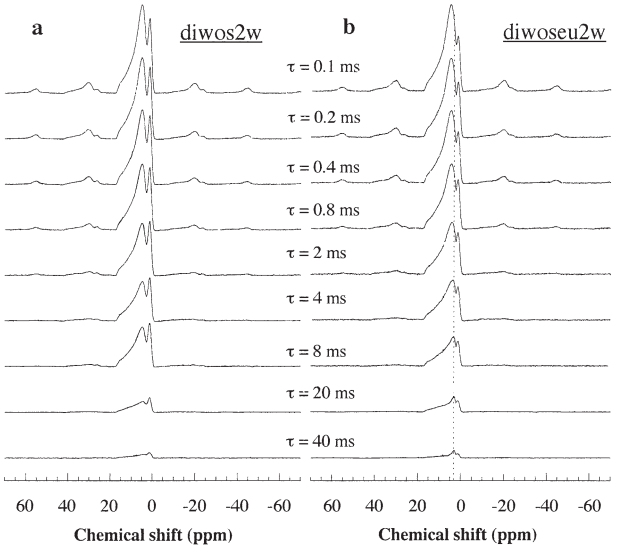

Fig. 7. ^{1}H rotor-synchronized Hahn-echo MAS NMR spectra of (a) a C31.3M15.4S53.3 glass containing 1.8 wt% H_2O (diwos2w) (clear and homogeneous), and (b) a C30.3M11.2S58.5 glass containing 2.0 wt% H_2O (diwoseu2w) (milky white, phase-separated), both not doped with any paramagnetic impurities. Both sets of spectra have been acquired with a spectral width of 1 MHz, a sample spinning rate of 10 kHz, recycle delay times of 100 to 180 s, and evolution time period, τ values of 0.1 to 40 ms as indicated. The relative intensities for spectra of a given sample have been faithfully reproduced. The dotted line is a guide to the position near 3 ppm.

the presence of a fluid phase. The latter consists mostly of clear glass and only a small amount of quench crystals near capsule wall, and exhibited no appreciable weight loss after the capsule was pierced and heated at 110°C overnight. The increased tendency of quench crystal formation for the former was due to the combined effect of 0.2 wt% Gd_2O_3 addition and larger sample size. The ^{1}H MAS NMR spectra for both samples (Fig. 8a and c) contain a sharp peak near 4.8 ppm with a FWHM of ~0.35 ppm on top of broader peaks similar to those of clear, quench crystal-free glasses described above. The sharp peak has a shorter T_1 than the broader peaks, similar to water species on the surface of hydrated minerals (Xue et al., 2002) and silica gels (Bronnimann et al., 1988), and could thus be attributed to mobile fluids trapped in the quench crystals. Subtraction of two ^{1}H MAS NMR spectra acquired with the DEPTH sequence and different recycle delay times (120 s and 40 s) for the sample without paramagnetic impurities (di2w) completely eliminates the sharp peak, resulting in a spectrum (Fig. 8b) similar to those of quench crystal-free glasses of similar compositions (Fig. 2b and c). The absence of a sharp peak near 4.8 ppm and the lack of differential relaxation of different peaks in the ^{1}H MAS NMR spectra shown in Figure 2 to 4 represent additional evidences that those samples were indeed completely glassy.

As described in section 2.1, two of the more silica-rich samples containing 2 wt% H_2O (diseu2w and diwoseu2w) were milky white in appearance and show signs of phase separation. All the added water were retained in the glass structure, judging from the lack of change in sample weight after the recovered sample capsules were pierced and heated at 110°C overnight, and the lack of sharp peaks attributable to mobile water in the ^{1}H MAS NMR spectra. The ^{1}H MAS NMR spectra for both samples (Fig. 9) are composed of a narrow peak near 1.1 to 1.3 ppm and a broader higher-frequency peak with a maximum near 4.5 ppm. The higher-frequency peak is somewhat broader than those of the clear, homogeneous glasses shown in Figure 2 to 4. Measurement with different recycle delay times revealed that these spectra contain an additional, small component with a longer T_1. Subtraction of two ^{1}H MAS NMR spectra taken with the DEPTH pulse sequence and different recycle delay times (120 s and 40 s) yielded a small peak near 3.0 ppm with a FWHM of ~1.5 ppm for both samples (Fig. 9). This component also has somewhat different behavior in the rotor-synchronized ^{1}H Hahn-echo MAS NMR spectra. In Figure 7b are shown the ^{1}H Hahn-echo MAS NMR spectra for the C30.3M11.2S58.5 glass sample containing 2 wt% H_2O (diwoseu2w). The component near 3.0 ppm becomes more prominent with increasing τ, and is the dominant peak in the high-frequency region for τ values of 20 to 40 ms, suggesting that it is in an environment with very weak homonuclear H-H dipolar interaction. The same behavior is observed for the other milky white glass sample (diseu2w) (not shown). The peak near 3.0 ppm resembles those of SiOH groups in silica glasses with low water contents around 0.12 wt% (Kohn et al., 1989a; Zeng et al., 1999b) (also our unpublished data). The inferred very weak homonuclear H-H dipolar interaction is also consistent with the isolated nature of the latter. A previous Raman spectroscopic study of anhydrous glasses in the two-liquid region of

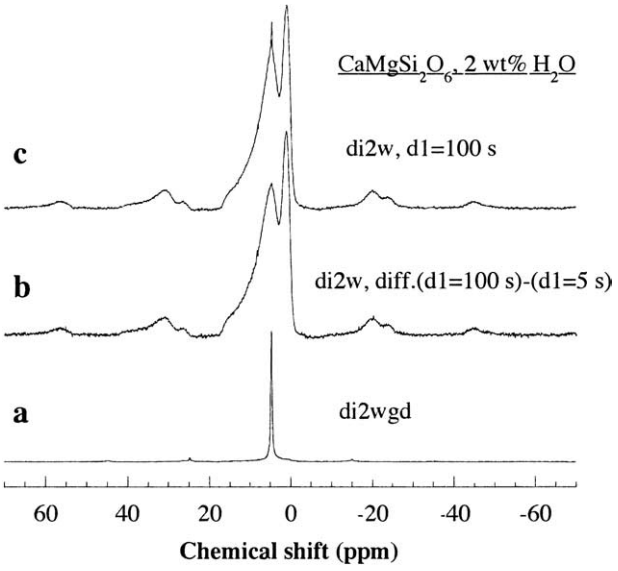

Fig. 8. ^{1}H MAS NMR spectra for (a) a $CaMgSi_2O_6$ sample (quench crystal + minor glass) with 0.2 wt% Gd_2O_3 and 1.9 wt% H_2O added (di2wgd), and (b), (c) a $CaMgSi_2O_6$ sample (glass + minor quench crystal) not doped with any paramagnetic impurities and containing 2 wt% H_2O (di2w). (a) was acquired using the Hahn-echo pulse sequence, with a spectral width of 500 kHz, a sample spinning rate of 8 kHz, an evolution time period, τ value of 0.125 ms and a recycle delay of 10 s; (c) was acquired using the DEPTH pulse sequence with a spectral width of 1 MHz, a sample spinning rate of 10 kHz, and a recycle delay (d1) of 100 s. (b) is the difference between (c) and another spectrum acquired on the same sample with a recycle delay of 5 s and with all other parameters as (c). The sharp peak near 4.8 ppm is completely eliminated in the difference spectrum (b), suggesting that it has a shorter ^{1}H T_1 than the broad peaks.

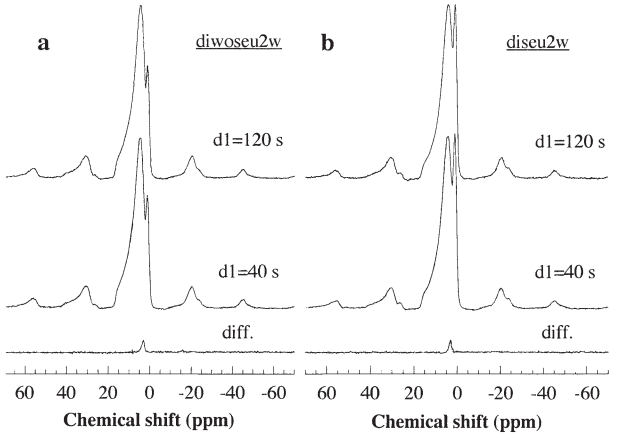

Fig. 9. ^{1}H MAS NMR spectra for the two phase-separated glasses not doped with any paramagnetic impurities. (a) C30.3M11.2S58.5 glass containing 2.0 wt% H_2O (diwoseu2w); (b) C21.7M21.7S56.6 glass containing 2.0 wt% H_2O (diseu2w). The top two spectra for each were acquired using the DEPTH pulse sequence with a spectral width of 1 MHz, a sample spinning rate of 10 kHz, and a recycle delay (d1) of 120 s or 40 s as indicated. The bottom spectra are the difference spectra of the top two, showing the component with longer ^{1}H T_1.

the CMS system at ambient pressure also suggested that one of the two phases resembles silica glass (McMillan, 1984). We have attempted deconvolution for the ^{1}H MAS NMR spectra of these glasses with one unconstrained Gaussian for the 1.1 to 1.3 ppm peak, five Gaussians for the higher-frequency peak with chemical shifts and widths constrained to those of homogeneous glasses of the nearest compositions, and in addition, one other Gaussian for the silicalike phase with a fixed chemical shift (3.0 ppm) and FWHM (1.5 ppm). The estimated relative areas for the 3.0-ppm peak in the fully relaxed spectra with a recycle delay of 120 s are ~3 to 4% for both samples. The estimated relative abundances of free hydroxyls (peak near 1.1 to 1.3 ppm) in the main phase (excluding the peak near 3.0 ppm) are in reasonable agreement with those of the homogeneous glasses (see Fig. 6).

3.1.2. *^{1}H-NMR results for other compositions*

In Figure 10 are shown the ^{1}H MAS NMR spectra for hydrous $Na_2Si_4O_9$, $Na_2Si_2O_5$, $Na_2CaSi_4O_{10}$, and $Li_2Si_2O_5$ glasses containing 0.5 to 3.8 wt% H_2O, and for comparison, the spectrum for a C23.3M23.3S53.3 glass containing 1.8 wt% H_2O (dis2wgd). All these samples were doped with 0.2 wt% Gd_2O_3 to reduce the ^{29}Si T_1. Before proceeding to discuss the spectral features of these samples, it is useful to first clarify the effect of the added Gd_2O_3 on the ^{1}H MAS NMR spectra, as already outlined in section 2.2. From comparison of the ^{1}H MAS spectrum of the C23.3M23.3S53.3 glass containing 1.8 wt% H_2O and doped with 0.2 wt% Gd_2O_3 (dis2wgd) (Fig. 10g) with that of a glass with a similar composition, but not doped with any paramagnetic impurities (dis2w) (Fig. 2d), it is clear that peaks are significantly broadened with 0.2 wt% Gd_2O_3 addition. Similar differences in peak widths are also observed for glasses of a different composition (C33.6M16.5S49.9) containing ~2 wt% H_2O (spectrum for the 0.2 wt% Gd_2O_3-doped sample (diwo2wgd) not shown; that of the Gd_2O_3-free sample (diwo2w) shown in Figure 3a). The rotor-synchronized ^{1}H Hahn-echo MAS NMR spectra for glasses doped with 0.2 wt% Gd_2O_3 show much more rapid intensity decay with increasing τ than those not doped with any paramagnetic impurities (compare Fig. 7 and 11). This suggests that the added Gd_2O_3 causes a significant reduction in both the ^{1}H T_1 and ^{1}H spin-spin relaxation time (T_2). The intensities in the ^{1}H MAS NMR spectra of the glass samples (CMS or alkali silicates) doped with 0.2 wt% Gd_2O_3 account for only ~50 to 70% of those expected from the total water contents. The loss of intensity may be a result of irreversible magnetization decay during the dead time for signals with very small T_2. The greater effect of the doped Gd_2O_3 on the ^{1}H-NMR spectra than expected for ^{29}Si-NMR spectra could be due to more effective dipolar interaction between protons and unpaired electrons of Gd, coupled with effective proton spin diffusion, or closer spatial association of Gd with water species, or both. It is likely that some of the Gd may be directly bonded to water species forming GdOH or $GdOH_2$ linkages. Despite this complication, the overall features of the ^{1}H-NMR spectra (number of peaks and their chemical shifts) are similar for glass samples doped or not doped with 0.2 wt% Gd_2O_3 (compare Fig. 2d and 10g), and these results should thus be useful qualitatively.

The ^{1}H MAS NMR spectra for the $Na_2Si_4O_9$ glasses containing 1.0 and 3.7 wt% H_2O (Fig. 10a,b) are in general similar

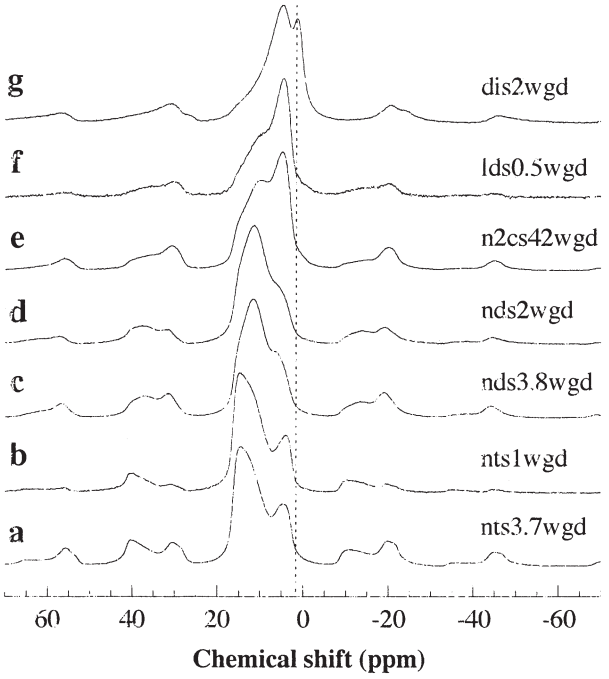

Fig. 10. ^{1}H MAS NMR spectra of (a) a $Na_2Si_4O_9$ glass containing 3.7 wt% H_2O (nts3.7wgd), (b) a $Na_2Si_4O_9$ glass containing 1.0 wt% H_2O (nts1wgd), (c) a $Na_2Si_2O_5$ glass containing 3.8 wt% H_2O (nds3.8wgd), (d) a $Na_2Si_2O_5$ glass containing 1.9 wt% H_2O (nds2wgd), (e) a $Na_2CaSi_4O_{10}$ glass containing 2.0 wt% H_2O (n2cs42wgd), (f) a $Li_2Si_2O_5$ glass containing 0.5 wt% H_2O (lds0.5wgd), and (g) a C23.3M23.3S53.3 glass containing 1.8 wt% H_2O (dis2wgd), all doped with 0.2 wt% Gd_2O_3. (a) was acquired with a single-pulse of 3.8 μs (π/2), all others were acquired with the DEPTH pulse sequence. The sample spinning rate was 10 kHz for all, and the recycle delay times were 10 to 60 s. The dotted line is a guide to the position near 1.3 ppm.

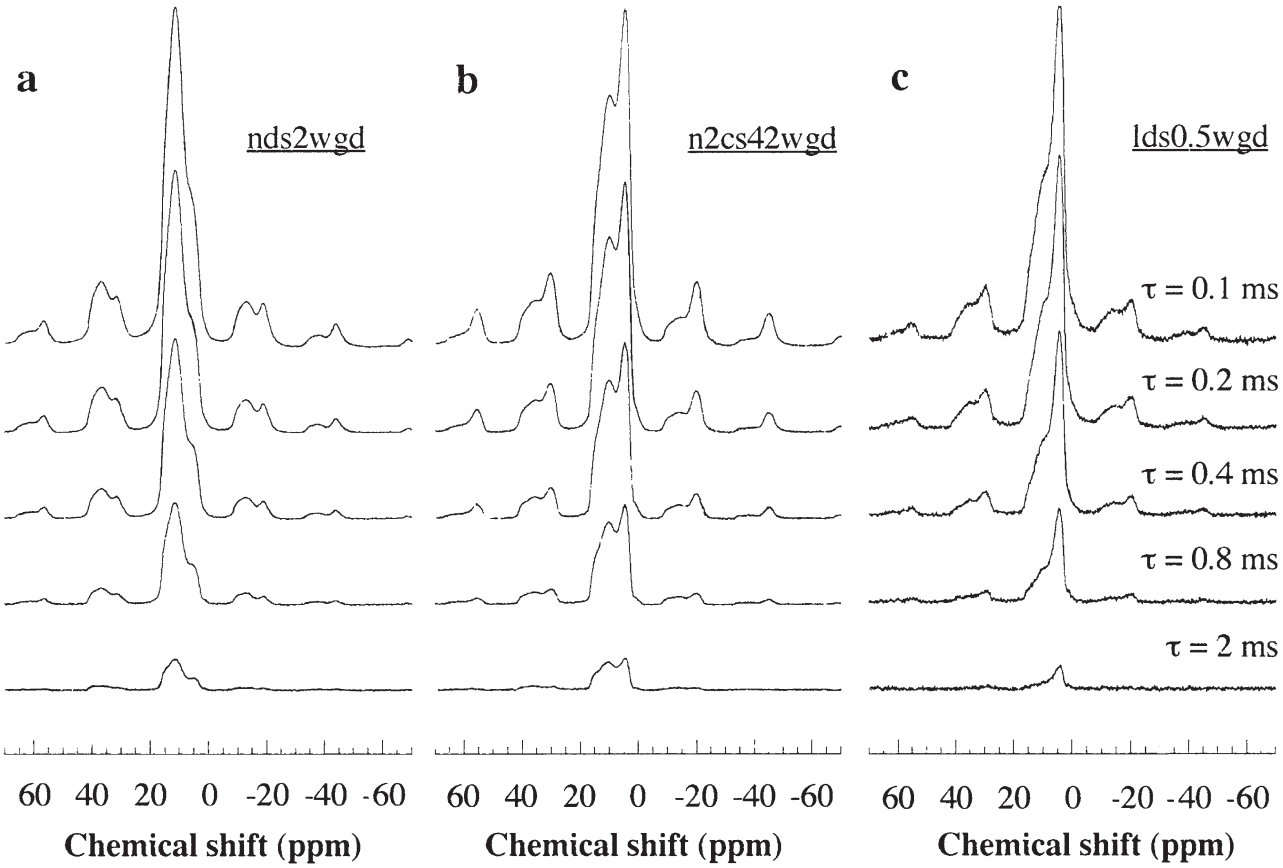

Fig. 11. ^{1}H rotor-synchronized Hahn-echo MAS NMR spectra of (a) a $Na_2Si_2O_5$ glass containing 1.9 wt% H_2O (nds2wgd), (b) a $Na_2CaSi_4O_{10}$ glass containing 2.0 wt% H_2O (n2cs42wgd), and (c) a $Li_2Si_2O_5$ glass containing 0.5 wt% H_2O (lds0.5wgd), all doped with 0.2 wt% Gd_2O_3. All the spectra have been acquired with a spectral width of 500 MHz, a sample spinning rate of 10 kHz, recycle delay times of 10 to 20 s, and evolution time period, τ values of 0.1 to 2 ms as indicated. The relative intensities for the spectra of a given sample are faithfully reproduced.

to those reported for similar glasses without paramagnetic impurities (Kümmerlen et al., 1992; Schaller and Sebald, 1995; Robert et al., 2001). There are two partially resolved peaks with maxima near 14.8 ppm and 4.0 (1.0 wt% H_2O sample) to 4.9 ppm (3.7 wt% H_2O sample). Each of these peaks consists of more than one component, as is clear from their asymmetric shapes in the central band and splitting in the spinning sidebands. The spinning sidebands of the lower-frequency composite peak extend to a further frequency range (more than 100 kHz) than the higher-frequency peak, suggesting greater H-H dipolar interaction. With decreasing water content, the relative intensity of the composite lower-frequency peak decreases; the decrease is more prominent in the spinning sidebands than in the central bands. Thus, part of the intensities for the lower-frequency peak could be attributed to molecular H_2O, whose abundance decreases with decreasing water content. In the rotor-synchronized ^{1}H Hahn-echo MAS NMR spectra (not shown), the relative intensity of the composite lower-frequency peak near 4 to 5 ppm decreases slightly in the central band and more rapidly in the spinning sidebands with increasing τ, again consistent with contribution from both molecular H_2O and SiOH groups in this region. Robert et al. (2001) has also contributed part of the intensities for the lower-frequency peak in a $Na_2Si_4O_9$ glass containing 1.28 wt% H_2O to molecular H_2O and the remaining intensities in the entire frequency range to SiOH groups, on the basis of results from double-quantum-filtered ^{1}H dipolar correlation experiment. The spinning sidebands of the lower-frequency composite band contain two partially resolved components with estimated chemical shifts near 5.5 and 3.5 ppm (Fig. 10a,b), suggesting the presence of two groups of molecular H_2O with different strength of hydrogen bonding. An examination of the ^{1}H-^{29}Si HETCOR spectrum in Robert et al. (2001) also reveals that the ^{1}H sites that only cross-polarize with Si Q^4 sites at a contact time of 2 ms give two peak maxima near these positions. Although not suggested by the original authors, it is more likely that these two peak maxima represent two populations of molecular H_2O species in the vicinity of Si Q^4 sites, rather than SiOH groups because of the distance of the latter from Si Q^4 sites. Zeng et al. (1999a) have also identified two molecular H_2O species from ^{1}H-NMR studies of hydrous $Na_2Si_4O_9$ and $NaAlSi_3O_8$ glasses. The higher-frequency peak with a maximum near 14.8 ppm is asymmetric, with intensities decaying slowly at lower frequency and more abruptly at higher frequency (Fig. 10a,b). The position of this peak corresponds to the highest-frequency shoulder in the ^{1}H-NMR spectra of hydrous CMS glasses described in section 3.1, and is also similar to those of SiOH

Table 3. ^{1}H chemical shifts (δ_i^H) and O-H . . . O distances for SiOH, CaOH, MgOH and H_2O groups in low-pressure crystalline silicate, phosphate and hydroxide phases from the literature.

Phase	Site	δ_i^H(ppm)	R(O-H . . . O)[a] (Å)	NMR Method	Reference[b] NMR	Reference[b] Structure
$Ca_2(OH)(HSiO_4)$(α-dicalcium	SiOH	9.6	2.679	CRAMPS	[1]	[11]
silicate hydrate)	CaOH	2.4	3.093			
$Ca_2(OH)_2(SiO_3)$	CaOH	4.1		CRAMPS	[2]	
$Ca_6(OH)_2(Si_6O_{17})$(xonolite)	CaOH	2		CRAMPS	[2]	
$Ca_5(OH)_2(SiO_4)_2$	CaOH	1.7		CRAMPS	[1]	
$Ca_{16}(OH)_8(Si_2O_5)_{12}\cdot nH_2O$	CaOH	1.3		CRAMPS	[1]	
	H_2O	5.0				
$Ca_4(OH)_2(Si_3O_9)$	CaOH	1.2		CRAMPS	[1]	
$Ca_6(OH)_2(SiO_4)(Si_2O_7)$	CaOH	0.2, −0.8		CRAMPS	[1]	
$Ca_6(OH)_6(Si_2O_7)$	CaOH	−2.0		CRAMPS	[1]	
$Ca(OH)_2$(portlandite)	CaOH	1.4	3.337	CRAMPS	[1]	[12]
$Ca_5(OH)(PO_4)_3$(hydroxyapatite)	CaOH	0.2	3.444	MAS	[3]	[13]
$Mg_5Si_2O_8(OH)_2$ (chondrodite)	MgOH	1.1	3.031	MAS	[4]	[14]
$Mg_3Si_4O_{10}(OH)_2$ (talc)	MgOH	1.1	3.367	MAS	[5]	[15]
$Ca_2Mg_5Si_8O_{22}(OH)_2$(tremolite)	MgOH	0.7	3.288	MAS	[5]	[16]
$Mg(OH)_2$ (brucite)	MgOH	−0.5 ± 2	3.215	static, multipulse	[6]	[17]
$Ca_3Si_3O_8(OH)_2$ (rosenhahnite)	SiOH	6.7	2.681	CRAMPS	[1]	[18]
	SiOH	11.3	2.575			
$Ca_3(HSiO_4)_2\cdot 2H_2O$(afwillite)	SiOH	12.1	2.540	CRAMPS	[1]	[19]
	SiOH	8.1	2.583			
	H_2O	4.1				
$Ca_2Na(HSi_3O_9)$(pectolite)	SiOH	15.8	2.482	MAS	[5]	[20]
$Ca_2Na(HSi_3O_9)\cdot nH_2O$	SiOH	14.9		CRAMPS	[1]	
	H_2O	5.1				
$CaNa(HSiO_4)$	SiOH	12.7	2.53	CRAMPS	[1]	[21]
$NaHSi_2O_5\cdot 2H_2O$(makatiite)	SiOH/H_2O	5.8[c]		MAS	[7]	
$NaHSi_2O_5\cdot 3H_2O$(kanemite)	SiOH	15	2.488	MAS	[8]	[22]
	H_2O	5				
$NaHSi_4O_9\cdot 4H_2O$(octosilicate)	SiOH	16		MAS	[7]	
	H_2O	3.6				
$NaHSi_7O_{15}\cdot 4.5H_2O$(magadiite)	SiOH	14.9		MAS	[9]	
	H_2O	3.5				
$KHSi_2O_5$	SiOH	15.6	2.460	MAS	[10]	[23]

[a] Parameter for O-H . . . O pair with the shortest H . . . O distance when multiple hydrogen-bonds exist;

[b] Reference: [1] Heidemann (1994); [2] Rosenberger and Grimmer (1979); [3] Yesinowski and Eckert (1987); [4] Phillips et al. (1997); [5] Yesinowski et al. (1988); [6] Sears et al. (1988); [7] Almond et al. (1997); [8] Hayashi (1997); [9] Almond et al. (1994); [10] Deng et al. (1989); [11] Marsh (1994); [12] Desgranges et al. (1993); [13] Sänger and Kuhs (1992); [14] Lager et al. (2001); [15] Perdikatsis and Burzlaff (1981); [16] Papike et al. (1969); [17] Elleman and Williams (1956); [18] Wan et al. (1977); [19] Malik and Jeffery (1976); [20] Prewitt (1967); [21] Cooksley and Taylor (1974); [22] Garvie et al. (1999); [23] Malinovskii and Belov (1979).

[c] A single peak with only weak spinning sidebands due to rapid chemical exchange or spin diffusion.

groups with very strong hydrogen bonds in silicate minerals (see compilation in Table 3).

The ^{1}H MAS NMR spectra for the $Na_2Si_2O_5$ glasses containing 2 and 3.76 wt% H_2O both contain a main peak with a maximum near 11.6 ppm and an unresolved lower-frequency shoulder near 6 ppm (Fig. 10c,d). These spectra are similar to that of a $Na_2Si_2O_5$ glass containing 7.8 wt% H_2O reported previously (Kohn et al., 1989a), except that the latter contain more intense spinning sidebands. The lower-frequency shoulder becomes resolved in the spinning sidebands, because it gives more intense spinning sidebands than the main peak. The relative intensity of this lower-frequency peak decreases with decreasing water content, and this decrease is more prominent in the spinning sidebands than in the central band. All these features are again consistent with partial contribution of the lower-frequency peak from water species with strong H-H dipolar interaction, most likely molecular H_2O. We have estimated the ^{1}H chemical shift of molecular H_2O from the positions of the spinning sidebands for the sample with higher water content. The resultant value (around 6.3 ppm) is somewhat larger than that estimated for molecular H_2O in silica glasses (near 4.2 ppm: Kohn et al., 1989a), and is close to the estimation for one of the two molecular H_2O populations of higher chemical shift (5.5 ppm) for the $Na_2Si_4O_9$ glasses described above. The moderately larger ^{1}H chemical shifts of molecular H_2O in depolymerized sodium silicate glasses than in silica glasses correspond to somewhat stronger hydrogen bonding that may be related to the presence of Na, for example, through direct bonding of molecular H_2O to Na and/or hydrogen bonding with nonbridging oxygens. These ^{1}H chemical shifts are within the range for molecular H_2O in crystalline silicates (see Table 3 for examples). In the rotor-synchronized ^{1}H Hahn-echo MAS NMR spectra (Fig. 11a), the relative intensity of the lower-frequency shoulder decreases slightly in the central band, and deceases more rapidly in the spinning sidebands with increasing τ, again consistent with partial contribution from molecular H_2O. The main peak near 11.6 ppm clearly has a higher-frequency shoulder near 15 ppm in both the

^{1}H single-pulse and Hahn-echo MAS NMR spectra (Fig. 10c,d, 11a) corresponding to the peak maximum in the high-frequency region of the ^{1}H MAS NMR spectra for the $Na_2Si_4O_9$ glasses. Thus SiOH groups in both $Na_2Si_4O_9$ and $Na_2Si_2O_5$ glasses have a range of strength of hydrogen bonding, with large populations of very strong hydrogen bonding.

The ^{1}H MAS NMR spectra for both the $Li_2Si_2O_5$ glass containing 0.5 wt% H_2O and the $Na_2CaSi_4O_{10}$ glass containing 2 wt% H_2O show a major peak with a maximum near 4.5 to 4.8 ppm, a partially resolved higher-frequency peak with a maximum near 10 ppm and an even higher-frequency shoulder that extends to ~17 ppm (Fig. 10e,f). The rotor-synchronized ^{1}H Hahn-echo MAS NMR spectra for the $Na_2CaSi_4O_{10}$ glass containing 2 wt% H_2O (Fig. 11b) show similar behavior to those of $Na_2Si_2O_5$ glasses with 2 to 3.76 wt% H_2O: the relative intensity of the 4.8-ppm peak in the central band decreases slightly, and those in the spinning sidebands decease more rapidly with increasing τ, consistent with partial contribution of the 4.8-ppm peak from molecular H_2O. The rotor-synchronized ^{1}H Hahn-echo MAS NMR spectra for the $Li_2Si_2O_5$ glass containing 0.5 wt% H_2O (Fig. 11c) show somewhat different behavior: the relative intensity of the 4.5 ppm-peak increases slightly with τ, opposite to the trend expected if it has a significant contribution from molecular H_2O. The abundance of molecular H_2O is probably minor for the $Li_2Si_2O_5$ glass, as is expected from its low water content. The relative intensities in the higher-frequency region from 10 to 17 ppm are somewhat lower for the $Li_2Si_2O_5$ glass than for the $Na_2CaSi_4O_{10}$ glass, and both are much lower than those of the $Na_2Si_2O_5$ glasses. This suggests that the relative populations of SiOH groups with strong hydrogen bonding decrease in the same order. This follows the same trend of decreasing relative population of strongly hydrogen-bonded SiOH groups with increasing field strength of cations (Na < Na + Ca < Li; Ca < Mg) as shown by the CMS glasses above. The implications of these systematic changes with composition will be discussed in section 3.3.

It is also note-worthy that in the ^{1}H MAS NMR spectra for both the $Li_2Si_2O_5$ and the $Na_2CaSi_4O_{10}$ glasses, there is a clear break in slope near the low-frequency tail, which may be an indication of the presence of a small component near 1.5 ppm (Fig. 10e,f and 11b,c). An even smaller component near this position may also be present in the spectra of $Na_2Si_4O_9$ and $Na_2Si_2O_5$ glasses (Fig. 10a,b,c,d and Fig. 11a). This shoulder may correspond to the major peak near 1.2 to 1.5 ppm observed for the CMS glasses, and could be an indication of a very small amount of free hydroxyl groups (LiOH, (Ca,Na)OH and NaOH). It is also possible, though, that this shoulder may merely reflect peak broadening due to H-H dipolar interaction and/or the presence of paramagnetic impurities. In either case, it is clear that the abundances of OH groups contributing to the intensity near 1.5 ppm are much smaller in the $Na_2Si_4O_9$, $Na_2Si_2O_5$, $Li_2Si_2O_5$, and $Na_2CaSi_4O_{10}$ glasses than in CMS glasses.

3.2. ^{29}Si MAS and ^{1}H-^{29}Si CP-MAS NMR Results

3.2.1. ^{29}Si-NMR results for the CaO-MgO-SiO$_2$ system

The ^{29}Si MAS NMR spectra for some of the anhydrous glasses along the $CaMgSiO_4$-SiO_2 join are shown in Figure 12.

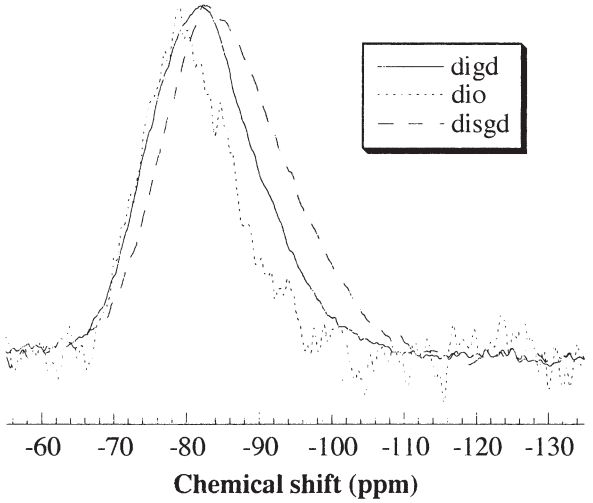

Fig. 12. ^{29}Si MAS NMR spectra for anhydrous C26.5M26.5S47 (dio) (not doped with paramagnetic impurities), $CaMgSi_2O_6$ (digd) and C23.3M23.3S53.3 (disgd) glasses (both doped with 0.2wt% Gd_2O_3) along the $CaMgSiO_4$-SiO_2 join. The spectra for the C26.5M26.5S47 and $CaMgSi_2O_6$ glasses were acquired with the DEPTH sequence and a recycle delay of 1600 s and 50 s, respectively; the spectrum for the C23.3M23.3S53.3 glass was acquired with a single pulse of 2.2 μs (π/4) and a recycle delay of 20 s. The spinning rate was 8 kHz for all.

The ^{29}Si MAS NMR spectrum of the anhydrous $CaMgSi_2O_6$ glass that is doped with 0.2 wt% Gd_2O_3 (digd) contains an asymmetric peak with a maximum near −82.0 ppm and a FWHM of 16.6 ppm, similar to those reported previously (e.g., Murdoch et al., 1985; Kirkpatrick et al., 1986; Brandriss and Stebbins, 1988). There is an obvious shoulder on the higher-frequency side, and a more slowly decaying tail to the lower-frequency side. The ^{29}Si MAS NMR spectrum of a more silica-rich C23.3M23.3S53.3 glass (disgd), also doped with 0.2 wt% Gd_2O_3, consists of a single, asymmetric broad peak that has a maximum near −82.3 ppm and a FWHM of 19.2 ppm. Compared with that of the anhydrous $CaMgSi_2O_6$ glass, the higher-frequency shoulder is less pronounced, and the lower-frequency side is more intense. The ^{29}Si MAS NMR spectrum of a less silica-rich C26.5M26.5S47 glass, not doped with any paramagnetic impurities (dio), is noisier due to long ^{29}Si T_1, but nevertheless clearly shows a narrower FWHM (13 ppm) than that of the $CaMgSi_2O_6$ glass, with peak maximum near the high-frequency shoulder of the latter (−79 ppm). Thus with increasing NBO/T along the $CaMgSiO_4$-SiO_2 join, the relative intensity in the higher-frequency region systematically increases, and that in the lower-frequency region decreases, although no separate components are clearly discernible. The ^{29}Si MAS NMR spectrum of an anhydrous C33.6M16.5S49.9 glass doped with 0.2 wt% Gd_2O_3 (diwogd) is similar to that of the $CaMgSi_2O_6$ glass, with a peak maximum near −81.0 ppm and a FWHM of 15.7 ppm (Fig. 13b). The ^{29}Si MAS NMR spectra of alkali and alkaline earth silicate glasses are generally regarded to be composed of two or more components due to Si of different Q^n species. For alkali silicate compositions, peaks for the individual Q^n species are narrower and thus partially resolved (see section 3.2.2). For alkaline earth silicate glasses, these components are in general not clearly resolved in single-pulse ^{29}Si MAS NMR spectra (e.g., Murdoch et al., 1985), but

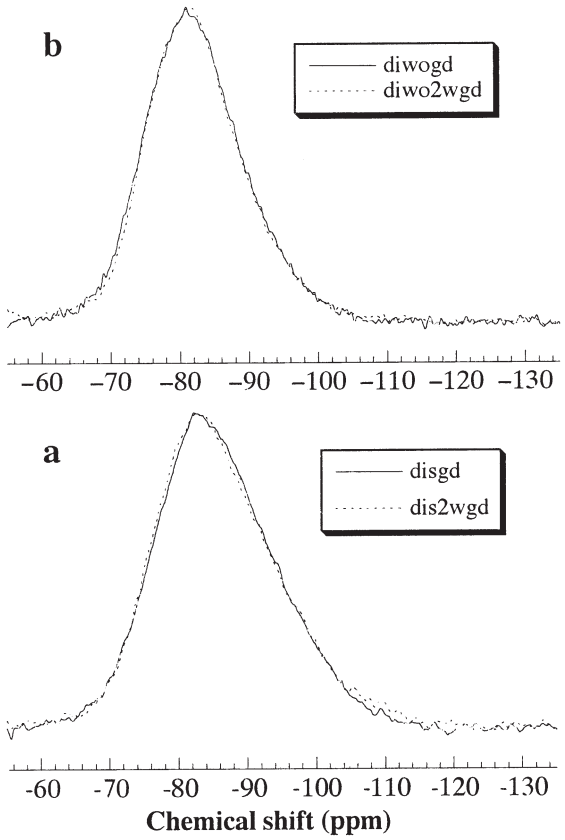

Fig. 13. ^{29}Si MAS NMR spectra for (a) anhydrous (disgd) and hydrous C23.3M23.3S53.3 glass containing 1.8 wt% H_2O (dis2wgd); (b) anhydrous (diwogd) and hydrous C33.6M16.5S49.9 glass containing 1.8 wt% H_2O (diwo2wgd), all doped with 0.2 wt% Gd_2O_3. The spectra of (a) were acquired with a single pulse of 2.2 μs (π/4) and a recycle delay of 20 s; the spectra of (b) were acquired with the DEPTH pulse sequence and recycle delay times of 64 and 120 s. The spinning rate was 8 kHz for all.

have been shown to be resolvable in more sophisticated two-dimensional ^{29}Si-NMR spectra (Zhang et al., 1997). The systematic changes we have observed for the ^{29}Si MAS NMR spectra of anhydrous glasses along the $CaMgSiO_4$-SiO_2 join (Fig. 12) may be a result of gradual increase in the relative proportions of less polymerized Q^n species with increasing NBO/T.

The ^{29}Si MAS NMR spectra of anhydrous and hydrous C23.3M23.3S53.3 (dis2wgd) (on the Di-Qz join) and C33.6M16.5S49.9 (diwo2wgd) (on the Di-Wo join) glasses with 1.8 wt% H_2O, all doped with 0.2 wt% Gd_2O_3, are compared in Figure 13. Changes between the anhydrous and hydrous glasses are small for both compositions. The ^{29}Si MAS NMR spectrum of a more depolymerized C26.5M26.5S47 glass with 1.0 wt% H_2O that was not doped with any paramagnetic impurities (dio1w) (not shown) is indistinguishable from that of the anhydrous glass (Fig. 12) within noise level. Thus for all three compositions, changes in the ^{29}Si MAS NMR spectra due to the dissolution of ~1 to 2 wt% H_2O are small. We have not attempted deconvolution for these spectra, because of the very small changes between anhydrous and hydrous glasses, coupled with the lack of resolution for different Si species. Nevertheless, it is clear that the lack of significant spectral changes with dissolution of ~1 to 2 wt% H_2O is not simply a result of insensitivity. For example, if all the 1.8 wt% dissolved water in the C23.3M23.3S53.3 glass were in the form of SiOH, an increase in the bulk NBO/T of ~0.22 would be expected (NBO in a broad sense, including SiOM and SiOH, see discussions in the next section). This is almost equivalent to the difference in NBO/T between the anhydrous C23.3M23.3S53.3 glass (NBO/T = 1.75) and $CaMgSi_2O_6$ glass (NBO/T = 2). The observed spectral changes with water dissolution are significantly less than the latter (see Fig. 12). In addition, as will be described in the next section, sodium- and sodium-calcium silicate glasses show more significant spectral changes with dissolution of a similar amount of H_2O, even though some of the latter spectra have comparable peak widths. These results thus indicate that changes in the overall degree of polymerization of the silicate network structure with dissolution of ~1 to 2 wt% H_2O are relatively small for the CMS glasses investigated.

These results are in broad agreement with the ^{1}H MAS NMR results described in section 3.1. For both C23.3M23.3S53.3 and C33.6M16.5S49.9 glasses containing 1 to 2 wt% H_2O, we have estimated that ~20% or more of the dissolved hydroxyls are free hydroxyls (Table 2). As will be further illustrated in section 4.2, while the formation of a SiOH group increases the total number of nonbridging oxygens (in a broad sense, including SiOM and SiOH) by one, the formation of a MOH group has an opposite effect. Thus, the effect of free hydroxyls on the polymerization of the network structure roughly cancel out that of an equivalent amount of SiOH, so that the net change in the degree of polymerization is caused by only ~60% or less of the total dissolved hydroxyls for these two compositions. The lack of discernible changes in the ^{29}Si MAS NMR spectra for the anhydrous and hydrous C23.3M23.3S53.3 and C33.6M16.5S49.9 glasses with 1.8 wt% H_2O must be due to the combined effect of free hydroxyls and broad peak widths. For the C26.5M26.5S47 glass containing 1 wt% H_2O (dio1w), we have estimated that at least 29% of the dissolved hydroxyls are free hydroxyls (Table 2). From a similar argument, the net change in polymerization of the structure is caused by an equivalence of 42% or less of the total dissolved hydroxyls ($\leq$ 0.42 wt% H_2O). It is thus not surprising that no discernible changes were observed between the ^{29}Si MAS NMR spectra of the anhydrous and hydrous glasses.

The ^{1}H-^{29}Si CP-MAS NMR spectra of the C23.3M23.3S53.3 and C33.6M16.5S49.9 glasses containing 1.8 wt% H_2O (dis2wgd and diwo2wgd) are somewhat displaced to higher frequencies, compared with the corresponding single-pulse spectra (Fig. 14). An analysis of the intensities of the ^{1}H-^{29}Si CP MAS NMR spectra against contact time in the range of 0.05 to 14 ms yields a cross-polarization time constant, T_{SiH} of 0.17 ms, and ^{1}H spin-lattice relaxation in the rotating frame time constant, $T_{1\rho}$ of 6.3 ms for the C23.3M23.3S53.3 glass with 1.8 wt% H_2O, and T_{SiH} of 0.30 ms and $T_{1\rho}$ of 8.1 ms for the C33.6M16.5S49.9 glass with 1.8 wt% H_2O. These T_{SiH} values are similar to, though somewhat smaller than the estimated values for Si Q^1, Q^2 and Q^3 groups in hydrous $Na_2Si_4O_9$ glasses (0.5 to 1.4 ms) (Kümmerlen et al., 1992) and hydrated $Na_2Si_2O_5$ glasses (0.24 to 0.68 ms) (Uchino et al., 1992a). We may also compare these results with data for crystalline sili-

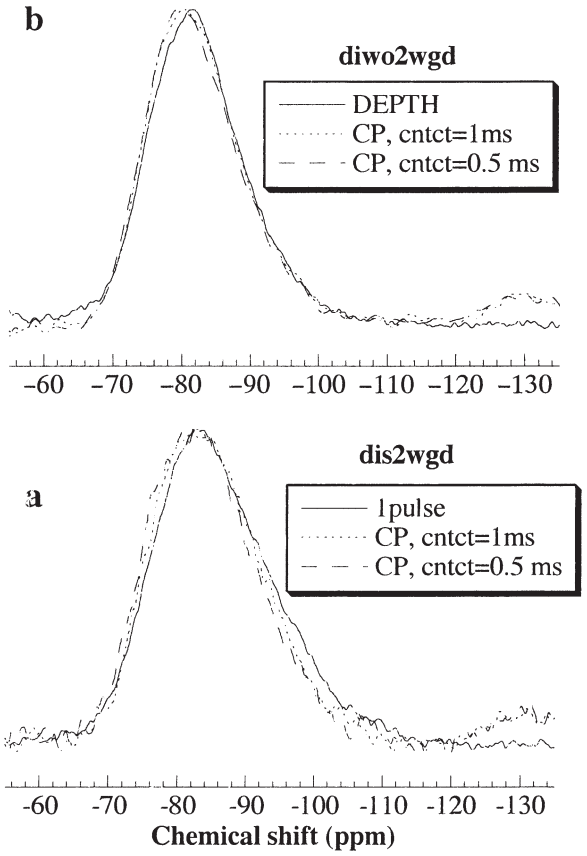

Fig. 14. ^{29}Si MAS NMR spectra acquired with a single pulse or DEPTH pulse sequence, and ^{1}H-^{29}Si CP-MAS NMR spectra with a contact time (cntct) of 0.5 and 1 ms for (a) C23.3M23.3S53.3 glass containing 1.8 wt% H_2O (dis2wgd); and (b) C33.6M16.5S49.9 glass containing 1.8 wt% H_2O (diwo2wgd), both doped with 0.2 wt% Gd_2O_3.

cates. Oglesby and Stebbins (2000) have collected ^{1}H-^{29}Si CP-MAS NMR spectra for several crystalline silicates containing SiOH groups, including $Ca_3Si_3O_8(OH)_2$ rosenhahnite and $KHSi_2O_5$, and have shown that the T_{SiH} values exhibit a general correlation with the Si-H distances. All the SiOH groups from their collection of data give T_{SiH} values between 0.6 to 1.3 ms, and the mineral talc that only contains MgOH group gives a larger T_{SiH} value of 3.7 ms. Two of the Si sites from their data (Q^3(1Al) in ussingite, and Q^2 in rosenhahnite), that are not directly coordinated to any OH groups, but are each bonded to a nonbridging oxygen that is strong hydrogen-bonded to a neighboring SiOH group, also yield small T_{SiH} values (0.74 and 1.5 ms). Hayashi (1997) has reported similar T_{SiH} values (0.35, 1.3 ms) for two SiOH sites in a kanemite ($NaHSi_2O_5.xH_2O$) sample. Phillips et al. (1997) has reported ^{1}H-^{29}Si CP-MAS NMR results for several hydrous magnesium silicate phases synthesized at pressures above 10 GPa, in which all the structural water are MgOH groups. Their reported T_{SiH} value for condrodite is 1.1 ms, overlapping with the range shown by SiOH groups, whereas the T_{SiH} values for phase B and superhydrous B are larger (2.2 to 40 ms). It may be inferred from these data that small T_{SiH} values below 1.5 ms are typical of, but not restricted to, samples containing SiOH groups. The very short T_{SiH} of our hydrous glass samples are consistent with the presence of some SiOH groups.

3.2.2. ^{29}Si-NMR results for other compositions

In contrast to the CMS system described above, there are in general larger changes between anhydrous and hydrous glasses containing 1 to 2 wt% H_2O for the $Na_2Si_4O_9$, $Na_2Si_2O_5$ and $Na_2CaSi_4O_{10}$ compositions, as described below.

3.2.2.1. $Na_2Si_4O_9$ glasses. The ^{29}Si MAS NMR spectrum for the anhydrous $Na_2Si_4O_9$ glass contains two partially resolved peaks with maxima near −105 ppm attributable to Q^4 species, and near −93 ppm attributable to Q^3 species (Fig. 15a). The dissolution of only 1 wt% water causes a

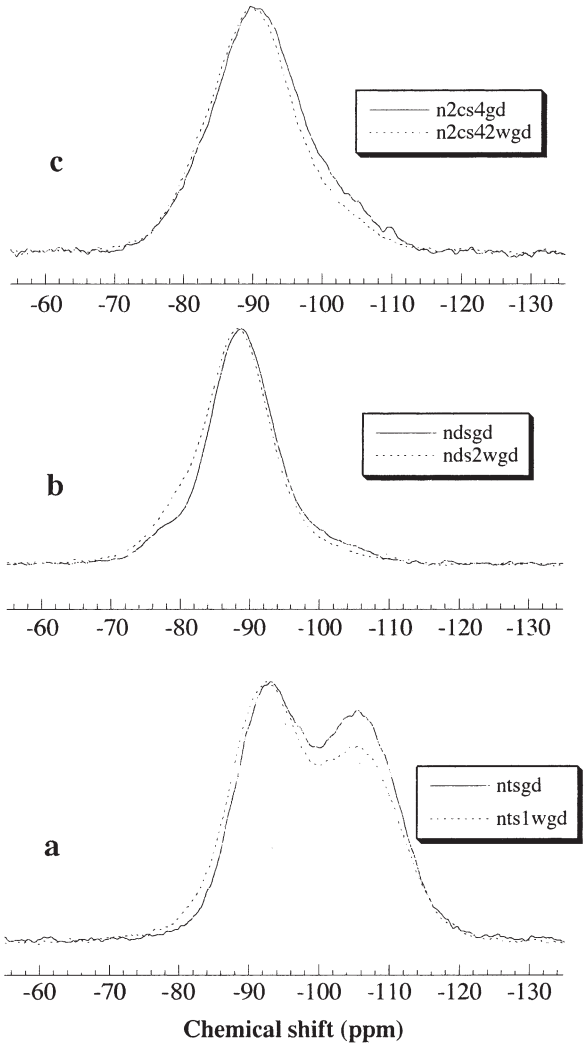

Fig. 15. ^{29}Si MAS NMR spectra for (a) anhydrous (ntsgd) and hydrous $Na_2Si_4O_9$ glass containing 1.0 wt% H_2O (nts1wgd), (b) anhydrous (ndsgd) and hydrous $Na_2Si_2O_5$ glass containing 1.9 wt% H_2O (nds2wgd), (c) anhydrous (n2cs4gd) and hydrous $Na_2CaSi_4O_{10}$ glass containing 2.0 wt% H_2O (n2cs42wgd), all doped with 0.2 wt% Gd_2O_3. The spectra were acquired with either a single pulse of 2.2 μs (π/4) and a delay time of 20 s, or the DEPTH pulse sequence and delay times of 40 to 60 s. Spinning rate was 8 kHz for all.

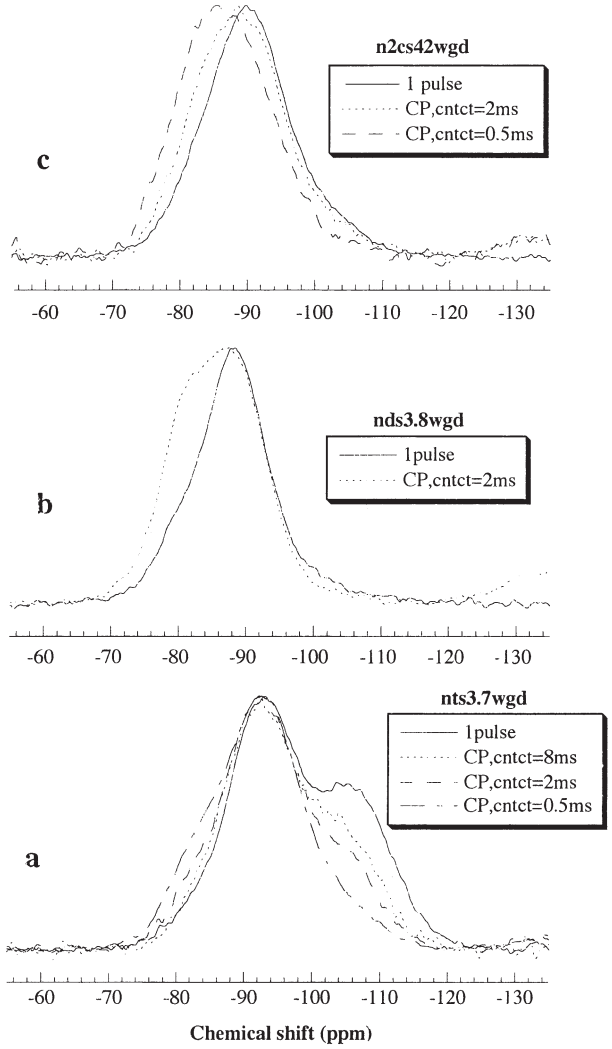

Fig. 16. (a) ^{29}Si single-pulse MAS NMR spectrum and ^{1}H-^{29}Si CP-MAS NMR spectra with contact times (cntct) of 0.5, 2 and 8 ms for the $Na_2Si_4O_9$ glass containing 3.7 wt% H_2O (nts3.7wgd), (b) ^{29}Si single-pulse MAS NMR spectrum and ^{1}H-^{29}Si CP-MAS NMR spectra with a contact time of 2 ms for the $Na_2Si_2O_5$ glass containing 3.8 wt% H_2O (nds3.8wgd), (c) ^{29}Si single-pulse MAS NMR spectrum and ^{1}H-^{29}Si CP-MAS NMR spectra with contact times of 0.5 and 2 ms for the $Na_2CaSi_4O_{10}$ glass containing 2.0 wt% H_2O (n2cs42wgd). All the samples were doped with 0.2 wt% Gd_2O_3. The sample spinning rate was 4 kHz for the CP-MAS spectra and 6 to 8 kHz for the single-pulse spectra.

marked decrease in the relative intensity of the peak near −105 ppm, relative to that of the peak near −93 ppm (Fig. 15a). These results are in general agreement with those of Kümmerlen et al. (1992) and Zotov and Keppler (1998) for $Na_2Si_4O_9$ glasses containing 2.62 to 10.0 wt% H_2O. We have also collected ^{1}H-^{29}Si CP-MAS NMR spectra with a range of contact times between 0.25 and 8 ms for the sample containing 3.7 wt% H_2O (Fig. 16a). The ^{1}H-^{29}Si CP-MAS NMR spectra with short contact times of 0.25 and 0.5 ms contain a main peak near the position for Q^3 (−93 ppm) and a pronounced asymmetric shoulder to higher frequency. With increasing contact time, the relative intensity of the higher-frequency shoulder decreases, whereas a lower-frequency shoulder grows. These changes are again similar to those reported previously (Kümmerlen et al., 1992). The higher-frequency shoulder has been attributed to Q^2 and the lower-frequency shoulder to Q^4 by the latter authors.

We have attempted deconvolution for the ^{29}Si MAS NMR spectra to obtain a more quantitative picture of the extent of changes in the network structure. Intensities in the spinning sidebands were also taken into account, because the abundance of Q^4 is in general over-represented in the central band as a result of smaller chemical shift anisotropy. The ^{29}Si MAS NMR spectrum of the anhydrous glass can be deconvoluted with two Gaussian peaks of unconstrained parameters. The resultant Q^n speciation distribution is consistent with that expected from chemical composition (Table 4). The ^{29}Si MAS NMR spectra of the hydrous glasses also contain two peaks at nearly the same positions, but in addition show a small higher-frequency shoulder corresponding to the more pronounced shoulder attributable to Q^2 in the CP-MAS NMR spectra. These spectra were thus deconvoluted with three Gaussians representing Q^4, Q^3 and Q^2. The parameters for all peaks were unconstrained for the sample containing 3.8 wt% H_2O, but the parameters of Q^2 were constrained to those of above for the sample containing 1 wt% H_2O because of its small intensity. The resultant chemical shifts and peak widths for Q^3 and Q^4 of the hydrous glasses are similar to those of the anhydrous glass (Table 4). This deconvolution procedure is similar to those of Kümmerlen et al. (1992) and Zotov et al. (1998), and the estimated Q^n abundances (Table 4) are also in good agreement with the latter. If all the dissolved water are assumed to be in the form of either SiOH or molecular H_2O, the estimated NBO/T are consistent with ~67 and 54% of the dissolved water in the form of SiOH in the glasses containing 1.0 and 3.7 wt% H_2O, respectively.

The estimated increase in the bulk NBO/T with water dissolution requires that some of the Q^3 and Q^2 are not true Q^n(Na) species with n bridging oxygen and 4-n nonbridging oxygen (SiONa) neighbors like those in the anhydrous glasses, but Q^n(H,Na) and/or Q^n(H) species with n bridging oxygen neighbors and one or more OH neighbors. The deconvolution procedure above implicitly assumes indistinguishable features for the true Q^n(Na) and Q^n(H) species. The reliability of these results thus largely depends on the validity of this assumption. From studies of silica gels and hydrous silica glasses (e.g., Maciel and Sindorf, 1980; Farnan et al., 1987), it is known that the ^{29}Si chemical shifts for Q^3(H) groups are near −100 ppm, half way between those of Q^3(Na) (−92.5 ppm) and Q^4 (−105.8 ppm) in the anhydrous $Na_2Si_4O_9$ glass, and the ^{29}Si chemical shifts for Q^2(H) groups are around −91 ppm, similar to those of Q^3(Na) in the latter. The Q^3(H) in the crystalline $H_2Si_2O_5$ phases also yield ^{29}Si chemical shifts in the range −98.4 to −110 ppm (Engelhardt and Michel, 1987), more negative than those of Q^3(Na) in α-$Na_2Si_2O_5$ (−94.5 ppm) (Murdoch et al., 1985). These data seem to suggest that the chemical shifts of Q^n(H) species are different from those of true Q^n(Na) species. However, there are also evidences that suggest the contrary. For example, the four Q^3(H) and Q^3(Na) sites in $NaHSi_2O_5.2H_2O$ makatite all yield ^{29}Si chemical shifts in a small range between −92 and −94 ppm (Almond et al., 1997), close to that of Q^3(Na) in α-$Na_2Si_2O_5$. The Q^3(H) and Q^3(K) groups in crystalline $KHSi_2O_5$ are crystallographically indistinguishable due to strong hydrogen bonding and H positional

Table 4. Deconvolution results for ^{29}Si MAS NMR spectra of sodium silicate glasses.

Composition[a]	Water content (wt%)	Q^1 δ_i^{Sib} (ppm)	Q^1 FWHM (ppm)	Q^1 abundance (%)	Q^2 δ_i^{Sib} (ppm)	Q^2 FWHM (ppm)	Q^2 abundance (%)	Q^3 δ_i^{Sib} (ppm)	Q^3 FWHM (ppm)	Q^3 abundance (%)	Q^4 δ_i^{Sib} (ppm)	Q^4 FWHM (ppm)	Q^4 abundance (%)	Bulk NBO/T[c]
$Na_2Si_4O_9$	0							−92.5	10.6	50.0	−105.8	12.5	50.0	0.50
	1.0				−81.6[d]	8.3[d]	2.0	−92.0	10.8	51.7	−105.7	13.3	46.4	0.56
	3.7				−81.6	8.3	5.0	−92.5	11.1	57.3	−105.9	13.0	37.7	0.67
$Na_2Si_2O_5$	0				−77.5	6.1	7.2	−88.6	9.6	80.8	−99.2	12.6[d]	11.9	0.95
	2.0	−72.4	6.9[d]	1.8	−79.0	7.1	11.0	−88.2	9.8	78.6	−98.3	12.6[d]	8.6	1.06
	3.8	−72.3	6.9[d]	1.9	−79.3	6.8	13.0	−88.1	9.8	76.4	−97.6	12.6[d]	8.6	1.08

[a] All samples doped with 0.2 wt% Gd_2O_3.
[b] ^{29}Si chemical shifts.
[c] Estimated assuming negligible amounts of free oxygens and free hydroxyls; here, NBO includes both SiONa and SiOH.
[d] Values fixed during deconvolution.

disorder, and give a single ^{29}Si-NMR peak at −91.2 ppm (Oglesby and Stebbins, 2000), comparable to those of Q^3(K) in crystalline $K_2Si_2O_5$ (−91.5 to −94.5 ppm) (Murdoch et al., 1985) and low-pressure $K_2Si_4O_9$ phase (−91.8 and −92.7 ppm) (Kanzaki et al., 1998). The two Q^2(H,Ba) sites in $BaSi_2O_4(OH)_2.2H_2O$ krauskopfite have ^{29}Si chemical shifts of −80.3 and −84.1 ppm (Oglesby and Stebbins, 2000), overlapping with that of Q^2(Ba) in crystalline $BaSiO_3$ (−80 ppm) (Smith et al., 1983). The similarities in the ^{29}Si chemical shifts for Q^n(H), Q^n(H,M), and Q^n(M) in the latter cases must arise from the presence of M cations and nonbridging oxygens, perhaps through interactions between M cations and oxygens in the Si(M)OH groups and hydrogen bonding between SiOH and nonbridging oxygens. It is thus reasonable to assume that large parts of the Q^3(H) species in the hydrous $Na_2Si_4O_9$ glasses yield ^{29}Si chemical shifts similar to those of Q^3(Na) species in the anhydrous glass. The similarities in the resultant parameters for Q^3 and Q^4 from unconstrained deconvolution of the ^{29}Si MAS NMR spectra for both the anhydrous and hydrous $Na_2Si_4O_9$ glasses support such an inference. Thus, the deconvolution procedure described above is probably largely reasonable. It cannot be excluded, though, that for relatively polymerized silicate compositions, some of the Q^3(H) groups may be in a region largely free from alkalis, and give more negative ^{29}Si chemical shifts, like those of hydrous silica glasses. If the latter is true for the $Na_2Si_4O_9$ glasses, the actual SiOH abundance could be even larger than those estimated above. In any case, it is clear that the dissolution of only 1 wt% H_2O causes significant depolymerization of the network structure for the $Na_2Si_4O_9$ glass, which is in contrast to the results for the CMS glasses.

3.2.2.2. $Na_2Si_2O_5$ glasses. The ^{29}Si MAS NMR spectrum of the anhydrous $Na_2Si_2O_5$ glass contains a main peak near −88.6 ppm attributable to Q^3, a shoulder to higher frequency attributable to Q^2 and a tail to lower frequency attributable to Q^4 (Fig. 15b), similar to those reported in the literature (e.g., Stebbins, 1987; Maekawa et al., 1991). The ^{29}Si MAS NMR spectra of the hydrous $Na_2Si_2O_5$ glasses show a more enhanced, but less resolved high-frequency shoulder, and a less intense low-frequency tail. The spectral change between the anhydrous glass and the glass containing 2 wt% H_2O (Fig. 15b) is more prominent than those of CMS glasses of comparable water content. Compared with the single-pulse spectrum, the ^{1}H-^{29}Si CP-MAS NMR spectra for the hydrous $Na_2Si_2O_5$ glasses show a large increase in the high-frequency shoulder near −80 ppm attributable to Q^2, and also contain a small component to even higher frequency (near −72 ppm), attributable to Q^1 (Fig. 16b), similar to that of a hydrated $Na_2Si_2O_5$ glass containing ~3 wt% H_2O reported previously (Uchino et al., 1992a). In the latter study, Uchino and coauthors reported ^{1}H-^{29}Si CP-MAS NMR spectra for hydrated $Na_2Si_2O_5$ glasses with water contents up to 28 wt% that all show three partially resolved components near −88 to −91 ppm, −80 to −85 ppm, and −71 to −78 ppm, corresponding to the three components observed in our spectra. Uchino and coauthors assigned these peaks to Q^3(Na), Q^2(Na,H), and Q^1(Na, 2H) respectively, and an unresolved shoulder near −93 to −96 ppm to Q^3(H). As discussed in section 3.2.2.1, the chemical shifts of Q^n(H) and Q^n(Na,H) are expected to be similar to those of Q^n(Na), so that the general assignment of the three resolved components to Q^3, Q^2 and Q^1 are probably reasonable, but the number of H neighbors to each is more uncertain. The lowest frequency shoulder near −93 to −96 ppm could be due to either Q^3(H), or more likely Q^4.

We have also attempted deconvolution for the ^{29}Si MAS NMR spectra of the $Na_2Si_2O_5$ glasses. Even the spectrum for the anhydrous glass cannot be uniquely deconvoluted without constraints. We have compared ^{29}Si MAS NMR spectra for anhydrous sodium silicate glasses with a range of silica contents from $Na_2Si_4O_9$ and $Na_2Si_3O_7$, to $Na_4Si_3O_8$ compositions, for which peaks due to different Q^n species are better resolved (see Tsujimura et al., 2004). The FWHM for a given Q^n species do not show appreciable variations with silica content, whereas their chemical shifts move systematically to less negative values with decreasing silica content. Similar results have also been reported from previous studies (e.g., Maekawa et al., 1991). We have thus deconvoluted the ^{29}Si MAS NMR spectrum for the anhydrous $Na_2Si_2O_5$ glass with the FWHM of Q^4 fixed to 12.6 ppm and with all other parameters unconstrained. Varying the fixed FWHM of Q^4 within a reasonable range (±0.5 ppm) does not change the chemical shifts and widths for Q^2 and Q^3 appreciably, but does affect the chemical shift of Q^4, the overall abundances of Q^n and accordingly the estimated bulk NBO/T (within about ± 0.005). The deconvolution results are reported in Table 4.

The ^{29}Si MAS NMR spectra for the hydrous $Na_2Si_2O_5$ glasses were deconvoluted with four Gaussians of increasing

frequencies representing the Q^4, Q^3, Q^2, and Q^1 species. Again some constraints are necessary. The widths of the small components for Q^4 and Q^1 on either side of the spectra were fixed, whereas all other parameters were unconstrained during the deconvolution. The deconvolution results are shown in Table 4. The chemical shifts and widths of the dominant Q^3 and Q^2 species are relatively insensitive to the values chosen for the fixed widths of Q^4 and Q^1, but the chemical shifts of the latter and the overall abundances of Q^n and thus the bulk NBO/T show more variations. For example, when the FWHM of Q^1 is varied between 6.9 ± 0.7 ppm and the FWHM of Q^4 varied between 12.6 ± 0.5 ppm, the estimated bulk NBO/T varies by about ± 0.008. Under the assumption that all the dissolved water are present as either SiOH or H_2O, the proportion of dissolved water in the form of SiOH can be estimated to be ~53 and 33% for the $Na_2Si_2O_5$ glasses containing 2.0 and 3.7 wt% H_2O, respectively. Considering the uncertainties with the deconvolution, these values should be viewed with a large error. Nevertheless, they support the conclusion from visual inspection that the dissolution of only 2 wt% H_2O causes significant depolymerization in the network structure.

3.2.2.3. $Na_2CaSi_4O_{10}$ glasses. The ^{29}Si MAS NMR spectra of the anhydrous $Na_2CaSi_4O_{10}$ glass has an asymmetric shape with a maximum near −89.7 ppm and a tail to lower frequency side (Fig. 15c). The FWHM of the peak is ~14.2 ppm, comparable to that of the C33.6M16.5S49.9 glass described in section 3.2.1. With dissolution of 2 wt% H_2O, the ^{29}Si MAS NMR peak becomes narrower with a small increase in intensity on the higher-frequency side, and a larger decrease in intensity for the lower-frequency tail (Fig. 15c). The ^{1}H-^{29}Si CP-MAS NMR spectra with contact times of 0.5 and 2 ms show an increase in intensity on the high-frequency side of the peak and a corresponding decrease on the lower-frequency side, than the single-pulse spectrum. As for the $Na_2Si_2O_5$ glasses, these changes may be interpreted as an increase in the abundance of Q^2 and possibly also Q^1, and a decrease in the abundance of Q^4, relative to Q^3, with water dissolution. We have not attempted deconvolution for these spectra, because none of them have resolved features to allow unequivocal choice of components. The spectral changes for the $Na_2CaSi_4O_{10}$ glasses are, nevertheless, more pronounced than those of the C33.6M16.5S49.9 glasses with a similar amount of dissolved water described in section 3.2.1.

3.3. Ab Initio MO Calculation Results

3.3.1. SiOH groups

The ^{1}H chemical shifts of SiOH groups in silicates have been the subject of a number of previous ab initio MO studies using clusters of various sizes (e.g., Fleischer et al., 1993; Xue and Kanzaki, 1998; Casanovas et al., 1999; Civalleri et al., 1999; Xue and Kanzaki, 2001). It is now clear from both ab initio calculations and experimental ^{1}H-NMR data (e.g., Yesinowski and Eckert, 1987; Eckert et al., 1988; Heidemann, 1994) that the ^{1}H chemical shifts for acidic OH groups (e.g., SiOH, POH and SOH) and molecular H_2O all show a general correlation with hydrogen bonding distance. One of the incentives of this study was to seek a theoretical understanding of the observed

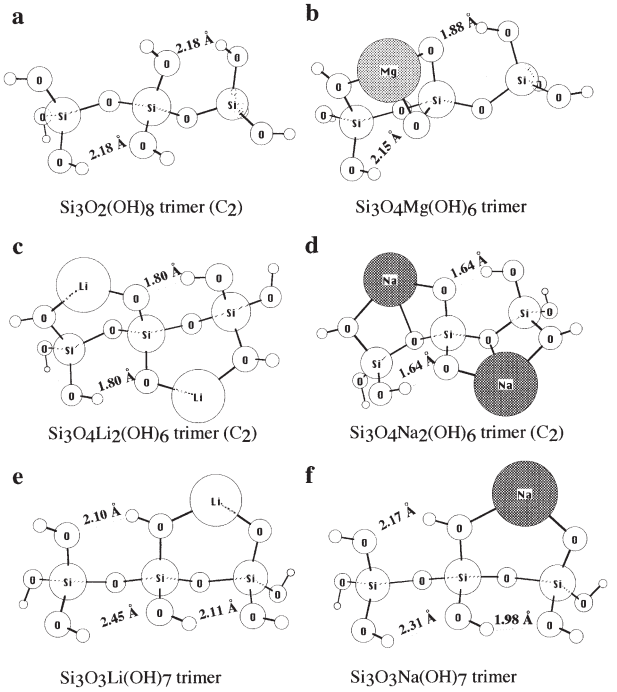

Fig. 17. Representative clusters modeling hydrogen-bonded SiOH groups in hydrous silica and alkali and alkaline earth silicates. All geometries were optimized at B3LYP/6-31+G(d,p). Unlabeled small open circles stand for hydrogen atoms. Numbers labeled are the H . . . O distances.

distributions in ^{1}H chemical shifts for SiOH groups in hydrous silica and alkali and alkaline earth silicate glasses containing different types of network-modifying cations as described in section 3.1.

3.3.1.1. SiOH groups in hydrous silica glasses. Clusters modeling SiOH groups in the SiO_2-H_2O system can be constructed by neutralizing linked SiO_4 tetrahedra of various sizes at the peripheries by protons (see Fig. 17a for an example). We have reported results for a number of such clusters in our previous papers (Xue and Kanzaki, 1998, 2001). While the main objective of those studies was to unravel the general correlation between the ^{1}H chemical shift and hydrogen bonding distance, we revisit this system here to evaluate the applicability of different models to hydrous silica glasses (and more generally to hydrous silicate glasses) in terms of hydrogen bonding strength.

Non-hydrogen-bonded SiOH groups in various clusters in the SiO_2-H_2O system, such as $Si_2O(OH)_6$ dimer and $Si_3O_2(OH)_8$ linear trimer optimized at B3LYP/6-31+G(d,p), yield ^{1}H chemical shifts in a small range between 2.1 and 2.3 ppm (Table 5). Similar ^{1}H chemical shifts (around 1.4 to 2.3 ppm) have been reported for non-hydrogen-bonded SiOH in clusters of various sizes in the SiO_2-H_2O system, calculated with robust basis sets similar to that used here for shielding and with a wider range of methods for geometry optimization (e.g., Fleischer et al., 1993; Xue and Kanzaki, 1998; Casanovas et al., 1999; Civalleri et al., 1999; Xue and Kanzaki, 2001). Hydrogen bonds of SiOH within a single cluster are in general relatively weak. For example, the O-H . . . O distances for hydrogen-

Table 5. Geometry parameters, and ^{1}H isotropic shielding (σ_i^H) and chemical shifts (δ_i^H) of OH groups in clusters optimized at B3LYP/6-31 + G(d,p). The shieldings were calculated at HF/6-311 + G(2df,p).

Cluster[a]	Linkage	R(O-H) (Å)	R(H . . . O) (Å)	R(O-H . . . O) (Å)	O-H . . . O angle (°)	σ_i^H (ppm)	δ_i^H (ppm)
TMS						32.1	0.0
$Si(OH)_4$ (S_4)	SiOH	0.964				29.8	2.3
$Si_2O(OH)_6$ dimer (C_2)	SiOH	0.964				29.8	2.3
SiOSi angle =	SiOH . . . O	0.969	2.39	3.14	134.01	28.8	3.3
128.21°	SiOH	0.964				29.9	2.2
$Si_3O_2(OH)_8$ linear	SiOH	0.964				29.9	2.2
trimer (C_2)	SiOH	0.965				29.6	2.5
SiOSi angle =	SiOH	0.964				30.0	2.1
138.19°	SiOH . . . O	0.970	2.18	2.98	138.55	28.3	3.8
$Si_3O_4Li_2(OH)_6$ linear	SiOH	0.964				29.9	2.2
trimer (C_2)							
SiOSi angle =	SiOH	0.965				29.8	2.3
119.52°	SiOH . . . O	0.998	1.80	2.73	153.16	23.5	8.6
$Si_3O_4Na_2(OH)_6$ linear	SiOH	0.964				30.1	2.0
trimer (C_2)							
SiOSi angle =	SiOH	0.964				30.1	2.0
123.18°	SiOH . . . O	1.018	1.64	2.61	157.81	20.7	11.4
$Si_3O_4K_2(OH)_6$ linear	SiOH	0.964				30.3	1.8
trimer (C_2)							
SiOSi angle =	SiOH	0.964				30.4	1.7
124.95°	SiOH . . . O	1.028	1.59	2.58	160.03	19.5	12.6
$Si_3O_4Mg(OH)_6$ linear	SiOH	0.964				30.2	1.9
trimer (C_2)	SiOH	0.964				29.6	2.5
SiOSi angles =	SiOH	0.963				30.1	2.0
114.05°, 130.14°	SiOH	0.968				29.0	3.1
	SiOH . . . O	0.983	1.88	2.78	151.58	25.4	6.7
	SiOH . . . O	0.976	2.15	2.82	124.88	27.4	4.7
$Si_3O_4Ca(OH)_6$ linear	SiOH	0.964				30.4	1.7
trimer (C_2)	SiOH	0.963				29.9	2.2
SiOSi angles =	SiOH	0.964				30.3	1.8
115.12°, 129.45°	SiOH	0.968				29.4	2.7
	SiOH . . . O	0.989	1.80	2.73	155.15	24.6	7.5
	SiOH . . . O	0.982	2.00	2.76	131.71	26.4	5.7
$Si_3O_3Li(OH)_7$ linear	SiOH	0.964				29.7	2.4
trimer	SiOH	0.964				30.3	1.8
SiOSi angle =	$Si^{center}OH$ . . . O(H)	0.975	2.11	2.92	139.71	27.2	4.9
124.28°, 126.62°	Si^{center}(Li)OH . . . O(H)	0.974	2.10	2.93	141.19	27.4	4.7
	SiOH	0.964				29.8	2.3
	SiOH	0.964				30.4	1.7
	$Si^{end}OH$ . . . O(H)	0.970	2.45	3.19	132.71	28.7	3.4
$Si_3O_3Na(OH)_7$ linear	SiOH	0.964				29.7	2.4
trimer	SiOH	0.964				30.4	1.7
SiOSi angle =	$Si^{center}OH$ . . . O(H)	0.978	1.98	2.82	143.07	26.4	5.7
125.47°, 129.01°	Si^{center}(Na)OH . . . O(H)	0.973	2.17	2.98	140.05	28.0	4.1
	SiOH	0.964				29.9	2.2
	SiOH	0.964				30.4	1.7
	$Si^{end}OH$ . . . O(H)	0.971	2.31	3.08	135.46	28.3	3.8
$Si_3O_3K(OH)_7$ linear	SiOH	0.964				29.8	2.3
trimer	SiOH	0.964				30.5	1.6
SiOSi angle =	$Si^{center}OH$ . . . O(H)	0.980	1.91	2.77	144.66	26.0	6.1
125.72°, 134.24°	Si^{center}(K)OH . . . O(H)	0.971	2.29	3.07	−137.24	28.6	3.5
	SiOH	0.964				30.0	2.1
	SiOH	0.964				30.4	1.7
	$Si^{end}OH$ . . . O(H)	0.972	2.27	3.05	136.61	28.3	3.9
$Mg^{VI}_{12}(OH)_{13}$	Mg^{VI}_3OH (central)	0.963				32.7	−0.6
(brucite-like cluster)	Mg^{VI}_3OH (2nd shell)	0.963				31.8	0.3
	Mg^{VI}_3OH (3rd shell)	0.970				31.7	0.4
	Mg^{VI}_3OH (3rd shell)	0.967				32.1	0.0
$(OH)Mg^{VI}_2Mg^{V}(OH)_3(OH_2)_9$	$Mg^{VI}_2Mg^{V}OH$	0.963				31.6	0.5
[+2]	Mg^{VI}_2OH	0.963				32.1	0.0
	$Mg^{VI}Mg^{V}OH$	0.962				32.1	0.0
	$Mg^{VI}Mg^{V}OH$	0.965				31.5	0.6
$(OH)Mg^{VI}_3(OH)_3(OH_2)_9$	Mg^{VI}_3OH	0.963	2.81	3.49	128.29	31.5	0.6
+ H_2O [+2]	Mg^{VI}_2OH	0.963				32.8	−0.7
	Mg^{VI}_2OH	0.960				32.1	0.0
	Mg^{VI}_2 OH	0.963				31.9	0.2

Table 5. (Continued)

Cluster[a]	Linkage	R(O-H) (Å)	R(H . . . O) (Å)	R(O-H . . . O) (Å)	O-H . . . O angle (°)	σ_i^H (ppm)	δ_i^H (ppm)
$(OH)Mg^{VI}Mg^{V}_2(OH)_3(OH_2)_5$	$Mg^{VI}Mg^{V}_2OH$	0.962				32.0	0.1
[+2]	$Mg^{VI}Mg^{V}OH$	0.963				31.9	0.2
	$Mg^{VI}Mg^{V}OH$	0.962				32.1	0.0
	Mg^{V}_2OH	0.961				31.9	0.2
$(OH)Mg^{V}_3(OH)_3(OH_2)_6$	Mg^{V}_3OH	0.962				32.1	0.0
[+2]	Mg^{V}_2OH	0.961				31.9	0.2
$(OH)Mg^{V}_3(OH)_3(OH_2)_6$ + OSi_2H_6[+2]	Mg^{V}_3OH . . . O	0.963	2.48	3.34	148.22	31.7	0.4
$OHMg^{IV}_3(OH_2)_9$ [+5] (C_3)	Mg^{IV}_3OH	0.976				31.9	0.2
$(OH)Mg^{IV}_2(OH_2)_6$ [+3] dimer(C_2)	Mg^{IV}_2OH	0.973				31.2	0.9
$(OH)Ca^{VI}_3(OH)_3(OH_2)_9$	Ca^{VI}_3OH	0.965				31.6	0.5
[+2]	Ca^{VI}_2OH	0.965				31.7	0.4
$(OH)Ca^{VI}_3(OH)_3$	Ca^{VI}_3OH . . . O	0.969	2.30	3.26	174.38	30.6	1.5
$(OH_2)_9$ + OSi_2H_6 [+2]	Ca^{VI}_2OH	0.965				31.6	0.5
$(OH)Li^{IV}_4(OH_2)_8$ [+3]	Li^{IV}_4OH	0.970				32.5	−0.4
$(OH)Li^{IV}_4(OH_2)_8$ + OSi_2H_6 [+3]	Li^{IV}_4OH . . . O	0.978	2.13	3.10	180.00	30.0	2.1
$(OH)Li^{IV}_2(OH_2)_6$ [+1] dimer (C_2)	Li^{IV}_2OH	0.965				32.2	−0.1
$(OH)Na^{V}_4(OH_2)_{12}$ [+3]	Na^{V}_4OH	0.968				34.4	−2.3

[a] Numbers in square brackets are the net cluster charges.

bonded SiOH in $Si_2O(OH)_6$ dimer and $Si_3O_2(OH)_8$ linear trimer clusters are 3.14 and 2.98 Å at B3LYP/6-31+G(d,p), corresponding to ^{1}H chemical shifts of 3.3 and 3.8 ppm, respectively (see Fig. 17a and Table 5).

These calculation results can be compared with experimental NMR data for hydrous silica glasses and silica gels. The reported ^{1}H MAS NMR data for hydrous silica glasses containing 0.12 to 2.5 wt% H_2O all contain peaks near 2.8 to 3.3 ppm attributable to SiOH groups (Kohn et al., 1989a; Zeng et al., 1999b). The ^{1}H CRAMPS spectra of silica gels yield a sharp peak near 1.7 ppm and an asymmetric peak near 3.0 ppm, which have been attributed, respectively, to isolated and hydrogen-bonded SiOH groups on the surface (e.g., Bronnimann et al., 1988). Thus, whereas isolated silanols on the surface of silica gels yield ^{1}H chemical shifts (near 1.7 ppm) similar to those calculated for non-hydrogen-bonded SiOH, silanols in hydrous silica glasses yield larger ^{1}H chemical shifts (2.8 to 3.3 ppm) indicative of some hydrogen bonding. The lack of non-hydrogen-bonded SiOH groups in silica glasses could be a natural consequence of protons being in the neighborhood of other oxygens in the bulk glass structure. In another word, protons in the bulk glass structure must have some interaction, weak or strong, with neighboring oxygens, so that isolated hydrous species is not applicable. The ^{1}H chemical shifts of hydrogen-bonded SiOH groups in the calculated clusters are in good agreement with those of hydrous silica glasses.

3.3.1.2. SiOH groups in hydrous alkali and alkaline earth silicate glasses. As shown in section 3.1 and also pointed out by previous NMR and vibrational spectroscopic studies (e.g., Scholze, 1959a,b; Kohn et al., 1989a; Zotov and Keppler, 1998), hydrogen bonds for SiOH groups in alkali and alkaline earth silicate glasses are in general stronger than those in hydrous silica glasses, and the relative population of strong hydrogen bonds also increase with decreasing field strength of network-modifying cations. This fact has often been postulated to be related to the presence of nonbridging oxygens (e.g., Scholze, 1959b; Wu, 1980; Kohn et al., 1989a). Strongly hydrogen-bonded SiOH groups are also common in crystalline silicates, especially those containing large alkali metals such as Na and K (see examples in Table 3). The more systematic and gradual variations in hydrogen bonding strength with compositions for SiOH groups in glasses than in crystalline phases may be related, in part, to the lack of long-range order in the former that removes constraints imposed by the requirements of strict periodicity on bond lengths and angles, so that the range of these parameters in glasses may better reflect those determined by local bonding requirements and thus may be more directly comparable to results from ab initio calculations for small clusters (cf. Navrotsky et al., 1985). In this section, we present calculation results for SiOH groups in clusters that contain nonbridging oxygens, and compare them with experimental observations.

In silicate crystals and also likely in glasses, nonbridging oxygens are in general coordinated to three or more network-modifying M cations in addition to a Si; the M cations normally have greater oxygen coordination numbers than Si, due to more ionic characters of the M-O bonds. Much large clusters than described in the previous section are necessary if the complete oxygen coordinations of both Si and M cations are included. However, because we are mainly interested in the effect of nonbridging oxygens on the hydrogen bond forming tendency and ^{1}H chemical shifts of SiOH groups, but not the NMR parameters of nonbridging oxygens themselves, a simplified model should be useful at least semiquantitatively. The approach adopted here as well as in a number of previous studies (e.g., de Jong and Brown, 1980; Uchino et al., 1991; e.g., Uchino et al., 1992a,b) is to include only sufficient number of M cations to satisfy the charge requirement of the nonbridging oxygens (e.g., 1 Na per NBO, 1 Mg for every two NBO's), without trying to complete the oxygen coordination sphere of the M cations. In the optimized structure, each nonbridging oxygen is coordinated to only one M cation, and each M cation is coordinated to two or three oxygens.

Two factors may conceivably contribute to the enhanced hydrogen bonding of a SiOH group in hydrous alkali and

alkaline earth silicates: one is the presence of nonbridging oxygens as good hydrogen-bond acceptor (SiOH . . . O_{nbr}), and the other is the direct coordination of a M cation to the oxygen in the SiOH group (Si(M)OH). We have adopted two series of linear trimer clusters to evaluate each of these factors. One set of clusters is $Si_3O_4M_n(OH)_6$ (where $n = 1$ for alkaline earth cations, and 2 for alkali cations), in which two oxygens of the central SiO_4 tetrahedron are nonbridging oxygens, and two of the SiOH groups from the two end SiO_4 tetrahedra each form hydrogen bonding with a nonbridging oxygen (see Fig. 17b, c and d for examples). This type of hydrogen bonding resembles those observed in minerals, such as $Ca_3Si_3O_8(OH)_2$ rosenhahnite (Wan et al., 1977). We have systematically varied the type of M cations (K, Na, Li, Ca to Mg), and the calculation results are tabulated in Table 5. The hydrogen bonding distances between the SiOH group and the nonbridging oxygen in the optimized clusters are in general shorter than those between two SiOH groups in the $Si_3O_2(OH)_6$ trimer, a crude model for hydrous silica glasses. There is also a general trend of decreasing hydrogen bonding distances with decreasing field strength of the M cations (H > Mg > Ca > Li > Na > K) (Table 5 and Fig. 17). The ^{1}H chemical shifts of these SiOH groups increase systematically from 3.8 ppm for M = H, to 4.7~6.7 ppm for M = Mg, to 5.7~7.5 ppm for M = Ca, and to 11.4 ppm for M = Na (Table 5). This qualitatively reproduces the trend shown for SiOH groups in silica and binary alkali and alkaline earth silicate glasses.

To evaluate whether SiOH groups with their oxygens coordinated to M cations (Si(M)OH) can also produce the observed trend for glasses, we have also performed calculations for another series of linear trimer clusters, $Si_3O_3M(OH)_7$ (where M = Li, Na, K), in which a nonbridging oxygen resides on an end SiO_4 tetrahedron, and a SiOH group from the middle SiO_4 tetrahedron has its oxygen coordinated to the M cation (see Fig. 17e and f for examples). Our calculation revealed that although the coordination of a M cation to the oxygen in the SiOH group does induce hydrogen bonding (Si^{center}(M)OH . . . O(H) in Table 5), such hydrogen bonds are relatively weak, and with decreasing field strength of the M cation, there is a small increase in the O-H . . . O distance, and a slight decrease in the ^{1}H chemical shift of the Si(M)OH group (4.7 ppm for M = Li, 4.1 ppm for M = Na, and 3.5 ppm for M = K), opposite to the trend observed for alkali and alkaline earth silicate glasses. This suggests that direct bonding of SiOH groups to M cations cannot be the principle factor for the observed trend of hydrogen bonding with cation types. In this series of clusters, another SiOH group on the central SiO_4 tetrahedron forms a hydrogen bond with a SiOH from the end SiO_4 tetrahedron that contains the nonbridging oxygen (Si^{center}OH . . . O(H) in Table 5; also see Fig. 17e and f). The hydrogen bonding distance decreases and the ^{1}H chemical shift increases moderately with decreasing field strength of the M cations (4.9 ppm for M = Li, 5.7 ppm for M = Na, and 6.1 ppm for M = K). Thus, not only nonbridging oxygens, but also other oxygens bonded to the same Si as nonbridging oxygens can serve as hydrogen-bond acceptors, contributing to the observed trend of hydrogen bonding with cation type, although such hydrogen bonds are weaker than those formed directly with nonbridging oxygens. This observation may be attributed to the nonlocalized effect of M cations, i.e., the presence of a M cation not only affects the electronic state of the oxygen to which it is directly bonded (NBO), but also induce electron redistributions on oxygens that are bonded to the same Si as the NBO, enhancing its hydrogen-bond accepting ability. The nonlocalized effect of M cations has previously also been invoked to account for the bond length (strength) variations of bridging and nonbridging oxygens bonded to a common Si (M-O_{nbr}-Si-O_{br}-Si-) (oscillation pattern of bond energies): the weaker the M-O bonds, the stronger the adjacent Si-O_{nbr} bond, and the weaker the next Si-O_{br} bond (e.g., de Jong and Brown, 1980; Uchino et al., 1991, 1992b). We have also observed similar patterns for Si-O bond lengths in the clusters described in our study. It may be a general quantum chemical phenomenon related to the nonlocalized nature of electron distributions.

In brief, our calculations confirmed that hydrogen bonding between SiOH and nonbridging oxygens is the principle factor for the increasing tendency for strong hydrogen bonding with decreasing cation field strength. Direct coordination of M cations with the oxygens in SiOH groups may enhance the hydrogen bond formation, but cannot be the principle cause for strong hydrogen bonding. Interactions between SiOH and oxygens bonded to the same Si as nonbridging oxygens may also result in moderate hydrogen bonding. These factors could altogether contribute to the range of strength of hydrogen bonding observed for SiOH groups in silicate glasses.

The H . . . O hydrogen bond is generally regarded to be formed through interaction between hydrogen (electron acceptor) and the lone electron pair on oxygen (electron donor) (e.g., Pimentel and McClellan, 1960). Consider an A-O1-H . . . O2-BC pair, where A is a cation coordinated to an oxygen, O1, and B and C are cations coordinated to an oxygen, O2. The tendency for hydrogen bonding can be related to the Lewis acidity (basicity) of the cations, defined as the tendency of the cations to attract the lone electron pair on oxygen to form covalent bonds. The stronger the basicity of cation B (or C) is, the greater the tendency is for O2 to share its lone electron pair with a neighboring hydrogen to form hydrogen bond. This would be consistent with the trend of strong hydrogen bonding between SiOH and nonbridging oxygens of cations with low field strength described above. On the other hand, the stronger the acidity of cation A is, the greater the extent of the lone electron pair on O1 is attracted to cation A than to the hydrogen, and thus the greater the tendency is for the hydrogen to form hydrogen bond with a neighboring oxygen, O2. This is in accord with the observation for crystalline phases that A cations of large field strength, such as Si, P and S, are among those that form the strongest hydrogen bonds; whereas A cations of low field strength, such as alkali and alkaline earth cations, do not tend to form hydrogen bonding (see the next section). These trends may also be regarded as a manifestation of the general phenomenon of nonlocalized electron distributions described above.

The SiOH groups in the clusters considered here show a general trend of decreasing ^{1}H chemical shift with increasing H . . . O and O-H . . . O distances (Fig. 18), consistent with previous ab initio calculation results (Xue and Kanzaki, 1998, 2001). These results are also in good agreement with experimental data for SiOH groups in crystalline silicates (Fig. 18). A linear correlation for ^{1}H chemical shift over the entire range of O-H . . . O distances is often adopted to estimate the

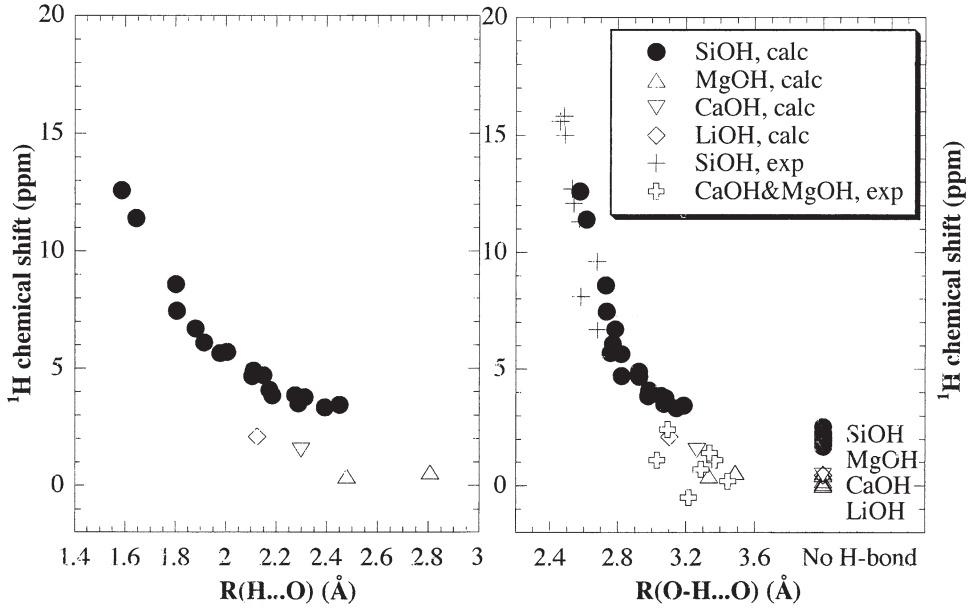

Fig. 18. ^{1}H chemical shift as a function of H . . . O and O-H . . . O distances for SiOH and free hydroxyl (CaOH, MgOH, and LiOH) groups calculated for small clusters (Table 5). Also shown for comparison are experimental data for SiOH, CaOH and MgOH groups in crystalline silicate, phosphate and hydroxide phases (see Table 3).

O-H . . . O distances of OH groups (e.g., Yesinowski and Eckert, 1987). However, our present and previous calculation results clearly indicate that the slope decreases below ~5 ppm (Fig. 18) (also see Xue and Kanzaki, 1998, 2001). Such a change in slope is difficult to discern from experimental data because very few data for crystalline phases are available for SiOH groups within the weak hydrogen bonding region. The smaller slopes render the ^{1}H chemical shift parameter less sensitive to hydrogen bonding distance within the range of weak hydrogen bonding. Furthermore, as will be illustrated below, the effect of cation type on ^{1}H chemical shift becomes significant within this range.

3.3.2. *Free hydroxyl groups*

We have constructed various clusters to simulate the geometries of free hydroxyl groups in silicates. We have referred to such groups simply as MOH thus far, but some clarification is demanding at this point. Like nonbridging oxygens that are often expressed as SiOM, oxygens in free hydroxyl groups are normally coordinated to two or more M cations, because of the ionic character of M-O bonds. In the rest of this paper, we will continue to refer to free hydroxyl groups simply as MOH for general discussions, but will use $(OH)M_n$ or M_nOH (where n stands for the number of M cations coordinated to OH) when their local structures are of concern. Unlike the preceding section for SiOH in depolymerized silicates, we are now interested in the NMR characteristics of free hydroxyls themselves, so it is important to accurately reproduce the local structures. For cations such as Si, it is known that the chemical shift is dominated by the first neighbor environments and to a lesser extent by the second neighbors and beyond. For example, ab initio calculations on Si-centered clusters modeling SiO_2 polymorphs have revealed that inclusion of the correct first neighbors (Si^{center}-O) are essential to produce approximate values of ^{29}Si chemical shifts, and inclusion of the complete third-neighbor (Si^{center}-O-Si-O) shells (the complete SiO_4 neighbors to the central SiO_4) accurately reproduces the ^{29}Si chemical shifts of the central Si (Xue and Kanzaki, 2000). If the ^{1}H chemical shift behaves analogously, H-centered clusters with appropriate representation of the oxygen coordinations of M cations in a $(OH)M_n$ group could be reasonable. In crystalline hydrous silicates, phosphates (for Ca and Mg), and hydroxides (for Ca, Mg, Li and Na), the oxygen coordination numbers of M cations in $(OH)M_n$ groups are normally four for Li, five for Na, six for Mg and six or higher for Ca, and the number of M cations (n) that are coordinated to each OH group is generally three for Mg and Ca, and four or larger for Li and Na. Similar and perhaps more flexible oxygen and M cation coordinations may be expected for free hydroxyls in silicate melts and glasses. We have simulated clusters containing OH groups linked to three Mg's of four-, five- and six-oxygen coordinations (Mg^{IV}, Mg^{V} and Mg^{VI}), to three Ca's of six oxygen coordinations (Ca^{VI}), to four Li's of four oxygen coordinations (Li^{IV}), and to four Na's of five oxygen coordinations (Na^{V}). These clusters are terminated mostly by OH_2 at the peripheries. Some examples are shown in Figure 19 and a full list can be found in Table 5. A $(OH)Mg_3$-centered cluster started with three edge-sharing MgO_6 octahedra, similar to those in the $Mg(OH)_2$ brucite structure, ended up as $(OH)Mg_2^{VI}Mg^{V}$ because one of the peripheral H_2O is no longer connected to Mg in the optimized structure (see Fig. 19b). A $(OH)Ca_3^{VI}$-centered cluster of similar geometry, on the other hand, remains stable after optimization at B3LYP/6-31+G(d,p) (see Fig. 19e). While it is most likely that free hydroxyl groups are coordinated to three or more M cations, we have also constructed clusters containing two corner-sharing MgO_4 or LiO_4 clusters ($(OH)Mg_2^{IV}$ and $(OH)Li_2^{IV}$)

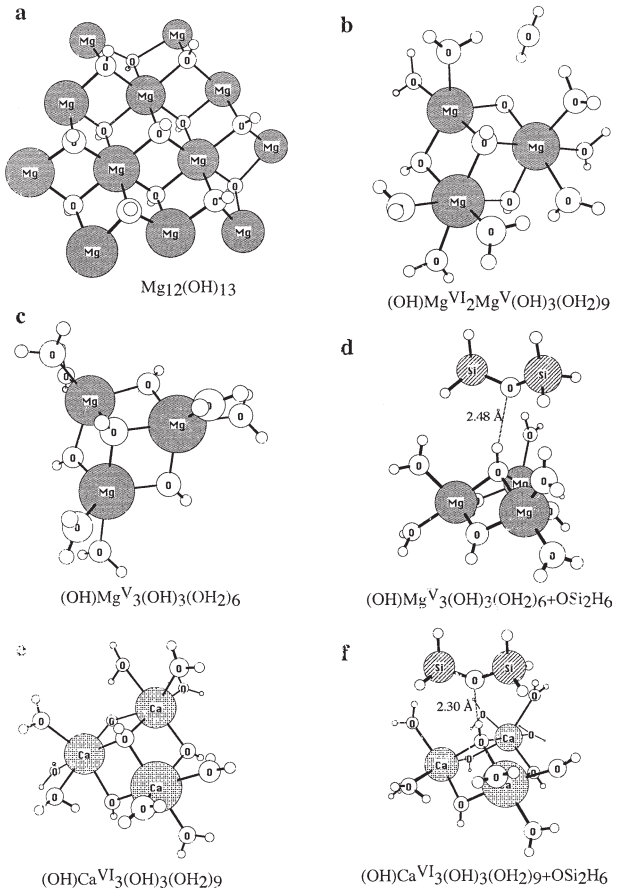

Fig. 19. Representative clusters modeling isolated and hydrogen-bonded free hydroxyl groups bonded to different cations. All geometries were optimized at B3LYP/6-31+G(d,p). Unlabeled small open circles stand for hydrogen atoms. Numbers labeled are the H . . . O distances.

to evaluate the effect of the cation coordination numbers of oxygens on the ^{1}H chemical shifts of free hydroxyls (Table 5). Some of the (OH)Mg_3- and (OH)Ca_3-centered clusters ((OH)$M_3(OH)_3(OH_2)_m$) also contain non central OH groups that are shared by two M cations (see Fig. 19b to f). To test the effect of terminating atoms on the ^{1}H-NMR chemical shift of the central (OH)M_n group, we have also constructed a cluster ($Mg_{12}(OH)_{13}$) that is more representative of a fragment of the brucite structure. All the OH groups in this cluster have a (OH)Mg_3 configuration and the peripheral Mg atoms (forth neighbors to the central H) have incomplete oxygen coordination (Fig. 19a). The ^{1}H chemical shifts of the central (OH)M_n groups in all the clusters show only a limited range of values: −0.6 to 0.9 ppm for (OH)Mg_3 and (OH)Mg_2, regardless of Mg and O coordination numbers; 0.5 ppm for (OH)Ca_3, −0.1 to −0.4 ppm for (OH)Li_4 and (OH)Li_2, and −2.3 ppm for (OH)Na_4. Even the edge-sharing (OH)Mg_2 and (OH)Ca_2 linkages (third-neighbor oxygens to the central H) in the (OH)$M_3(OH)_3(OH_2)_n$ clusters (see Fig. 19b,c and e) and all the noncentral (OH)Mg_3 groups in the $Mg_{12}(OH)_{13}$ brucitelike cluster, yield similar ^{1}H chemical shifts (Table 5). Therefore the ^{1}H chemical shifts of non-hydrogen-bonded (OH)M_n groups of alkali and alkaline earth cations are relatively insensitive to the coordination numbers of M cations or the connectivity of the MO_x polyhedra.

To simulate hydrogen-bonded free hydroxyl groups, we have attempted to construct clusters of (OH)M_n groups freely interacting with H_2O, bridging oxygen (OSi_2H_6), SiOH or nonbridging oxygen. However, with the exception of bridging oxygen, these other molecules tend to migrate away from the central OH group to coordinate to a M cation, or to form hydrogen bond with a peripheral OH_2 group, upon geometry optimization. Representative clusters of hydrogen-bonded M_nOH . . . OSi_2 groups are shown in Figure 19d and f, and their geometries and ^{1}H chemical shifts are tabulated in Table 5. Despite the net positive charge for these clusters, which is expected to enhance hydrogen bonding, the resultant hydrogen bonds are in general very weak. The O-H . . . O distances of the hydrogen-bonded (OH)M_n groups are between 3.1 and 3.9 Å, and their ^{1}H chemical shifts are between 0.4 and 2.1 ppm, only moderately larger than those without hydrogen bonding (Table 5).

In Table 3, we have tabulated the reported ^{1}H chemical shifts for CaOH and MgOH groups in crystalline hydrous silicate, phosphate and hydroxide phases stable near ambient pressure for comparison. Almost all the data fall in the range of −0.8 to 2.4 ppm (with one at 4.1 ppm). MgOH groups in hydrous magnesium silicates synthesized at pressures greater than 10 GPa (phases A, B and superhydrous B) are known to form somewhat stronger hydrogen bonds and correspondingly yield larger ^{1}H chemical shifts (3.7 to 5.0 ppm) (Phillips et al., 1997; Kagi et al., 2000), possibly as a result of increased density at high pressure. The results for low-pressure minerals are probably more relevant to the present discussion. Our calculated ^{1}H chemical shift values for CaOH and MgOH groups are in good agreement with the experimental data for low-pressure crystalline phases. MOH groups of alkali cations, such as NaOH and LiOH, are common in alkali hydroxides and hydroxide hydrates, and are known not to form hydrogen bonding with other oxygens (cf. Wells, 1986). Dupree et al. (1990) has reported ^{1}H MAS NMR results for a crystalline LiOH·H_2O sample. The spectrum consists of a broad peak centered at ~4.6 ppm with extensive spinning sidebands due to strong homonuclear H-H dipolar interactions. Fourier transform from the second rotational echo resulted in a narrower peak centered at 5.0 ppm, which was assigned to LiOH by the authors. However, a close inspection reveals that the peak actually has a pronounced shoulder to lower frequency (near ~0 ppm). In the crystal structure of LiOH·H_2O, each hydrogen in molecular H_2O forms a hydrogen bond with LiOH (Alcock, 1971). Thus, molecular H_2O is expected to yield larger ^{1}H chemical shifts than LiOH. It is more likely that the main peak near 5.0 ppm is due to H_2O, and the smaller shoulder near 0 ppm is due to LiOH. Our calculation results for LiOH (−0.4 to 2.1 ppm) are thus in agreement with the experimental data.

In Figure 18 we have plotted the ^{1}H chemical shift vs. O-H . . . O distance for both MOH and SiOH groups from our calculations and experimental data for crystalline phases for comparison. Clearly, the data for MOH groups are clustered near weak to very weak hydrogen bonding region, and yield lower ^{1}H chemical shifts than the correlation defined by SiOH groups. Whereas the ^{1}H chemical shifts for SiOH groups seem to converge toward values (1.7 to 2.3 ppm) for non-hydrogen-

bonded SiOH groups; those of MOH groups converge toward lower values (−2.3 to 0.6 ppm) for non-hydrogen-bonded MOH groups. This is an important point often overlooked. Although within the region of strong to very strong hydrogen bonding, the hydrogen bonding distance is the dominant factor in controlling the ^{1}H chemical shifts of all OH groups and molecular H_2O, its effect becomes secondary within the region of weak to very weak hydrogen bonding (below ~5 ppm). ^{1}H chemical shifts within the latter region should be particularly informative about the type of OH groups.

In summary, our calculation results are in good agreement with experimental data for crystalline phases, and both suggest that (1) free hydroxyls of alkali and alkaline earth cations do not have strong tendency for hydrogen bonding, and yield smaller ^{1}H chemical shifts than SiOH groups; (2) within the region of weak to very weak hydrogen bonding (below ~5 ppm), the nature of cations bonded to the OH groups plays a large role in determining the ^{1}H chemical shifts, so that any attempt to estimate the O-H . . . O distance from ^{1}H chemical shifts alone without due consideration of the nature of the cations could be misleading.

4. DISCUSSION

4.1. Interpretations of the ^{1}H MAS NMR Spectra

In light of the above ab initio calculation results, we revisit the issue of peak assignments for the ^{1}H MAS NMR spectra of hydrous silicate glasses presented in section 3.1. Let us first consider the assignment of the major peak near 1.2 to 1.5 ppm in the ^{1}H MAS NMR spectra of hydrous CMS glasses. Among the three possible candidates, molecular H_2O, SiOH and MOH groups, molecular H_2O can be excluded because this peak gives very weak spinning sidebands, indicative of weak H-H dipolar interactions. The possibility of contribution from SiOH groups can be evaluated in the context of hydrogen bonding. As inferred in section 3.3, some interaction between protons and neighboring oxygens, whether weak or strong, is expected for all hydrous species in the bulk structure of silicate glasses; therefore isolated SiOH groups, although known to yield ^{1}H chemical shifts near this region, is not applicable. Furthermore, because the hydrogen bonding strength of SiOH groups tends to be enhanced by the presence of nonbridging oxygens, we may take the ^{1}H chemical shifts of SiOH groups in hydrous silica glasses (2.7 to 3.3 ppm: Kohn et al., 1989a; Zeng et al., 1999b) as the minimum limit for those of depolymerized alkali and alkaline earth silicate glasses. This suggests that the peak near 1.2 to 1.5 ppm is unlikely to be due to SiOH groups. On the other hand, there are compelling evidences for the assignment of this peak to free hydroxyl groups. As is clear from both ab initio calculations and experimental ^{1}H-NMR data for crystalline phases, free hydroxyl groups of alkali and alkaline metals are not in favor of strong hydrogen bonding, and give ^{1}H chemical shifts around this range. We are thus confident that the peak near 1.2 to 1.5 ppm observed for hydrous CMS glasses can be best assigned to the (Ca,Mg)OH, free hydroxyl groups. The relative abundance of free hydroxyls in these glasses increases systematically with increasing NBO/T and decreasing Ca/(Ca + Mg) ratio. For the hydrous $Na_2Si_4O_9$, $Na_2Si_2O_5$, $Li_2Si_2O_5$ and $Na_2CaSi_4O_{10}$ glasses, intensities near this region are weak, suggesting that the abundances of NaOH, LiOH and (Ca,Na)OH free hydroxyl groups in the them are minor, if any. These compositional variations are consistent with more favorable formation of free hydroxyls by (1) more depolymerized melts, and (2) network-modifying cations of higher field strength (Mg > Ca > Li, Na).

The above argument does not imply that all ^{1}H-NMR peaks with small chemical shifts are due to free hydroxyl groups, or vice versa. For example, for aluminosilicate compositions, the ^{1}H-NMR characteristics of OH groups involving aluminum must also be considered. Our previous ab initio calculations (Xue and Kanzaki, 2001) have shown that $Al^{IV}OH$ groups (Al^{IV}: tetrahedral Al) are also among those that do not have strong tendency for hydrogen bonding and yield smaller ^{1}H chemical shifts than SiOH groups (around 0 to 2.5 ppm for weakly hydrogen-bonded $Al^{IV}OH$ groups, and −2 to 0 ppm for non-hydrogen-bonded $Al^{IV}OH$ groups). A ^{1}H-NMR peak near 1.5 ppm has been previously identified for alkali aluminosilicate glasses and was found to grow with increasing $NaAlO_2$/SiO_2 ratio for the $NaAlO_2$-SiO_2 system (Zeng et al., 1999a; Schmidt et al., 2001). From the ab initio calculation results alone, this peak could be attributed to either $Al^{IV}OH$ or NaOH (and KOH) groups, but not SiOH as argued by some (e.g., Liu et al., 2002). Considering the experimental results for aluminum-free silicate glasses from the present study, it is most likely that this peak is due to $Al^{IV}OH$ groups, supporting the earlier interpretations (Zeng et al., 1999a; Schmidt et al., 2001). On the other hand, the hydrogen bond forming tendency of MOH groups are expected to increase with further increase in the field strength of the M cations. For example, $Zn^{IV}OH$ and $Al^{VI}OH$ groups (Zn^{IV}: tetrahedral Zn; Al^{VI}: octahedral Al) in hydroxides ($Zn(OH)_2$ and $Al(OH)_3$) and oxyhydroxides (AlOOH) are known to form moderate hydrogen bonding (cf. Wells, 1986). The observed greater tendency of hydrogen bond formation for $Al^{VI}OH$ than for $Al^{IV}OH$ is possibly related to the number of aluminum coordinated to each OH (two or three for the former, and one for the latter). Finally, at very high pressure when the densities of silicate melts are substantially increased, the hydrogen bonding distances and accordingly the ^{1}H chemical shifts of all water species may increase to some extent.

As described in section 3.1, peaks between 4 to 17 ppm are also observed in the ^{1}H MAS NMR spectra of hydrous alkali and alkaline earth silicate glasses of all compositions. Intensities near 4 to 6 ppm may be partly due to molecular H_2O, because they demonstrate features indicative of strong H-H dipolar interaction. The remaining intensities in the 4 to 17 ppm region can be attributed to OH groups. From similar argument to that developed above, we may infer that these OH groups are dominantly SiOH groups, rather than free OH groups, at least for alkali and alkaline earth silicate systems. The observed changes in peak shape within this region largely reflect changes in the distribution of hydrogen bonding distances for the SiOH groups. The relative population of strong to very strong hydrogen bonding (8 to 17 ppm region) increases systematically with decreasing field strength of the network-modifying cation. It is worth mentioning that IR and Raman spectroscopic techniques are also often applied to gain information about hydrogen bonding, on the basis of similar correlations between O-H stretching frequency and hydrogen-bonding distances as ^{1}H

chemical shift (e.g., Nakamoto et al., 1955; Novak, 1974). Particularly when strongly hydrogen-bonded hydroxyl groups are present, ^{1}H MAS NMR is more advantageous, because whereas the peak shape in ^{1}H MAS NMR directly reflects the distribution of O-H . . . O distances (by a linear factor), the region of O-H stretching vibrations for strongly hydrogen-bonded hydroxyls in IR and Raman spectra (below ~2800 cm^{-1}) tends to be complicated by strong anharmonicity and possible Fermi resonance interactions between OH stretching bands and bending overtones (e.g., Novak, 1974). Until the recent work of Zarubin (1999), such problems had been neglected in almost all the IR and Raman studies of silicate glasses.

4.2. Water Dissolution Mechanisms in Depolymerized Silicate Melts and Glasses

As outlined in the Introduction, the dissolution mechanisms of water in silicate melts have been the subject of extensive past studies and discussions. The experimental and ab initio calculation results from our study place new constraints that allow us to evaluate and systematize the various models proposed thus far. Our study clearly indicates that substantial parts of the dissolved water in quenched hydrous CMS melts are in the form of (Mg,Ca)OH free hydroxyl groups, in addition to SiOH groups and molecular H_2O, and the distribution of these water species are dependent on the melt composition. These speciation distributions largely reflect those of the corresponding melts near Tg. Below we discuss the relations among these hydrous species and the network structure in alkali and alkaline earth silicate melts in terms of compositional variations, assuming that the temperature effect due to possible variations in Tg is secondary.

For anhydrous metal oxide-silica melts, the following homogeneous reaction expresses the relations among bridging oxygens, nonbridging oxygens and free oxygens in the melt:

$$\text{SiOSi (melt)} + \text{MOM (melt)} = 2\ \text{SiOM (melt)} \qquad (1)$$

Here MOM is a longhand form of free oxygen, and carries no connotations of the coordination number of the oxygen. The equilibrium constant of this reaction can be expressed as the following:

$$K_1 = [\text{SiOM}]^2/[\text{SiOSi}][\text{MOM}]$$

where [SiOM], [SiOSi] and [MOM] stand for the activities of the respective oxygen species. Numerous studies have indicated that reaction 1 is favored to the right (i.e., greater K_1) with decreasing field strength for the network-modifying cations from Mg to Na (see reviews in Fraser, 1977; Hess, 1995; Navrotsky, 1995). This compositional dependence may be a combined effect of (1) less stability of free oxygens that are coordinated only with cations of lower field strength, due to the unsatisfied bond valence requirement of oxygens, and (2) greater weakening of the Si-O-Si bonds due to the nonlocalized effect of cations of lower field strength, as suggested by previous semiempiric and ab initio MO calculations (e.g., de Jong and Brown, 1980; Uchino et al., 1991, 1992b) and also described in section 3.3.1.2 (also see Ryerson, 1985). An equivalent view is in terms of acid-base reaction. According to the Lux-Flood concept, a basic oxide is an oxide that readily provides O^{2-} ions (e.g., MO, M_2O), and an acidic oxide is one that reacts with O^{2-} (e.g., SiO_2) (cf. Fraser, 1977). Like ordinary protonic acid-base systems, reaction 1 between acidic (SiO_2) and basic (MO, M_2O) oxides proceeds further to completion for more basic oxides (see Fraser, 1977). The abundances of free oxygens in anhydrous alkali and alkaline earth silicate melts and glasses with the range of silica contents studied here are generally regarded to be small. For sodium silicate glasses, free oxygens have been confirmed to be negligible from both estimations of bridging and nonbridging oxygen abundances using O1s X-ray photoelectron spectroscopy (XPS) (e.g., Bruckner et al., 1980; Goldman, 1986) and estimations of Q^n distribution using ^{29}Si MAS NMR (e.g., Maekawa et al., 1991). For alkaline earth silicate glasses, however, peaks in both types of spectra are unresolved (e.g., Murdoch et al., 1985 for NMR, also see section 3.2.1.; Hochella and Brown, 1988 for XPS), rendering them insensitive to small amounts of free oxygens. Analysis of a two-dimensional ^{29}Si MAS NMR spectrum of a $CaSiO_3$ glass yielded a Q^n speciation distribution that corresponds to a bulk Ca/Si ratio of 0.972 ± 0.006, somewhat lower than that analyzed by EPMA (0.99 ± 0.01), which may be an indication of a small fraction (~1%) of the oxygens present as free oxygens (Zhang et al., 1997). For more depolymerized CMS glasses, there are stronger evidences for the presence of free oxygens. Raman studies of Mg_2SiO_4-$CaMgSiO_4$ glasses (Mysen et al., 1980a; McMillan, 1984; Cooney and Sharma, 1990) and a ^{29}Si-NMR study of Mg_2SiO_4 glass (Tangeman et al., 2001) all revealed an asymmetric peak that may contain components for not only Q^0 species, but also more polymerized species; the presence of the latter requires simultaneous occurrence of some free oxygens. It is likely that free oxygens are also present, though only in small amounts, in the more silica-rich anhydrous CMS glasses investigated in our study.

The dissolution of water in silica melts can be expressed by the following familiar homogeneous reaction described by Stolper (1982a)

$$\text{SiOSi (melt)} + H_2O\ \text{(melt)} = 2\ \text{SiOH (melt)} \qquad (2)$$

with an equilibrium constant, $K_2 = [\text{SiOH}]^2/[\text{SiOSi}][H_2O]$. Reaction 2 is analogous to reaction 1 in a sense that both cause rupture of the silicate network structure. In fact, H_2O can be regarded as the very large field strength extreme of the M_2O series (a very weak base).

The dissolution of water in metal oxide-silica melts may involve multiple reactions, because water could interact with either the silica or the metal oxide component. For the former, a reaction analogous to 2 may be invoked to account for the formation of SiOH groups. This reaction may be responsible for the observed depolymerization of sodium- and sodium-calcium-silicate glass structure with water dissolution. Although reaction 2 does not explicitly include species of network-modifying cations or nonbridging oxygens, the presence of the latter may affect the reaction indirectly in two ways. Firstly, strong hydrogen bonding interaction may enhance the stability of SiOH groups (e.g., Kurkjian and Russell, 1957; Wu, 1980). SiOH groups in metal oxide-silica glasses are involved in much stronger hydrogen bonding than those in silica glasses

because of the presence of nonbridging oxygens, and the population of strong hydrogen bonding increases with decreasing field strength of the network-modifying cation from Mg to Na. Secondly, as discussed for reaction 1, the Si-O-Si bonds in metal oxide-silica glasses may be weakened due to the nonlocalized effect of M cations. Both factors would result in greater equilibrium constant K_2 for metal oxide-silica melts than for silica melts, and greater K_2 for metal cations with smaller field strength. Previous IR spectroscopic studies have reported that the OH/H_2O ratios are greater in alkali-dominated silicate glasses than in silica glasses (e.g., Acocella et al., 1984; Zotov and Keppler, 1998; Behrens and Stuke, 2003), consistent with this trend.

The interaction between water and metal oxide component in metal oxide-silica melts can be expressed by the following homogeneous reaction between free oxygens and H_2O in the melt structure:

$$\text{MOM (melt)} + H_2O\text{ (melt)} = 2\text{ MOH (melt)} \quad (3)$$

with an equilibrium constant $K_3 = [MOH]^2/[MOM][H_2O]$. The formation of MOH has previously been suggested to become favorable in more basic silicate melts, out of the expectation that H_2O may show amphoteric properties and switches role from a basic oxide in reaction 2 for relatively acidic melt compositions, to an acidic oxide in reaction 3 for more basic melt compositions (e.g., Uys and King, 1963; Fraser, 1977). Uys and King (1963) further suggested that strong bases are also those that form stable hydroxides from oxides, and thus have greater tendency to form stable MOH groups in silicate melts. Indeed, a compilation of more recent data (cf. Chase, 1998) for the standard enthalpies of formation of hydroxides from oxides ($M^{2+}O$ (crystalline) + H_2O (gas) = $M^{2+}(OH)_2$ (crystalline) or $M^{+}{}_2O$ (crystalline) + H_2O (gas) = $2M^{+}OH$ (crystalline)) at 298.15 K (ΔH^0) shows greater stability of hydroxides for cations with lower field strength ($\Delta H^0 = -81.6$ kJ/mol for Mg, -109.2 kJ/mol for Ca, -129.3 kJ/mol for Li, -192.0 kJ/mol for Na, and -244.4 kJ/mol for K). It is tempting to infer that the large stability of alkali and alkaline earth hydroxides relative to oxides may suggest large equilibrium constant, K_3 for reaction 3 in the melts as well. However, our ^{1}H-NMR results revealed an opposite order of cation type dependency from above for the abundance of MOH groups in silicate glasses, suggesting that reaction 3 may not be the controlling factor determining the stability of such groups in silicate melts.

We may combine reactions 1 and 3 to obtain a more straightforward expression for the relation between MOH and the network structure as the following:

$$2\text{SiOM (melt)} + H_2O\text{ (melt)} = \text{SiOSi (melt)} + 2\text{ MOH (melt)} \quad (4)$$

The equilibrium constant of reaction 4 is: $K_4 = [SiOSi][MOH]^2/[SiOM]^2[H_2O] = K_3/K_1$

This reaction may, in a way, be regarded as the hydrous equivalence of reaction 1. It gives a straightforward expression that the formation of MOH alone would result in an increase in the degree of polymerization of the silicate network structure. Our ^{1}H-NMR data suggest that the formation of MOH is favored by higher field strength cations (Mg > Ca > Na), and thus K_4 may increase in the same order, parallel to the trend shown by K_1. This sequence of stability is also manifested by the structures of crystalline silicates: whereas MgOH and CaOH groups are common hydroxyl species in hydrous magnesium and calcium silicates, NaOH groups are rarely observed in hydrous sodium silicates (Table 3). As for the anhydrous reaction 1, the inferred increase in K_4 with increasing field strength of M cation may be the combined effect of (1) more favorable formation of MOH groups by higher field strength cations because of better satisfaction of the valence requirements of such oxygens; and (2) less destabilization of the Si-O-Si bonds from the nonlocalized effect of M cations. Equivalently, this trend may be accounted for by greater extent of reaction 4 to the left between the acidic SiO_2 and basic MOH, with increasing basicity of the MOH groups. Therefore, it is not the basicity of MOM with respective to acidic H_2O (reaction 3), but the basicity of MOH (and MOM) with respective to acidic SiO_2 (reaction 1 or 4), that determines the stability of MOH groups in alkaline and alkaline earth silicate melts. The contrasting fact of wide occurrence of alkali-OH groups in hydroxide and hydroxide hydrate phases and scarcity of such groups in crystalline hydrous silicate phases (cf. Wells, 1986) is most likely a natural consequence of such a relationship. It should be mentioned that reaction 4 has been proposed previously to account for apparent nonlinear variations of water solubility with silica content in silicate melts (Kurkjian and Russell, 1957; Uys and King, 1963), although as discussed above, Uys and King (1963) suggested an opposite trend for the cation type dependency.

We may also combine reactions 4 and 2 in different ways to relate MOH with SiOH. By combining the left side of reaction 4 with the right side of reaction 2, one gets the following:

$$\text{SiOM (melt)} + \text{SiOH (melt)} = \text{MOH (melt)} + \text{SiOSi (melt)} \quad (5)$$

Alternatively, by combining the left hand sides of both reactions, one can obtain the following

$$\text{SiOM (melt)} + H_2O\text{ (melt)} = \text{MOH (melt)} + \text{SiOH (melt)} \quad (6)$$

Reactions analogous to 6 have often been suggested as a cation exchange process between a proton and M cation.

In summary, reactions 1, 2 and 3 give a general description of the relations among the three anhydrous oxygen species (SiOSi, SiOM and MOM) and the three hydrous species (H_2O, SiOH and MOH). For relatively polymerized systems in which the amounts of free oxygens are small, reactions 2 and 4 may be sufficient to describe the relations among the three hydrous species and their correlation with the network structure (SiOSi, SiOM). These reactions may be combined to give different, though equivalent expressions.

The abundance of free hydroxyls may diminish to a level of insignificance for silica-rich alkali silicate melts. When the formation of free hydroxyls is negligible, reaction 2 becomes the dominant water dissolution mechanism, as thus far widely accepted. This dissolution mechanism alone causes a decrease in the degree of polymerization of the network structure. The formation of free hydroxyls, as exemplified by reaction 4,

becomes an important water dissolution mechanism for relatively depolymerized silicate melts with cations of relatively large field strength such as Ca and Mg. Other cations of similar or larger field strength, such as Fe, are also expected to favor the formation of free hydroxyls. As these compositions are directly applicable to mafic and ultramafic magmas, the formation of free hydroxyl groups must constitute an important water dissolution mechanism for mantle-derived mafic and ultramafic magmas. The dissolution mechanism described by reaction 4 alone, would cause an increase in the degree of polymerization of the network structure. At least for the compositions we have investigated, both dissolution mechanisms make significant contributions, and the net changes, determined by the competition of these two opposing mechanisms, may be a smaller reduction in the degree of polymerization of the silicate melt structure than with reaction 2 alone.

4.3. Relations with Melt Viscosity and Liquidus Phase Boundaries

The diverse dissolution mechanisms of water are expected to have direct consequences for the phase relations and physical properties of silicate melts. The latter information is indispensable for understanding and quantitatively modeling magmatic processes of various scales, from magma transport and fractional crystallization in magma chambers, to the differentiation of the Earth's mantle during its early evolution.

The viscosity of silicate melts is one of the physical properties that have been found to be closely related to the silicate network structure. The addition of alkali or alkaline earth oxides to silica is known to cause a drastic decrease in the melt viscosity, which can be related to the depolymerization of the silicate network as described by reaction 1. The dissolution of water in relatively polymerized silicate melts, such as rhyolite and andesite, has also been found to cause a large reduction in viscosity (see review in Lange, 1994). This can again be explained by the rupture of the silicate network through reaction 2, analogous to the addition of alkali metals. There are only limited studies concerning the effect of water on the viscosities of more depolymerized silicate melts (Scarfe, 1973; Persikov et al., 1990; Persikov, 1991; Whittington et al., 2000; Whittington et al., 2001). Scarfe (1973) measured the viscosities of hydrous silicate melts of several natural compositions at high pressure and high temperature and observed only a small reduction in viscosity for a tholeiite melt, and little changes for a more depolymerized olivine tholeiite melt, with addition of 4 wt% water. Persikov and coauthors (Persikov et al., 1990; Persikov, 1991) measured the melt viscosities for a series of synthetic and natural silicate samples at high temperature and high pressure, and concluded that the dissolution of water causes a smaller reduction in melt viscosity for intermediate and basic melts than for acidic melts. More recently, Persikov and Bukhtiyarov (2001) reported viscosity results for melts along the albite (Ab)-diopside join under saturated water pressure up to 5 kbar and noted that whereas the viscosities of the more acidic albite and $Ab_{25}Di_{75}$ melts show a drastic decrease with increasing water pressure, those of the more basic diopside melt show a small increase. However, these authors did not compare the data with those of the anhydrous melts under identical P-T conditions. Whittington et al. (2000, 2001) determined the viscosities of anhydrous melts of synthetic compositions similar to those of phonolite, trachyte, tephrite, and basanite (with estimated NBO/T up to 1.51) at ambient pressure and near the glass transition temperature, and confirmed that the effect of water is smaller for more depolymerized melts. Because the depolymerized melts investigated in these studies all contain abundant Ca and Mg, free hydroxyls may constitute an important water species. As described in the preceding section, the formation of free hydroxyls cause an increase in the degree of polymerization of the network structure through reaction 4, countering the effect of reaction 2 for the formation of silanols. Thus the above results may be at least partly attributed to smaller reductions in the polymerization of melt structure as the relative abundances of free hydroxyls increase with increasing NBO/T. Persikov and Bukhtiyarov (2001) have also interpreted their viscosity results in a similar way. The observed net depolymerization effect suggests that the abundances of free hydroxyl groups are smaller than those of SiOH groups in these melts.

Liquidus phase relations of silicates are also strongly affected by the melt structure. For anhydrous metal oxide-silica melts at ambient pressure, the liquidus boundaries of certain phases, such as the saturation surface of cristobalite-tridymite and the cotectic boundaries of forsterite-enstatite and enstatite-cristobalite, have been found to shift systematically to silica-rich compositions with decreasing field strength of the network-modifying cations (e.g., Kushiro, 1975; Ryerson, 1985). As the silica activities at these boundaries are buffered, the systematic shifts to higher silica contents may be interpreted as a decrease in silica activities in the melts at a given silica content. The latter may in turn be related to a decrease in the abundances of more polymerized species, as a result of greater equilibrium constant of reaction 1 (cf. Ryerson, 1985; Hess, 1995). Liquidus phase relations under hydrous conditions have also been extensively investigated because of the important role of water in magma genesis and evolution. It has been shown that in the forsterite-silica and forsterite-diopside-silica systems the dissolution of water shifts the liquidus boundaries of both forsterite-enstatite and enstatite-quartz to more silica-rich compositions at 10 to 20 kbar, analogous to the effect of adding alkali oxides (e.g., Kushiro et al., 1968; Kushiro, 1969; Warner, 1973). These results imply that the dissolution of water in the melts reduces the activities of more polymerized components, which may again be an indication of gross depolymerization of the melt structure (Kushiro, 1975; Fraser, 1977). The melt compositions near the forsterite-enstatite liquidus boundary of the anhydrous systems at 10 to 20 kbar have silica molar contents within the range of CMS glasses from our study, those of the enstatite-quartz liquidus boundaries are somewhat more silica-rich, and both have larger Mg/Ca ratios. Thus, assuming that the water dissolution mechanisms do not change appreciably between 2 kbar and 20 kbar, we may expect that both free hydroxyls and SiOH groups are important water species in these melts. The observed shifts in the liquidus boundaries may be taken to suggest that the depolymerization effect of SiOH (reaction 2) exceeds the opposing effect of free hydroxyls (reaction 4) under these conditions, implying greater abundances of the former than the latter. This is in broad agreement with the NMR results from our study and with the viscosity

data described above, although quantitative comparisons are difficult due to the different compositions and P-T conditions.

4.4. Relations with Water Solubility in Depolymerized Silicate Melts

The water dissolution mechanisms described in section 4.1 may be applied to explain the observed compositional dependence of water solubility in alkali and alkaline earth silicate melts. The early data measured near 1 atm often show conflicting trends with respect to compositions, which was a major source of the diverse water dissolution models proposed (e.g., Tomlinson, 1956; Walsh et al., 1956; Kurkjian and Russell, 1957; Franz and Scholze, 1963; Uys and King, 1963). McMillan and Holloway (1987) has compiled such solubility data and suggested that there is a general trend of increasing solubility with (1) decreasing silica content, and (2) cation types in the order Ca, Li, Na and K, for binary alkali and calcium silicate melts, a trend best shown by the data of Franz and Scholze (1963) determined using IR spectroscopy. Solubility data on alkali (Li, Na and K) silicate melts at ambient pressure reported more recently (Mesko and Shelby, 2001; Mesko et al., 2002) are in general agreement with those of Franz and Scholze (1963). Following Stolper (1982a), the solubility of water in silicate melts may be expressed by the following vapor-melt equilibrium,

$$H_2O\ (\text{vapor}) = H_2O\ (\text{melt}) \quad (7)$$

in addition to homogeneous reactions describing the relations between molecular H_2O and hydroxyl groups in the melt, both at the experimental temperature (rather than Tg). As suggested by Stolper (1982a), the compositional dependency of water solubility is likely to be dominated by the homogeneous reaction(s) involving the formation of hydroxyl groups, rather than the heterogeneous reaction 7. At the level of water solubility of these experiments (< 0.3 wt% H_2O), almost all of the dissolved water species are expected to be hydroxyl groups. Our study has shown that between the two forms of hydroxyl groups, SiOH and MOH, the latter is favored over the former by cations of higher field strength (Mg $>$ Ca $>$ Na). A likely explanation for the observed solubility trend is thus enhanced formation of SiOH in alkali silicate melts through the homogeneous reaction 2. As described above, the enhanced reaction 2 for quenched glasses can be related partly to the weakening of Si-O-Si bonds by the presence of network modifiers, and partly to the stabilization of SiOH groups by hydrogen bonding with nonbridging oxygens. High-temperature IR and Raman studies have suggested that hydrogen bonding may become less important at higher temperature for silicate liquids, to which the solubility data apply (e.g., Scholze, 1959c; Mysen, 1998). A more general structural factor for the stability of SiOH groups with decreasing field strength of cations may be the greater interaction between the protons on SiOH groups and nonbridging oxygens: such an interaction may manifest itself as static Si-O-H. . .O_{nbr} hydrogen bonding in the rigid glasses below Tg, and as a dynamic exchange of protons between the two types of oxygen sites in the liquid state at higher temperature.

A number of water solubility data have also been reported for alkali and alkaline earth silicate melts at high pressure (e.g., Rosenhauer and Eggler, 1975; Eggler and Rosenhauer, 1978; McMillan and Holloway, 1987; Mysen and Acton, 1999; Mysen and Wheeler, 2000; Mysen, 2002; Mysen and Cody, 2003). As suggested previously, molecular water must play an increasingly important role with increasing water solubility at high pressure (cf. Stolper, 1982a; McMillan and Holloway, 1987). The general compositional dependence of water solubility with the type of metal cations and with silica content seems to be retained at least up to ~10 kbar (cf. McMillan and Holloway, 1987), and may be explained in a similar way. At pressures above ~20 kbar, the compositional effect on water solubility seems to be much smaller, consistent with the dominant role of molecular water at large water contents (cf. Stolper, 1982a; McMillan and Holloway, 1987).

5. CONCLUSIONS

In conclusion, our ^{1}H and ^{29}Si-NMR data and ab initio calculation results strongly suggest that substantial parts of the dissolved water in silicate glasses (quenched melts) of the CaO-MgO-SiO_2 system are in the form of (Ca,Mg)OH, free hydroxyl groups. We have found that free hydroxyls are favored by (1) more depolymerized melts and (2) network-modifying cations of higher field strength (Mg $>$ Ca $>$ Li, Na). This dissolution mechanism could be particularly important for mantle-derived mafic and ultramafic magmas. The formation of free hydroxyls is expected to result in an increase in the polymerization and viscosity of silicate melts, contrary to the effect of SiOH formation. These diverse water dissolution mechanisms would also affect the liquidus phase relations and physical properties of silicate melts, and must be taken into account for any quantitative models of hydrous silicate melts and glasses.

Our ^{1}H MAS NMR data and ab initio calculations also yield insight into the hydrogen bonding strength of OH groups in hydrous silicate glasses. Whereas the hydrogen bonding strength of SiOH in all the studied alkali and alkaline earth silicate glasses covers a similar range from weak to very strong; the relative population of strong hydrogen bonding grows with decreasing field strength of the network-modifying cations. The ab initio calculations suggest that this trend may largely reflect hydrogen bonding with nonbridging oxygens. Interaction between SiOH and nonbridging oxygens could be an important factor contributing to the enhanced water solubility in alkali silicate melts near ambient pressure. Free hydroxyls tend not to form strong hydrogen bonding with other oxygens.

Acknowledgments—We are grateful to T. Kawamoto for stimulating discussions and for sample synthesis at the early stage of this project. We also thank S. Yamashita for permission to use the internally heated gas pressure apparatus, T. Matsuzaki for electron microprobe analysis, and D. G. Fraser for helpful discussions. The manuscript benefited from comments by three reviewers. All the calculations were performed on an Alpha server ES45, funded by the Ministry of Education, Culture, Sports, Science and Technology of Japan (MEXT). This study was supported by Grants-in-Aid for Scientific Research to M.K. and 21st century COE Program from the MEXT.

Associate editor: J. Rustad

REFERENCES

Acocella J., Tomozawa M., and Watson E. B. (1984) The nature of dissolved water in silicate glasses and its effect on various properties. *J. Non-Cryst. Solids* **65,** 355–372.

Alcock N. W. (1971) Refinement of the crystal structure of lithium hydroxide monohydrate. *Acta Crystallogr.* **B27,** 1682–1683.

Almond G. G., Harris R. K., and Graham P. (1994) A study of the layered alkali-metal silicate, magadiite, by one-dimensional and 2-dimensional ^{1}H and ^{29}Si NMR spectroscopy. *J. Chem. Soc. Chem. Commun.* **7,** 851–852.

Almond G. G., Harris R. K., and Franklin K. R. (1997) A structural consideration of kanemite, octosilicate, magadiite and kenyaite. *J. Mater. Chem.* **7,** 681–687.

Bartholomew R. F. and Schreurs J. W. H. (1980) Wide line NMR study of protons in hydrosilicate glasses of different water content. *J. Non-Cryst. Solids* **38/39,** 679–684.

Behrens H. and Stuke A. (2003) Quantification of H_2O contents in silicate glasses using IR spectroscopy—A calibration based on hydrous glasses analyzed by Karl-Fischer titration. *Glass Sci. Technol.* **76,** 176–189.

Bode B. M. and Gordon M. S. (1998) Macmolplt: A graphical user interface for GAMESS. *J. Mol. Graph. Mod.* **16,** 133–138.

Brandriss M. E. and Stebbins J. F. (1988) Effects of temperature on the structures of silicate liquids: ^{29}Si NMR results. *Geochim. Cosmochim. Acta* **52,** 2659–2669.

Bronnimann C., Zeigler R. C., and Maciel G. E. (1988) Proton NMR study of dehydration of the silica gel surface. *J. Am. Chem. Soc.* **110,** 2023–2026.

Bruckner R., Chun H.-U., Goretzki H., and Sammet M. (1980) XPS measurements and structural aspects of silicate and phosphate glasses. *J. Non-Cryst. Solids* **42,** 49–60.

Casanovas J., Pacchioni G., and Illas F. (1999) ^{29}Si solid state NMR of hydroxyl groups in silica from first principle calculations. *Mat. Sci. Eng.* **B68,** 16–21.

Chase M. W. J. (1998) *NIST-JANAF Themochemical Tables*. 4th ed. Monograph 9. J. Phys. Chem. Ref. Data. Monograph No. 9, American Institute of Physics.

Cheeseman J. R., Trucks G. W., Keith T. A., and Frisch M. J. (1996) A comparison of models for calculating nuclear magnetic resonance shielding tensors. *J. Chem. Phys.* **104,** 5497–5509.

Civalleri B., Garrone E., and Ugliengo P. (1999) Cage-like clusters as models for the hydroxyls of silica: Ab initio calculation of ^{1}H and ^{29}Si NMR chemical shifts. *Chem. Phys. Lett.* **299,** 443–450.

Cooksley B. G. and Taylor H. F. W. (1974) Crystal structure of monoclinic $NaCaHSiO_4$. *Acta Crystallogr.* **B30,** 864–867.

Cooney T. F. and Sharma S. K. (1990) Structure of glasses in the systems Mg_2SiO_4-Fe_2SiO_4, Mn_2SiO_4-Fe_2SiO_4, Mg_2SiO_4-$CaMgSiO_4$ and Mn_2SiO_4-$CaMnSiO_4$. *J. Non-Cryst. Solids* **122,** 10–32.

Cory D. G. and Ritchey W. M. (1988) Suppression of signals from the probe in Bloch decay spectra. *J. Magn. Reson.* **80,** 128–132.

de Jong B. H. W. S. and Brown G. E. Jr. (1980) Polymerization of silicate and aluminate tetrahedra in glasses, melts and aqueous solutions—II. The network modifying effects of Mg^{2+}, K^{+}, Na^{+}, Li^{+}, H^{+}, OH^{-}, F^{-}, Cl^{-}, H_2O, CO_2 and H_3O^{+} on silicate polymers. *Geochim. Cosmochim. Acta* **44,** 1627–1642.

Deng Z. Q., Lambert J. F., and Fripiat J. J. (1989) A puckered layered silicate, $KHSi_2O_5$: Hydrolysis products and alkylammonium intercalated derivatives. *Chem. Mater.* **1,** 375–380.

Desgranges L., Grebille D., Calvarin G., Chevrier G., Floquet N., and Niepce J. C. (1993) Hydrogen thermal motion in calcium hydroxide: $Ca(OH)_2$. *Acta Crystallogr.* **B49,** 812–817.

Dupree R., Holland D., Mortuza M. G., Smith M. E., Chen A., and James P. F. (1990) Multinuclear magnetic resonance study of Li_2O-SiO_2 sol-gel glasses. *Magn. Reson. Chem.* **28,** S89–96.

Eckert H., Yesinowski J. P., Silver L. A., and Stolper E. M. (1988) Water in silicate glasses: Quantitation and structural studies by ^{1}H solid echo and MAS-NMR methods. *J. Phys. Chem.* **92,** 2055–2064.

Eggler D. H. and Rosenhauer M. (1978) Carbon dioxide in silicate melts. II. Solubilities of CO_2 and H_2O in $CaMgSi_2O_6$ (diopside) liquids and vapors at pressures to 40 kb. *Am. J. Sci.* **278,** 64–94.

Elleman D. D. and Williams D. (1956) Proton positions in brucite crystals. *J. Chem. Phys.* **25,** 742–744.

Engelhardt G. and Michel D. (1987) *High-Resolution Solid-State NMR of Silicates and Zeolites.* Wiley.

Farnan I., Kohn S. C., and Dupree R. (1987) A study of the structural role of water in hydrous silica glass using cross-polarisation magic angle spinning NMR. *Geochim. Cosmochim. Acta* **51,** 2869–2873.

Fleischer U., Kutzelnigg W., Bleiber A., and Sauer J. (1993) ^{1}H NMR chemical shift and intrinsic acidity of hydroxyl groups. Ab initio calculations on catalytically active sites and gas-phase molecules. *J. Am. Chem. Soc.* **115,** 7833–7838.

Franz H. and Scholze H. (1963) Die Löslichkeit von H_2O-Dampf in Glasschmelzen verschiedener Basizität. *Glastech. Ber.* **36,** 347–356.

Fraser D. G. (1977) Thermodynamic properties of silicate melts. In *Thermodynamics in Geology* (ed. D. G. Fraser), pp. 301–325. Reidel.

Frisch M. J., Trucks G. W., Schlegel H. B. G. E. Scuseria, Robb M. A., Cheeseman J. R., Zakrzewski V. G. J. A. Montgomery J., Stratmann R. E., Burant J. C., Dapprich S., Millam J. M., Daniels A. D., Kudin K. N., Strain M. C., Farkas O. J. Tomasi, Barone V., Cossi M., Cammi R., Mennucci B., Pomelli C. C. Adamo, Clifford S., Ochterski J., Petersson G. A., Ayala P. Y. Q. Cui, Morokuma K., Rega N., Salvador P., Dannenberg J. J., Malick D. K., Rabuck A. D., Raghavachari K., Foresman J. B. J. Cioslowski, Ortiz J. V., Baboul A. G., Stefanov B. B., Liu G. A. Liashenko, Piskorz P., Komaromi I., Gomperts R., Martin R. L. D. J. Fox, Keith T., Al-Laham M. A., Peng C. Y., Nanayakkara A. M. Challacombe, Gill P. M. W., Johnson B., Chen W., Wong M. W. J. L. Andres, Gonzalez C., Head-Gordon M., Replogle E. S., and J. A. Pople. (1998) Gaussian 98. Gaussian Inc.

Garvie L. A. J., Devouard B., Groy T., Camara F., and Buseck P. R. (1999) Crystal structure of kanemite, $NaHSi_2O_5 \cdot 3H_2O$, from the Aris phonolite, Namibia. *Am. Mineral.* **84,** 1170–1175.

Gladden L. F., Carpenter T. A., and Elliot S. R. (1986) ^{29}Si MAS NMR studies of the spin-lattice relaxation time and bond-angle distribution in vitreous silica. *Phil. Mag.* **B53,** L81–L87.

Goldman D. S. (1986) Evaluation of the ratios of bridging to nonbridging oxygens in simple silicate glasses by electron spectroscopy for chemical analysis. *Phys. Chem. Glasses* **27,** 128–133.

Hayashi S. (1997) Solid-state NMR study of locations and dynamics of interlayer cations and water in kanemite. *J. Mater. Chem.* **7,** 1043–1048.

Heidemann D. (1994) Proton high-resolution solid-state NMR spectroscopy using CRAMPS techniques for studies in silicate and cement science. In *Application of NMR Spectroscopy to Cement Science* (eds. P. Colombet and A. R. Grimmer), pp. 77–102.

Hess P. C. (1995) Thermodynamic mixing properties and the structure of silicate melts. In *Structure, Dynamics and Properties of Silicate Melts*, Vol. 32 (eds. J. F. Stebbins, P. F. McMillan and D. B. Dingwell), pp. 145–189. Mineralogical Society of America.

Hochella M. F. Jr. and Brown G. E. Jr. (1988) Aspects of silicate surface and bulk structure analysis using X-ray photoelectron spectroscopy (XPS). *Geochim. Cosmochim. Acta* **52,** 1641–1648.

Kagi H., Parise J. B., Cho H., and Rossman G. R. (2000) Hydrogen bonding interactions in phase A $[Mg_7Si_2O_8(OH)_6]$ at ambient and high pressure. *Phys. Chem. Minerals* **27,** 225–233.

Kanzaki M., Xue X., and Stebbins J. F. (1998) Phase relations in Na_2O-SiO_2 and K_2O-SiO_2 systems up to 14 GPa and ^{29}Si NMR study of the new high-pressure phases: Implications to the structure of high-pressure silicate glasses. *Phys. Earth Planet. Int.* **107,** 9–21.

Kanzaki M. and Xue X. (2002) NMR evidence for a new water dissolution mechanism in alkaline earth silicate melts (abstract). *Geochim. Cosmochim. Acta* **66,** A345.

Kawamoto T. and Holloway J. R. (1997) Melting temperature and partial melt chemistry of H_2O-saturated mantle peridotite to 11 gigapascals. *Science* **276,** 240–243.

Kirkpatrick R. J., Oestrike R., and Weiss C. A. Jr. (1986) High-resolution ^{27}Al and ^{29}Si NMR spectroscopy of glasses and crystals along the join $CaMgSi_2O_6$-$CaAl_2SiO_6$. *Am. Mineral.* **71,** 705–711.

Kohn S. C. (2000) The dissolution mechanisms of water in silicate melts; a synthesis of recent data. *Mineral. Mag.* **64,** 389–408.

Kohn S. C., Dupree R., and Smith M. E. (1989a) Proton environments and hydrogen-bonding in hydrous silicate glasses from proton NMR. *Nature* **337,** 539–541.

Kohn S. C., Dupree R., and Smith M. E. (1989b) A multinuclear magnetic resonance study of the structure of hydrous albite glasses. *Geochim. Cosmochim. Acta* **53,** 2925–2935.

Kohn S. C., Dupree R., and Mortuza M. G. (1992) The interaction between water and aluminosilicate magmas. *Chem. Geol.* **96,** 399–409.

Koller H., Engelhardt G., and Felsche J. (1990) Si-29 NMR studies of the transformation of silicate anions in the system $Na_2O \cdot SiO_2 \cdot 9{,}5H_2O$ in crystals, melts and solution. *J. Chem. Soc.* **5,** 371–372.

Koller H., Engelhardt G., and Felsche J. (1995) Variable temperature ^1H, ^{23}Na and ^{29}Si MAS NMR studies on sodium silicate hydrates of composition $Na_2O \cdot SiO_2 \cdot nH_2O$ (n = 9, 6, 5): Local structure in crystals, melts, supercooled melts and glasses. *Z. Anorg. Allg. Chem.* **621,** 301–310.

Kubicki J. D. and Sykes D. (1993) Molecular orbital calculations on $H_6Si_2O_7$ with a variable Si-O-Si angles: Implications for the high pressure vibrational spectra of silicate glasses. *Am. Mineral.* **78,** 253–259.

Kurkjian C. R. and Russell L. E. (1957) Solubility of water in molten alkali silicates. *J. Soc. Glass Technol.* **41,** 130–144.

Kushiro I. (1969) The system forsterite-diopside-silica with and without water at high pressures. *Am. J. Sci.* **267A,** 269–294.

Kushiro I. (1972) Effect of water on the composition of magmas formed at high pressures. *J. Petrol.* **13,** 311–334.

Kushiro I. (1975) On the nature of silicate melt and its significance in magma genesis: Regularities in the shift of the liquidus boundaries involving olivine, pyroxene and silica minerals. *Am. J. Sci.* **275,** 411–431.

Kushiro I., Yoder H. S. J., and Nishikawa M. (1968) Effect of water on the melting of enstatite. *Geol. Soc. Am. Bull.* **79,** 1685–1692.

Kümmerlen J., Merwin L. H., Sebald A., and Keppler H. (1992) Structural role of H_2O in sodium silicate glasses: Results from ^{29}Si and ^1H NMR spectroscopy. *J. Phys. Chem.* **96,** 6405–6410.

Lager G. A., Ulmer P., Miletich R., and Marshall W. G. (2001) O-DO bond geometry in OD-chondrodite. *Am. Mineral.* **86,** 176–180.

Lange R. A. (1994) The effect of H_2O, CO_2 and F on the density and viscosity of silicate melts. In *Volatiles in Magmas*, Vol. 30 (eds. M. R. Carroll and J. R. Holloway), pp. 331–369. Mineralogical Society of America.

Levin E. M., Robbins C. R., and McMurdie H. F. (1964) *Phase Diagrams for Ceramists.* **1** American Ceramic Society.

Liu Y., Nekvasil H., and Long H. (2002) Water dissolution in albite melts: Constraints from ab initio NMR calculations. *Am. Mineral.* **23,** 4149–4163.

Maciel G. E. and Sindorf D. W. (1980) Silicon-29 nuclear magnetic resonance study of the surface of silica gel by cross-polarisation and magic-angle spinning. *J. Am. Chem. Soc.* **102,** 7606–7607.

Maekawa H., Maekawa T., Kawamura K., and Yokokawa T. (1991) The structural groups of alkali silicate glasses determined from ^{29}Si MAS-NMR. *J. Non-Cryst. Solids* **127,** 53–64.

Malik K. M. A. and Jeffrey J. W. (1976) A re-investigation of the structure of afwillite. *Acta Crystallogr.* **B32,** 475–480.

Malinovskii Y. A. and Belov N. V. (1979) Crystal structure of potassium disilicate $KHSi_2O_5$. *Dokolady Akademii Nauk SSSR* **246,** 99–103.

Marsh R. E. (1994) A revised structure for alpha-dicalcium silicate hydrate. *Acta Crystallogr.* **C50,** 996–997.

McMillan P. (1984) A Raman spectroscopic study of glasses in the system CaO-MgO-SiO_2. *Am. Mineral.* **69,** 645–659.

McMillan P. F. (1994) Water solubility and speciation models. In *Volatiles in Magmas*, Vol. 30 (eds. M. R. Carroll and J. R. Holloway), pp. 131–156. Mineralogical Society of America.

McMillan P. F. and Holloway J. R. (1987) Water solubility in aluminosilicate melts. *Contrib. Mineral. Petrol.* **97,** 320–332.

Mesko M. and Shelby J. (2001) Water solubility and diffusion in alkali silicate melts. *Phys. Chem. Glasses* **42,** 173–178.

Mesko M., Schader P., and Shelby J. (2002) Water solubility and diffusion in sodium silicate melts. *Phys. Chem. Glasses* **43,** 283–290.

Murdoch J. B., Stebbins J. F., and Carmichael I. S. E. (1985) High-resolution ^{29}Si NMR study of silicate and aluminosilicate glasses: The effect of network-modifying cations. *Am. Mineral.* **70,** 332–343.

Mysen B. (1998) Interaction between aqueous fluid and silicate melt in the pressure and temperatures regime of the Earth's crust and upper mantle. *N. Jb. Miner. Abh.* **172,** 227–244.

Mysen B. (2002) Water in peralkaline aluminosilicate melts to 2 GPa and 1400 degrees C. *Geochim. Cosmochim. Acta* **66,** 2915–2928.

Mysen B. and Acton M. (1999) Water in H_2O-saturated magma-fluid systems: Solubility behavior in K_2O-Al_2O_3-SiO_2-H_2O to 2.0 GPa and 1300°C. *Geochim. Cosmochim. Acta* **63,** 3799–3815.

Mysen B. O. and Virgo D. (1986) Volatiles in silicate melts at high pressure and temperature. 1. Interaction between OH groups and Si^{4+}, Al^{3+}, Ca^{2+}, Na^+ and H^+. *Chem. Geol.* **57,** 303–331.

Mysen B. O. and Wheeler K. (2000) Solubility behavior of water in haploandesitic melts at high pressure and high temperature. *Am. Mineral.* **85,** 1128–1142.

Mysen B. O. and Cody G. D. (2003) Solubility and solution mechanism of H_2O in alkali silicate melts at high pressure. *Geochim. Cosmochim. Acta* **67,** A316.

Mysen B. O., Virgo D., and Scarfe C. M. (1980a) Relations between the anionic structure and viscosity of silicate melts—A Raman spectroscopic study. *Am. Mineral.* **65,** 690–710.

Mysen B. O., Virgo D., Harrison W. J., and Scarfe C. M. (1980b) Solubility mechanism of H_2O in silicate melts at high pressures and temperatures: A Raman spectroscopic study. *Am. Mineral.* **65,** 900–914.

Nakamoto K., Margoshes M., and Rundle R. E. (1955) Streching frequencies as a function of distances in hydrogen bonds. *J. Am. Chem. Soc.* **77,** 6480–6486.

Navrotsky A. (1995) Energetics of silicate melts. In *Structure, Dynamics and Properties of Silicate Melts*, 32 (eds. J. F. Stebbins, P. F. McMillan and D. B. Dingwell), pp. 121–143. Mineralogical Society of America.

Navrotsky A., Geisinger K. L., McMillan P., and Gibbs G. V. (1985) The tetrahedral framework in glasses and melts—Inferences from molecular orbital calculations and implications for structure, thermodynamics and physical properties. *Phys. Chem. Minerals* **11,** 284–298.

Novak A. (1974) Hydrogen bonding in solids. Correlation of spectroscopic and crystallographic data. In *Structure and Bonding 18: Large Molecules* (eds. J. D. Dunitz, P. Hemerich, R. H. Holm, J. A. Ibers, C. K. Jorgensen, J. B. Neilands, D. Reimene, and R. J. P. Williams), pp. 177–216. Springer.

Oglesby J. V. and Stebbins J. F. (2000) ^{29}Si CPMAS NMR investigations of silanol-group minerals and hydrous aluminosilicate glasses. *Am. Mineral.* **85,** 722–731.

Papike J. J., Ross M., and Clark J. R. (1969) Crystal chemical characterization of clino-amphiboles based on five new structural refinements. Special Papers 2, pp. 117–136. Mineralogical Society of America.

Perdikatsis B. and Burzlaff H. (1981) Strukturverfeinerung am talk $Mg_3[(OH)_2Si_4O_{10}]$. *Z. Kristallogra.* **156,** 177–186.

Persikov E. S. (1991) The viscosity of magmatic liquids: Experiment, generalized patterns. a model for calculation and prediction. applications. In *Physical Chemistry of Magmas*, Vol. 9 (ed. L. L. Perchuk and I. Kushiro), pp. 1–40. Springer-Verlag.

Persikov E. S., Zharikhov V. A., Bukhtiyarov P. G., and Pol'skoy S. F. (1990) The effect of volatiles on the properties of magmatic melts. *Eur. J. Mineral.* **2,** 621–642.

Persikov E. S. and Bukhtiyarov P. G. (2001) The nature of anomalous dependence of viscosity of silicate and magmatic melts on lithostatic and water pressure. *Exp. Geosci.* **10,** 34–37.

Phillips B. L., Burnley P. C., Worminghaus K., and Navrotsky A. (1997) ^{29}Si and ^1H NMR spectroscopy of high-pressure hydrous magnesium silicates. *Phys. Chem. Minerals* **24,** 179–190.

Pimentel G. C. and McClellan A. L. (1960) *The Hydrogen Bond.* Freeman.

Prewitt C. T. (1967) Refinement of the structure of pectolite, $Ca_2NaHSi_3O_9$. *Z. Kristallogra.* **125,** 298–316.

Riemer T., Schmidt B., Behrens H., and Dupree R. (2000) H_2O/OH ratio determination in hydrous aluminosilicate glasses by static

proton NMR and the effect of chemical shift anisotropy. *Solid State Nucl. Magn. Reson.* **15,** 201–207.

Robert E., Whittington A., Fayon F., Pichavant M., and Massiot D. (2001) Structural characterization of water-bearing silicate and aluminosilicate glasses by high-resolution solid-state NMR. *Chem. Geol.* **174,** 291–305.

Rosenhauer M. and Eggler D. H. (1975) Solution of H_2O and CO_2 in diopside melt. *Carnegie Inst. Wash. Yearb.* **74,** 474–479.

Rosenberger H. and Grimmer A.-R. (1979) Zum Zusammenhang zwischen der chemischen Verschiebung der Protonen und dem Charakter der OH-Gruppen in einigen kristallinen Silicaten. *Z. Anorg. Allg. Chem.* **448,** 11–22.

Ryerson F. J. (1985) Oxide solution mechanisms in silicate melts: Systematic variations in the activity coefficient of SiO_2. *Geochim. Cosmochim. Acta* **49,** 637–649.

Sänger A. T. and Kuhs W. F. (1992) Structural disorder in hydroxyapatite. *Z. Kristallogra.* **199,** 123–148.

Scarfe C. M. (1973) Viscosity of basic magmas at varying pressure. *Nature* **241,** 101–102.

Schaller T. and Sebald A. (1995) One- and two-dimensional ^{1}H magic-angle spinning experiments on hydrous silicate glasses. *Solid State Nucl. Magn. Reson.* **5,** 89–102.

Schmidt B. C., Riemer T., Kohn S. C., Behrens H., and Dupree R. (2000) Different water solubility mechanisms in hydrous glasses along the Qz-Ab join: Evidence from NMR spectroscopy. *Geochim. Cosmochim. Acta* **64,** 513–526.

Schmidt B. C., Riemer T., Kohn S. C., Holtz F., and Dupree R. (2001) Structural implications of water dissolution in haplogranitic glasses from NMR spectroscopy: Influence of total water content and mixed alkali effect. *Geochim. Cosmochim. Acta* **65,** 2949–2964.

Scholze H. (1959a) Der Einbau des Wassers in Gläsern I. Der Einfluβ des im Glas gelösten Wassers auf das Ultrarot-Spektrum und die quantitative ultrarotspektroskopische Bestimmung des Wassers in Gläsern. *Glastech. Ber.* **32,** 81–88.

Scholze H. (1959b) Der Einbau des Wassers in Gläsern II. UR-Messungen an Silikatgläsern mit systematische variierter Zusammensetzung und Deutung der OH-Banden in Silikatgläsern. *Glastech. Ber.* **32,** 142–152.

Scholze H. (1959c) Der Einbau des Wassers in Gläsern IV. Der Einfluβ der Temperatur. *Glastech. Ber.* **32,** 314–320.

Sears R. E. J., Kaliaperumal R., and Manogaran S. (1988) ^{1}H shielding anisotropy in $Mg(OH)_2$: The isolated OH^- group. *J. Chem. Phys.* **88,** 2284–2288.

Smith K. A., Kirkpatrick R. J., Oldfield E., and Henderson D. M. (1983) High-resolution silicon-29 nuclear magnetic resonance spectroscopic study of rock-forming silicates. *Am. Mineral.* **68,** 1206–1215.

Stebbins J. F. (1987) Identification of multiple structural species in silicate glasses by ^{29}Si NMR. *Nature* **330,** 465–467.

Stolper E. (1982a) The speciation of water in silicate melts. *Geochim. Cosmochim. Acta* **46,** 2609–2620.

Stolper E. (1982b) Water in silicate glasses: An infrared spectroscopic study. *Contrib. Mineral. Petrol.* **81,** 1–17.

Sykes D., Kubicki J. D., and Farrar T. C. (1997) Molecular orbital calculation of ^{27}Al and ^{29}Si NMR parameters in Q^3 and Q^4 aluminosilicate molecules and implications for the interpretation of hydrous aluminosilicate glass NMR spectra. *J. Phys. Chem. A* **101,** 2715–2722.

Tangeman J. A., Phillips B. L., Navrotsky A., Weber J. K. R., Hixson A. D., and Key T. S. (2001) Vitreous forsterite (Mg_2SiO_4): Synthesis, structure and thermochemistry. *Geophys. Res. Lett.* **28,** 2517–2520.

Tomlinson J. W. (1956) A note on the solubility of water in a molten sodium silicate. *J. Soc. Glass Technol.* **40,** 2519.

Tsujimura T., Xue X., Kanzaki M., and Walter M. J. (2004) Sulfur speciation and network structural changes in sodium silicate glasses: Constraints from ^{29}Si MAS NMR and Raman spectroscopy. *Geochim. Cosmochim. Acta,*in press.

Uchino T., Sakka T., Ogata Y., and Iwasaki M. (1991) Ab initio molecular orbital calculations on the electronic structure of sodium silicate glasses. *J. Phys. Chem.* **95,** 5455–5462.

Uchino T., Sakka T., Ogata Y., and Iwasaki M. (1992a) Mechanism of hydration of sodium silicate glass in a steam environment: ^{29}Si NMR and ab initio molecular orbital studies. *J. Phys. Chem.* **96,** 7308–7315.

Uchino T., Sakka T., Ogata Y., and Iwasaki M. (1992b) Changes in the structure of alkali-metal silicate glasses with the type of network modifier cation: An ab initio molecular orbital study. *J. Phys. Chem.* **96,** 2455–2463.

Uys J. M. and King T. B. (1963) The effect of basicity on the solubility of water in silicate melts. *Trans. Metall. Soc. AIME* **227,** 492–500.

Walsh J. H., Chip J., King T. B., and Grant N. J. (1956) Hydrogen in steelmaking slags. *AIME Trans*. **206**.

Wan C., Ghose S., and Gibbs G. V. (1977) Rosenhahnite, $Ca_3Si_3O_8(OH)_2$: Crystal structure and the stereochemical configuration of the hydroxylated trisilicate group, $[Si_3O_8(OH)_2]$. *Am. Mineral.* **62,** 503–512.

Warner R. D. (1973) Liquidus relations in the system CaO-MgO-SiO_2-H_2O at 10 kb P_{H2O} and their petrologic significance. *Am. J. Sci.* **273,** 925–946.

Wells A. F. (1986) *Structural Inorganic Chemistry.* Oxford University Press.

Whittington A., Richet P., and Holtz F. (2000) Water and the viscosity of depolymerized aluminosilicate melts. *Geochim. Cosmochim. Acta* **64,** 3725–3736.

Whittington A., Richet P., Linard Y., and Holtz F. (2001) The viscosity of hydrous phonolites and trachytes. *Chem. Geol.* **174,** 209–223.

Wies C., Meise-Gresch K., and Muller-Warmuth W. (1990) ^{29}Si MAS NMR studies of sol-gel-derived glasses in the Li_2O-SiO_2 system. *J. Non-Cryst. Solids* **116,** 161–166.

Wu C.-K. (1980) Stable silicate glasses containing up to 10 weight percent of water. *J. Non-Cryst. Solids* **41,** 381–398.

Xue X. and Kanzaki M. (1998) Correlations between ^{29}Si, ^{17}O and ^{1}H NMR properties and local structures in silicates: An ab initio calculation. *Phys. Chem. Minerals* **26,** 14–30.

Xue X. and Kanzaki M. (2000) An ab initio calculation of ^{17}O and ^{29}Si NMR parameters for SiO_2 polymorphs. *Solid State Nucl. Magn. Reson.* **16,** 245–259.

Xue X. and Kanzaki M. (2001) An ab initio calculation of the ^{17}O and ^{1}H NMR parameters for various OH groups: Implications to the speciation and dynamics of dissolved water in silicate glasses. *J. Phys. Chem. B* **105,** 3422–3434.

Xue X., Kanzaki M., and Kawamoto T. (2001) NMR evidence for a new water dissolution mechanism in depolymerized silicate melts: Results for hydrous diopside composition (abstract). Presented at the Japan Earth and Planetary Science Joint Meeting.

Xue X., Kanzaki M., and Fraser D. G. (2002) The dissolution mechanisms of forsterite and enstatite: Constraints from ^{29}Si and ^{1}H MAS NMR (abstract). *Geochim. Cosmochim. Acta* **66,** A853.

Yesinowski J. P. and Eckert H. (1987) Hydrogen environments in calcium phosphates: ^{1}H MAS NMR at high spinning speeds. *J. Am. Chem. Soc.* **109,** 6274–6282.

Yesinowski J. P., Eckert H., and Rossman G. R. (1988) Characterization of hydrous species in minerals by high-speed ^{1}H MAS-NMR. *J. Am. Chem. Soc.* **110,** 1367–1375.

Zarubin D. P. (1999) Infrared spectra of hydrogen bonded hydroxyl groups in silicate glasses. A re-interpretation. *Phys. Chem. Glasses* **40,** 184–192.

Zeng Q., Nekvasil H., and Grey C. P. (1999a) Proton environments in hydrous aluminosilicate glasses: A ^{1}H MAS, ^{1}H/^{27}Al and ^{1}H/^{23}Na TRAPDOR NMR study. *J. Phys. Chem. B* **103,** 7406–7415.

Zeng Q., Stebbins J. F., Heaney A. D., and Erdogan T. (1999b) Hydrogen speciation in hydrogen-loaded, germania-doped silica glass: A combined NMR and FTIR study of the effects of UV irradiation and heat treatment. *J. Non-Cryst. Solids* **258,** 78–91.

Zhang P., Grandinetti P. J., and Stebbins J. F. (1997) Anionic species determination in $CaSiO_3$ glass using two-dimensional ^{29}Si NMR. *J. Phys. Chem. B* **101,** 4004–4008.

Zotov N. and Keppler H. (1998) The influence of water on the structure of hydrous sodium tetrasilicate glasses. *Am. Mineral.* **83,** 823–834.